Preparation and electrochemical performance of PEDOT – AuNPs nanocomposite layers for the selective detection of neurotransmitters

Dissertation

zur Erlangung des akademischen Grades

Doctoringenieur (Dr. Ing.)

vorgelegt der Fakultät für Elektrotechnik und

Informationstechnik der Technischen Universität Ilmenau

von

Gruia, Violeta - Tincuta

geboren am 23. Juli 1976 in Galati, Rumänien

vorgelegt am: 30.10.2015

Gutachter: 1. Univ.-Prof. Dr. rer. nat. habil. Dr. h. c. Andreas Bund

2. apl. Prof. Dr. rer. nat. habil. Uwe Ritter

3. Prof. Dr. Geta Carac

Verteidigung am: 12.04.2016

Verf.-Nr.: EI 382

Acknowledgments

Contents

Introduction and Motivation

In 2000, Alan J. Heeger, Alan G. MacDiarmid, and Hideki Shirakawa were awarded to the Nobel Prize for Chemistry "for their discovery and development of conducting polymers" (as written on their Nobel Prize certificate) [1]. A new class of chemical compounds, more exactly, the conductive polymers, (CP), have come into attention of the scientific world even before this time, but their importance was recognized in 2000 [1].

The electrochemist' interests in conducting polymers are especially in the preparation's method and electropolymerization mechanism. Mechanistic details play an important role in determining the quality of these materials because the most CPs were synthesized by the structures' modification [2].

The most common synthesized CPs are: polyphenylene (PP), polyphenylenevinylene, polypyrrole (PPy), polythiophene (PTh), polyaniline (PANI) [3-8]. These new systems have included substituted derivatives of the hydrocarbons and heterocycles but also novel compounds as 3,4-ethylenedioxythiophene (EDOT) which has considerably improved the properties of conducting materials [9-11]. The used method to synthesize conducting polymers, is the anodic oxidation of monomers, such as pyrrole, thiophene, or aniline [2].

Poly(3,4-ethylenedioxythiophene) (PEDOT) is one of the most widely used conducting polymers, due to its good electrochemical stability and high conductivity [11]. Since it was first synthesized in 1988 by Bayer AG, Leverkusen [11], intensive work has been done on this important CP [8-11]. Due to its promising future in many applications, e.g. antistatic coatings [8], energy storage [9], electrochromic devices [10], sensors [2] a considerable number of studies are on the influence of the electropolymerization conditions

1

on the surface morphology, electrical and sensing properties of PEDOT films [2].

PEDOT layers applications in sensors' field is the aim of this work. It is well known that very stable PEDOT films can be prepared by electrochemical polymerization in aqueous electrolytes [2, 11]. PEDOT shows good redox activity in aqueous media because of its hydrophilic surface imparted by the ether substituents in the 3 and 4 positions of the thiophene ring [2, 11]. In addition, the polymerization reaction mainly occurs via the 2 and 5 positions, and cross linking is reduced, which has positive impact on the electrochemical stability of the polymer [11].

A further advantage is the low oxidation potential of PEDOT in aqueous media (0.2 V vs Ag/AgCl), preserving high conductivity in broad potential range and making it suitable for electrochemical sensing for various analytes as catecholamines (dopamine and serotonin were studied in this work) [2, 11].

Another important feature of PEDOT layers is their stability with respect to the transition from the oxidized to the reduced state [12, 13]. The experimental method used in this study (Electrochemical Quartz Crystal Microbalance, EQCM, allows us to determine with high accuracy the ions species which are involved in the transition from one state to another.

The attention was focused recently on studying composite materials. Conducting polymers were used as a matrix on which different metals were deposited, such as Pt [14–16], Pd [14, 17-19], Ag [14, 20, 21], Au [22–29, 39], Cu [30–32], Ni [33–36], Pb [15, 37, 38]. These composite materials present special physical and chemical properties because they combine the polymer properties with those of metal particles. Thus, due to the presence of metal particles, the properties of nanocomposites like conductivity and catalytic

activities are significantly improved. So a promising application of composite films is developing different types of sensors.

Conducting polymer layers with incorporated metallic nanoparticles could have multiple applications for electronic components, sensors and catalysis, because they are lightweight, have large surface area, the potential for non-enzymatic detection, low cost, easy processing and scalable production [2].

In order to obtain a uniform distribution of nanoparticles a lot of work has done by several research groups [14-38] but their work was focused on particles deposition and not on polymer synthesis. The surface morphology of CP influences the particles distribution. Due to this reason our group has addressed this issue by systematically studying the influence of each involved polymerization parameter for PEDOT layer. It was found in this thesis the proper method for polymer electrodeposition in order to reach large amounts of metal nanoparticles in PEDOT layers, improving significantly the electrocatalytic properties as biosensor for neurotransmitters.

Catecholamines are a class of neurotransmitters which includes dopamine (DA) [40], serotonin (5-HT) [41], adrenalin (EP) [42]. These catecholamines control different biological processes and therefore it is very important their detection in the human body. Low levels of EP and DA have been found in patients with Parkinson's disease while 5-HT plays an important role in the emotional system together with other monoamine transmitters. These catecholamines coexist in biological medium with ascorbic acid (AA). AA is present in a concentration between 100 and 1000 time higher than catecholamines and interfere in their analytical detection because have similar oxidation potential [43].

Among the different analysis techniques the interest in electrochemical methods is higher because of their simplicity, selectivity, low costs, less time-

consuming and as well because they can be applied to a real-time in situ determination [40-42].

Electrochemical analysis on unmodified electrodes like glassy carbon (GC), or gold electrodes, used in our work, has limitations because of overlapping voltammetric peaks for different analytes due to the interference of high concentrations of AA [40-43].

The general objective of this work was to develop new modified electrodes using conducting polymers, PEDOT, and metal nanoparticles, gold nanoparticles, which are able to detect distinguish response of oxidation of analytes with respect of increase of concentration. It was also possible electroanalytical detection of neurotransmitters in the presence of AA without any interference, on PEDOT/Au nanoparticles modified electrode. The reproducibility was also studied and these data proved also that PEDOT nanocomposite layer can be a veritable candidate for an amperometric sensor for electrochemical detection of catecholamines.

1 Theoretical Background

In this chapter is presented the state of knowledge on conducting polymers and their applications. The first two sections give a brief introduction in conducting polymers and a summary classification also. The section 1.3 presents the polymerization mechanisms that govern their electrodeposition. The doping processes, which influence the polymer conductivity, presented in 1.4 are described by using the Electrochemical Quartz Crystal Microbalance (EQCM) technique. The piezoelectric effect, the principle behind the operation of the EQCM technique and a theoretical model to interpret the EQCM data for the charging and discharging process in electron-conducting polymer films are described in 1.5. Conducting polymers have several applications but the interesting one in this thesis is as biosensors for detection of neurotransmitters (1.7). For this reason their catalytic properties were improved by depositing gold nanoparticles on polymer surface (1.6). Section 1.7 presents the studied analytes in this work.

1.1 Introduction

For many years the main application of polymers has been as insulators and the electrical conducticity of polymers, was generally regarded as an undesirable property [2].

In the 1970s, a new class of polymers, which has high electronic conductivity, was discovered. This property is due to their oxidized or reduced state [44]. In 1862 Henry Letheby synthesised polyaniline by the anodic oxidation of aniline and showed that this polymer has electrochromic properties [8, 45]. Shirakawa and his colleagues prepared polyacetylene and together with the group led by MacDiarmid and Heeger discovered that the conductivity of polymer increased

strongly after the doping process. This was the starting point for new researches on the field of conducting polymers [46].

Electrochemistry plays an important role in the preparation and characterization of CPs [2, 44, 46] for at least two major reasons. The first one is focused on understanding the behavior of these systems, the mechanism of charge transfer during redox reactions of conducting polymers [47]. The second reason is the wide range of applications in the fields of energy storage, bioelectrochemistry, electroanalysis, electrocatalysis, organic electrochemistry, photoelectrochemistry, sensors, corrosion protection, electronic devices, electrochromic displays, microsystem technologies, microwave screening etc. [48-52].

The discovery of new systems brings new challenges. The complexity of those is given by the chemical changes like dimerization, cross-linking, ion-pair formation, but also by the changes in the morphology and slow relaxation.

The conductivity of this class of polymers is an attractive and useful property, but the most important one is the variability of their conductivity between their insulating and conducting states [45].

1.2 Classification of Electrochemically Active Polymers

Electrochemically active polymers can be classified regarding the way of charge propagation as [2]:

- electron-conducting polymers [2];
- proton (ion)-conducting polymers [2].

The electron-conducting polymers can be also classified into two classes, based on the mode of electron transport:

a) redox polymers, eg.: Poly(Tetracyanoquinodimethane) (PTCNQ) [53, 54],

Poly(Viologens) [55, 56], Poly(Tetrathiafulvalene) (PTTF) [57], Quinone Polymers [58–60]. They are ion exchange polymers and the redox active ions enter into the film as counterions. In the case of a cations exchange membrane, cations can be incorporated, which are held by covalent bonds [61].

b) electronically conducting polymers (Intrinsically Conducting Polymers—ICPs), eg.: Polyanilines (PANI) [62–71], Poly(o-Phenylenediamine) (PPD) [72], Poly(2-Aminodiphenylamine) (P2ADPA) [73, 74], Polypyrroles (PP) [75–83], Polythiophenes (PT) [84–95], Poly(3,4-Ethylenedioxythiophene) (PEDOT) [2, 10-12, 96–109] (the last one was used in this work).

1.3 Structure

1.3.1 Electropolymerization Mechanism for Conjugated Polymers

The deposition of conducting polymers, CPs, by electrochemical route is a unique process. Even if presents some similarities with the electrodeposition of metals like nucleation and phase-growth mechanism, the major difference is that the charged species of the deposited materials are initially produced by oxidation of the neutral monomer at the electrode surface [44]. That is interesting in electrochemical application, because thus it is easy to control the film thickness by the deposition charge, and also to characterize the polymer growth in situ. The various electrochemical and chemical reactions which are possible, make the electropolymerization mechanism a very complex problem [110-113].

The electrochemical stoichiometry of the electropolymerization reaction is in the range of 2.07-2.6 F/mol. The oxidation of the monomer requires only two electrons per molecule, 2 F/mol, so the excess of charge is the partial

reversible oxidation or doping charge of the conjugated polymer [110]. That means that every third to fourth monomeric subunit will be charged at the end of the electropolymerization [110].

1.3.1.1 Electropolymerization mechanism proposed by Roncalli

Roncalli proposed a mechanism for electropolymerization of heterocycles structures in two steps (Fig. 1) [110]. The first step (E), the electrochemical one, is the oxidation of the monomer to its radical cation. The concentration of radical cations near the electrode surface is supposed to be maintained high because the electron transfer reaction is faster than the diffusion of the monomer from the bulk solution. The second step (C), the chemical one, involves the coupling of two radicals to form a dimer, after loss of two protons and rearomatization. The rearomatization are actually the driving force of the chemical step. Due to the applied potential, the dimer, which is more easily oxidized than the monomer, forms its radical immediately, and a next coupling step with a radical cation happened and then the trimer loses the protons. Electropolymerization mechanism is formed from successive electrochemical and chemical steps until the oligomers become insoluble in the electrolyte and fall onto the electrode surface [110].
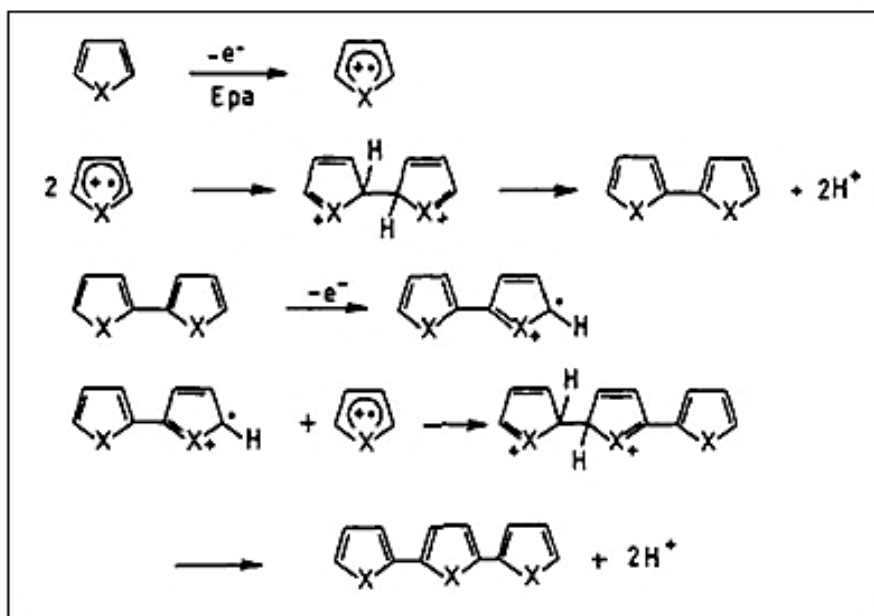
Fig. 1 Mechanism of electropolymerization proposed by Roncalli [110].

This mechanism proposed by Roncalli cannot answer to several questions, like the nature of the rate-limiting step, the role of oligomers in the initial deposition step, or the subsequent growth of the polymer chains. What is established is the oxidation of the monomer to its radical cation and the fact that the electropolymerization process is not limited by diffusion [110].

Reactivity of the monomers like pyrroles [75–83] and thiophenes [84–95], are always high but decrease drastically for oligomers [110], showing that the coupling tendency between oligomers and monomers decreases as a function of the oligomeric chain length [110]. Two possible explanations can be given for that: the first is the extremely high rate constant of dimerization for radical cations such as $Py^{\cdot+}$ or $Th^{\cdot+}$, about 10^9 M^{-1} s^{-1}. The second reason can be the proton elimination from the intermediate σ-dimers that may be rate determining step [110]. The experimental work of different scientific groups showed that rates of proton elimination from dimers diminish so drastically

that charged σ-dimers with more than four monomer units are stable [110]. The proton release can be correlated with the chain length criteria; the increasing chain length meaning a lower tendency for proton release [110].

1.3.1.2 Electropolymerization mechanism proposed by Heinze et al.

A similar mechanism to that of Roncalli was described by by Heinze et al. on donor-substituted thiophenes such as methylsulfanyl- or methoxy-substituted derivatives [111-113]. This mechanism confirms that the consecutive oligomerization of conducting polymers starts in solution and successive dimerization steps take place leading to an octameric coupling product (Fig. 2) [111].
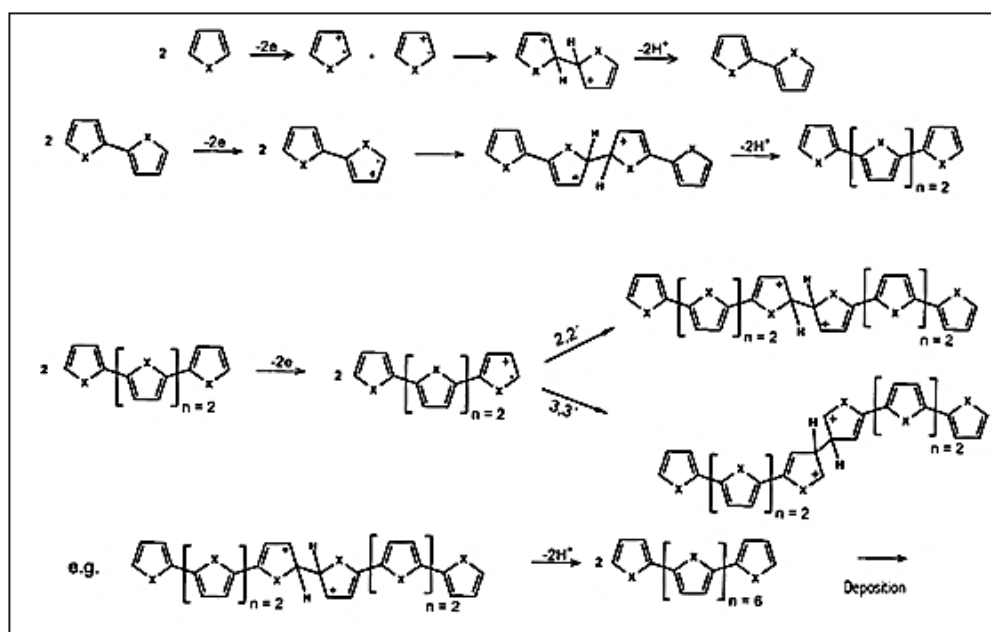
Fig. 2 Mechanism of electropolymerization proposed by Heinze [111].

If the concentration of the starting species is high then intermediates products like trimers, hexamers may occur due to the additional coupling reactions [111]. Also Lukkari et al. presented that, on initial step of electropolymerization,

oligomers are formed in solution and at the beginning of the deposition process oligomers with shorter or longer chains can be involved depending on the chemical nature and reactivity of the electrodes e.g ITO (indium tin oxide) or Pt [114].

Heinze et. al. also observed that the efficiency of electropolymerization and the amount of soluble oligomers formed during anodic oxidation strongly depend on the experimental parameters such as the polymerization potential, the concentration of the monomer, the experimental duration [111].

1.4 Doping of Polymers

Conjugated oligomers are oxidized at less positive potentials than their corresponding monomer and the polymer oxidation occurs concurrently with electrodeposition (see 1.3). The removal of one electron from the polymeric backbone at every three or four monomer units is responsible for polymer electronic conductivity [110-115]. To maintain film electroneutrality anions, are incorporated into the film. The term used for these anions is dopants [115].

The doping of polymers can be achieved by several methods but the most common are the chemical and the electrochemical ones [115]. Conjugated polymers can be both p-doped (oxidized) and n-doped (reduced). The electrochemical reduction (n-doping) of the neutral polymer was first reported by Inganas and co-workers [115].
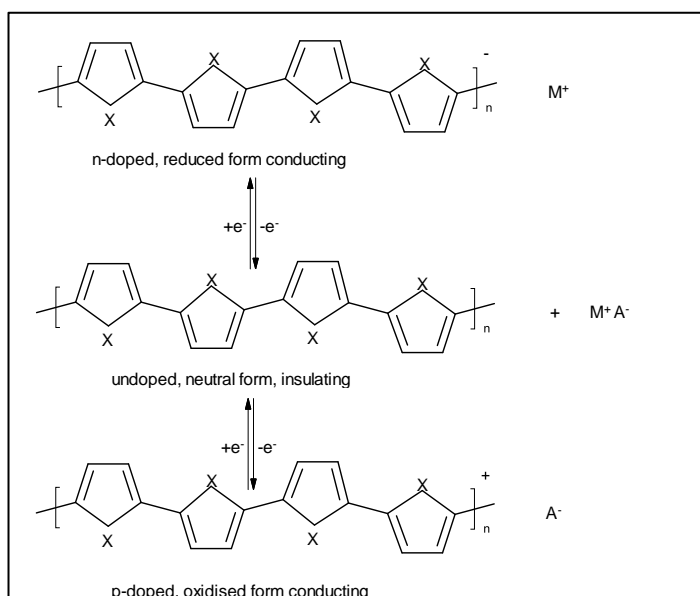
Fig. 3 The redox behaviour of a conducting polymer: neutral (undoped) form can be oxidized to the p-doped form or reduced to the n-doped form, X=NH, S or O [115].

During the p-doping the electrons are removed from the π-system of the polymer backbone resulting in a positively charged unit in the conjugated polymer [116]: During the n-doping, the electrons are introduced into the π-system of the polymer backbone forming a negatively charged unit in the conjugated system (Fig. 3) [116].

1.4.1 The electrochemically stimulated conformational relaxation, ESCR Model, by Otero et al.

During charging and discharging of the polymer layer a rearrangement of the chain configuration takes place, which is followed by the incorporation and expulsion of counterions. In order to explain this process Otero et al. [117, 118] have developed a model called "electrochemically stimulated conformational relaxation, ESCR" [118]. They supposed that the application of

an anodic overpotential to a neutral conjugated polymer leads to an expansion of the closed polymeric structure [118], partial oxidation takes place and counterions from the electrolyte enter under the influence of an electrical field [118]. During reduction reverse processes occur, the positive charges on the polymer are neutralized and counterions are expelled from opened channels that closed slowly as a function of waiting duration. Diffusion of the counterions becomes more and more difficult, as the structure closes [118].

A quantitative expression for the relaxation time τ needed to open the closed polymer structure is given by ESCR model (Eq. 1) [118.] Otero et al. assumed that the rate at which conformational changes in a conducting polymer film depend, as in other relaxation models, on structural and electrochemical variables through an Arrhenius type law [118]:

$$\tau = \tau_0 exp\frac{\Delta H}{RT} = \tau_0 exp\left[\frac{\Delta H^* + z_c(E_s - E_c) - z_r(E - E_0)}{RT}\right] \qquad \text{Eq. 1}$$

In Eq. 1 τ, the conformational relaxation time, is defined as the time required to change the conformation of a polymeric segment which previously was under the influence of a cathodic potential (E_c) and now it is oxidized by an anodic potential (E) at a given temperature (T). During the anodic pulse counterions enter from the solution. A polymeric segment is considered here as the minimum chain length whose conformational changes allow exchanges of ions between polymer and solution [118]. ΔH is the energy required for relaxing one mole of segments between two stationary states, as in any other conformational model. To describe the electrochemistry of the conducting polymers, this enthalpy includes three components: the first is ΔH^* the enthalpic increment of the system between two different stationary states, i.e., compacted and oxidized, in the absence of an external electric field. The second component is $z_c(E_s - E_c)$ is the electrochemical energy necessary to

13

reduce, close, and compact one mole of polymeric segments by cathodic potential (E_c). z_c is the charge consumed to reduce, close, and compact one mole of polymeric segments. The closure and compaction of the polymer is proportional to cathodic overpotential η_C (Eq. 2) [118]:

$$(\eta_C = E_S - E_C) \qquad \text{Eq. 2}$$

In Eq. 2 E_S is the experimental potential of closure and E_C is the compaction potential. In this situation, if the potential step is applied from a potential more anodic than E_S, the polymeric structure is relaxed, and the next oxidation will not be controlled by energetic requirements to open the polymeric network but only by counterion diffusion across the open structure [118].

The third term $z_r(E - E_0)$ is the electrochemical energy required to relax, oxidize, open, one mole of compacted polymeric segment. The energy required to relax one mole of compacted polymeric segment is supplied when an anodic overpotential, η, is applied to the compacted polymer (Eq. 3) [118]:

$$\eta = E - E_0 \qquad \text{Eq. 3}$$

This anodic overpotential refers to that potential where the oxidation of a relaxed conducting polymer begins (E_0). z_r is the charge consumed to relax one mole of compacted polymeric segments.

An important point is that during charging and discharging of CPs, the electroneutrality must be fulfilled. The mechanism of ion transport during charging and discharging of conducting polymers have been studied using several techniques: electrochemical quartz crystal microbalance (EQCM) [119-122], XPS (X-Ray Photoelectron Spectroscopy) measurements [123, 124] in order to prove that discharging involves not only the expulsion of anions but also the cations incorporation (Eq. 4, Eq. 5) [102]:

$$\left[(P_y)_4^+ A^-\right]_n + (n-m)e^- \rightarrow \left[(P_y)_{4n}^{m+} mA^-\right] + (n-m)A^-_{sol} \qquad \text{Eq. 4}$$

14

$$\left[\left(P_y\right)_{4n}^{m+} mA^-\right] + me^- + mM^+ \rightarrow \left(P_y\right)_{4n} + m[M^+, A^-]_{film} \quad \text{Eq. 5}$$
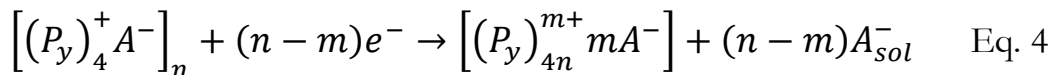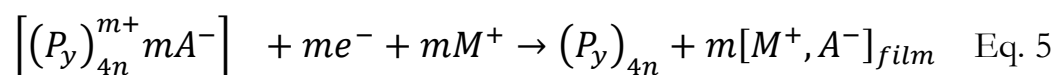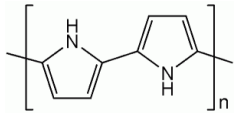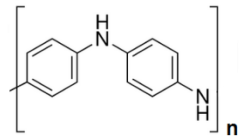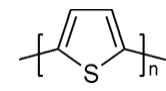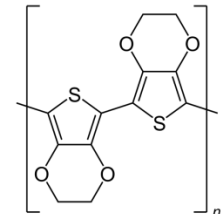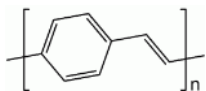
According to this model the partial oxidation of the conjugated polymer starts at the solution/polymer interface. This model has been criticized because its supposition was that the electrode potential cannot work at the solution/polymer interface and so excludes the driving forces in that domain.

1.4.2 Classification of CPs and their possible doping states

Table 1 List of conductive polymers with their possible doping states and applications.

Polymer	Structure	Specific Conductivity (S/cm)	Doping	Applications
Polypyrrole and derivatives (PPy)		40-200	p-	Electrochromic displays, sensors [64-70]
Polyaniline and derivatives (PANI)		5-30	n- p-	Sensors, electrochemical capacitors [40-50]
Polythiophene and derivatives (PTh)		10-200	n- p-	battery cathode material [71-78]
Poly(3,4-ethylenedioxythiophene) **(PEDOT)**		50-200	n- p-	Electrochemical capacitors, solar cells, battery cathode material, **sensors** [85-104]
Poly(para-phenylene vinylene) (PPV)		1-1000	p-	Photoconductors, solar cells, laser materials [33-36]

The range of conductivities of conducting polymers in charged and uncharged states was compared with different materials: insulators, semiconductors, and metallic conductors (Fig. 4) [2].
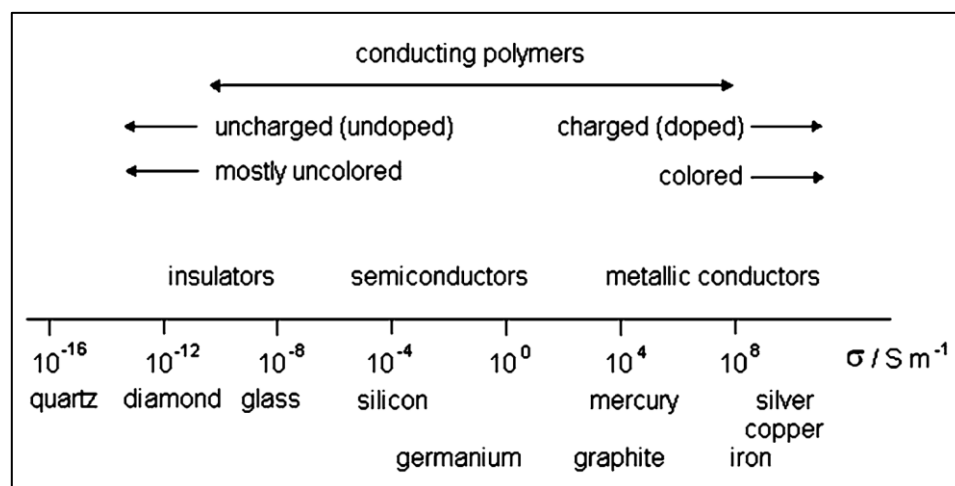
Fig. 4 Electronic conductivities of conducting polymers in comparison with those of other material [2]

The electronic conductivity has a broad range of values (up to 10–12 orders of magnitude) from its low value for the uncharged state of the polymer, similar as for insulator, to values of 1–1000 Scm^{-1} even up to 10^5 Scm^{-1} comparable to metals [2]. The type of used counterion affects the film conductivity [125]. For example, perchlorate anions, enhance the polymer conductivities [126].

1.5 Electrochemical Quartz Crystal Microbalance Technique

1.5.1 Piezoelectricity and the Quartz Crystal Microbalance

Piezoelectricity is a physical effect which denotes the appearance of an electric charge when a mechanical stress is applied. The word *piezoelectricity* derived from Greek and it means electricity resulting from pressure [126]. This property has only the materials that are acentric that means those that

crystallize in noncentrosymmetric space groups, like quartz, tourmaline, topaz, Rochelle salt, langasite, niobate, gallium-orthophosphate [126].

Even if the theoretical groundwork for the application of piezoelectricity was first pioneered by Rayleigh in 1885 [126], this effect was discovered in 1880 by French physicists Jacques and Pierre Curie [126].

A piezoelectric quartz crystal resonator is a precisely cut slab from a natural or synthetic crystal of quartz [127]. A quartz crystal microbalance (QCM) is formed from a thin quartz disk with electrodes plated on it and which presents acoustic resonances.

If an external electrical potential is applied to a piezoelectric material, as quartz is, that will produce an internal mechanical stress. An oscillating electric field will induce an acoustic wave that propagates through the crystal. The acoustic wave will have minimum impedance when the thickness of the quartz crystal is a multiple of a half wavelength of the acoustic wave [127].

For QCM technique the acoustic waves propagate in a direction perpendicular to the crystal surface [127]. To make this happen, the quartz crystal must be cuted to a specific orientation with respect to the crystal z-axis. AT-cut quartz crystals used in this work, are obtained by cutting the quartz wafer at approximately 35° with respect to z-axis. The dependence on the temperature of the resonance frequency of an AT-cut quartz can be neglected [127].

A resonant oscillation is obtained if the crystal is a part of an oscillation circuit where the electric and the mechanical oscillations are approximately the same as the fundamental frequency of the crystal is [127].

The oscillation frequency (f_0), depends on the quartz properties described by the parameters as the shear modulus (μ_q), the density (ρ_q) and the thickness of the quartz (t_q), are, as follows: $f_0 = (\mu_q/\rho_q)^{1/2}/2t_q$.

Sauerbrey has proved in 1959 that changes in the resonant frequency are directly related to the variation of mass accumulated on the crystal surface (Eq. 6) [128]:

$$\Delta f = -\frac{2f_0^2}{Z_q}\Delta m \qquad\qquad \text{Eq. 6}$$

In Eq. 6 Δf is the shift of the resonance frequency of the quartz crystal when a mass density, Δm, is deposited on top of one side of the resonator, $Z_q = (\mu_q \rho_q)^{1/2}$ is the mechanical impedance of quartz and f_0 is the resonance frequency of the unloaded quartz.

The Sauerbrey equation can be applied if the deposited layer has a uniform thickness and the deposited mass does not increases with more than 10% related to the mass of unloaded quartz and if the mechanical impedance of the deposited layers does not differ strongly from that of the quartz crystal.

The properly application of quartz crystal resonators is microgravimetry. Quartz crystal is suitable for electrochemical experiments, in order to monitor in-situ the mass changes at electrode surface. On this situation, the technique was named Electrochemical Quartz Crystal Microbalance, EQCM [129, 130].

When a crystal is immersed into a solution, the oscillating frequency depends on the physical properties of the electrolyte, like viscosity, density and electrical conductivity. Kanazawa and Gordon confirmed the linearity of the dependence of the frequency variation by the physical properties of the solvents [131]. The contact of quartz crystal with the liquid gives an additional frequency shift, Δf_l, which depends on density, ρ_l, and viscosity, η_l (Eq. 7) [131]:

$$\Delta f_l = -f_0^2 \frac{2}{\sqrt{\rho_q \mu_q}}\sqrt{\frac{n\rho_l\eta_l}{4\pi f_0}} \qquad\qquad \text{Eq. 7}$$

In Eq. 7 n is the number of the overtone ($n = 1, 3, 5, 7, ...$).

Theoretical Background

Their theory is based on a physical model, a simple one. According to this model the quartz is treated as a lossless elastic solid and the liquid as a viscous fluid. The frequency shift is from coupling the oscillation of the crystal, with the propagating shear wave in the liquid [131].

To explain the mechanism of oscillation of a crystal in solution, two electrical models are commonly used: the transmission line model and the Butterworth-van Dyke circuit [132]. These models were made in order to describe the propagation of the acoustic wave in analogy with the electrical waves [132].

The simplest electrical model to describe the QCM technique is an RLC circuit [127]. The electrical contact to a quartz crystal surface has been done by sputtering of an electrode to each face of the crystal. These electrodes bring an additional capacitance (C_0) in parallel with the series RLC as is shown in Fig. 5. On this principle is based Butterworth van Dyke (BvD) model.
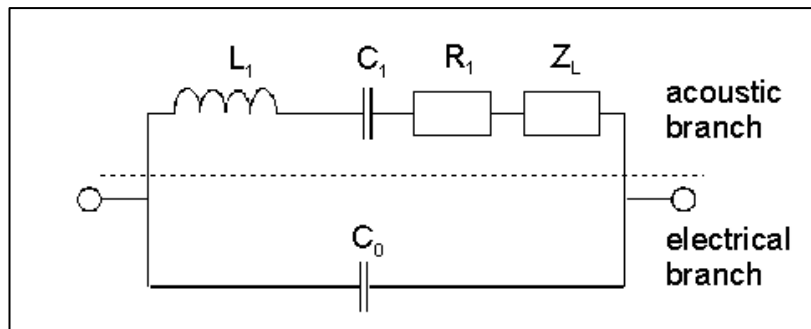
Fig. 5 Butterworth van Dyke Equivalent Circuit Model [127].

The BvD electrical model has two arms: one is the "shunt" arm, and it forms by the capacitor C_0, (electrical branch) that is the shunt capacitance of the crystal electrodes. The second arm, is the "motional" arm (acoustic branch) and it forms by the R-L-C circuit. Z_L is the mechanical load of a quartz due to the added the mass and is a component of "motional" arm (Fig. 5). L_1 is the motional inductance which is proportional to the mass. C_1 is the motional

20

capacitance which is inversely proportional to the stiffness. R_1 is the motional resistance which quantifies dissipative losses [127].

At the resonance frequency, the electrical impedance of the quartz crystal has a minimum and the admittance has a maximum. When an external potential is applied the admittance is proportional to the electrical current. It is a complex value that means it has a real and an imaginary component [127]. If a mass is deposited on the quartz crystal, than the resonance frequency will shift (Eq. 6). The complex shift in frequency is defined as (Eq. 8) [133]:

$$\Delta f^* = \Delta f + i\frac{\Delta w}{2} = (f - f_0) + i\frac{(w - w_0)}{2} \qquad\qquad \text{Eq. 8}$$

In Eq. 8 the real part is the shift of the position of the maximum of the resonance curve (Δf) and the imaginary part is the change of the half width at half maximum, FWHM, (Δw). As the displacement of the quartz surface is proportional to the piezoelectric current, the resonance curve can be represented by the real part of the admittance of the quartz crystal (Fig. 6). f_0 and w_0 are the fundamental resonance frequency and the full width at half maximum for the unloaded quartz.

Johannsmann et al. have shown that the complex frequency of AT-quartz is proportional to the mechanical impedance, Z_M^*, of an deposited layer (Eq. 9) [134]:

$$\frac{\Delta f^*}{f_0} = i\frac{Z_M^*}{\pi Z_q} \qquad\qquad \text{Eq. 9}$$

Based on Eq. 9 the mechanical impedance of the layer can be calculated as (Eq. 10) [133]):

$$Z_M^* = Z_M' + iZ_M'' = \frac{-\pi Z_q \Delta f}{f_0} + i\frac{\pi Z_q \Delta w}{2f_0} \qquad\qquad \text{Eq. 10}$$

The shift of frequency gives information about the mass deposited on top of quartz (Eq. 6), while FWHM represents a measure of the damping caused by a

viscoelastic layer [133]. Furthermore, from the data regarding the damping values semi-quantitative information about the roughness of the surface can be obtained in situ [131-136].
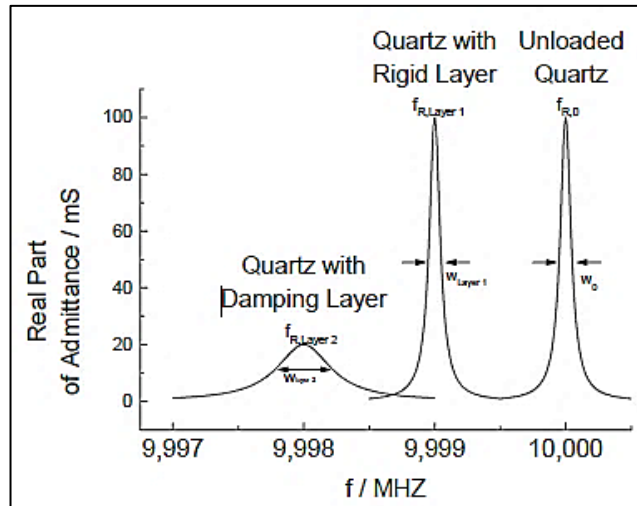
Fig. 6 Admittance diagrams of a quartz crystal near its resonance frequencies before and after application of a mechanical load. [133].

For viscoelastic or very rough layers it is better to characterize the electrical behavior of the resonator around its resonance frequency, by measuring the real part of the electrical admittance of the quartz crystal with a network analyzer or an impedance bridge (Fig. 6) [133-136]. The resonance curve can be described with a Lorentzian function (Fig. 6). The center of the curve lies at the resonance frequency, f, and the FWHM is proportional to the damping of the quartz crystal. When a smooth rigid layer is deposited on the quartz crystal the resonance curve shifts to lower frequencies but does not change its form (Fig. 6). When a damping layer deposited on the quartz crystal, the resonance curve shifts also to lower frequencies but at the same time becomes broader (Fig. 6).

1.5.2 Theoretical model to interpret the EQCM data for conducting polymers films proposed by Vorotyntsev et al.

A theoretical model to interpret the EQCM data for the charging and discharging process in conducting polymer films has been proposed by Vorotyntsev et al.. This model can be applied to the systems which do not have attached charged groups, or fixed charges [137]. Recently the EQCM technique has been used to obtain important informations on the electroactive polymer films [134]. With this technique it can be measured the variation of the mass of the film with the changing of external parameters, as it happens during cyclic voltammetry when potential varies in a chosen range. The driving force of the mass change is the electroneutrality condition for the film. A change of the film electronic charge is followed by the equivalent change of ions meaning an exchange of charged species between the film and solution [137].

In order to understand the complex process of charging in conducting polymers, Vorotyntsev et al. started from the simplest model for this system, to determine the most important parameters which govern this process and also to establish the qualitative relations between them [137].

In the case of equilibrium, the electrochemical potentials for anions and cations are equal in the film and in solution also (Eq. 11 and Eq. 12) [138]:

$$\mu_a^{0(s)} + KT log c_a^s + z_{K_a} e \emptyset^s = \mu_a^0 + KT log c_a + z_{K_a} e \emptyset^P + \Delta\mu_a^{int} \text{Eq. 11}$$

$$\mu_K^{0(s)} + KT log c_K^s - z_K e \emptyset^s = \mu_K^0 + KT log c_K - z_K e \emptyset^P + \Delta\mu_K^{int} \text{ Eq. 12}$$

In Eqs. 11 and 12 the symbols 'a' and 'k' are for anions (counter-ions) and cations (co-ions) respectively. The $\emptyset^s$ and $\emptyset^P$ are the potentials in solution and in the polymer and they can be considered as constant for the bulky electroneutrality of the film in the region faraway from both double layers [138]. $\mu_{a,K}^{0(s)}$ and $\mu_{a,K}^0$ are the standard chemical potentials. $c_{a,K}^s$, $c_{a,K}$ are the

concentrations of charged species in solution and polymer respectively. It has been supposed that the process occurs in a binary electrolyte therefore in Eq. 12 it can be considered that $z_{Ka} = -z_K$. The last terms $\Delta\mu_{a,K}^{int}$ represents the changes of the chemical potentials due to interactions between all charged components [138].

The potential drop $\emptyset^P - \emptyset^s$ at the polymer | solution interface can be excluded from Eqs. 11 and 12 (Eq. 13) [138]:

$$c_a c_K = c_s^2 exp\left(\frac{\Delta\mu_K^0 + \Delta\mu_a^0}{RT}\right) \equiv c_*^2 \qquad \text{Eq. 13}$$

In Eq. 13 $c_a \approx c_K \equiv c_s$ and $\Delta\mu_{a,K}^0 = \mu_{a,K}^{0(s)} - \mu_{a,K}^0$ [138]

To fulfill the electroneutrality condition for the film, the total electronic charge, $-Fc_e$, is compensated by the charge of intercalated anions, $-z_K Fc_a$, and cations, $-z_K Fc_{aK}$. During the anodic polymerization anions, c_a^b, are incorporated into the film and remain trapped there. The electrical charge of these trapped anions, $-z_K Fc_a^b$, was also included in the electroneutrality condition , as follows (Eq. 14) [138]:

$$c_e = c_a - c_b + c_a^b \qquad \text{Eq. 14}$$

For simplicity $z_K = 1$ and dimensionless variables have been used [138]:

$$\theta_a = \frac{c_a}{c_e^{max}} \qquad \theta_K = \frac{c_K}{c_e^{max}} \qquad \theta_a^b = \frac{c_a^b}{c_e^{max}} \qquad \theta_* = \frac{c_*}{c_e^{max}}$$

Fc_e^{max} represents the maximum electronic charge of the polymeric film. The shift of the frequency, Δf, due to the incorporation of anions or cations (with a molar mass M_a or M_K), is corrected for the mass of replaced or carried solvent (Eq. 15) [138]:

$$\Delta f = -F_0\left(\theta_a + \theta_K \frac{M_K}{M_a}\right) \qquad \text{Eq. 15}$$

In Eq.15 F_0 is the frequency shift at the maximum electronic charge. Eq. 15 takes into account that the solvent is transferred simultaneously with the charged species. From Eqs. 12–15 it was achieved the formula for frequency shift but in dimensionless variables (Eq. 16) [138]:

$$\frac{\Delta f}{F_0} = -\left(\frac{\theta}{2}\left(1 - \frac{M_K}{M_a}\right) + \left(1 + \frac{M_K}{M_a}\right)\sqrt{\frac{(\theta - \theta_a^b)^2}{4} + \theta_*^2}\right) \qquad \text{Eq. 16}$$

1.6 Composite Materials

Conducting polymers have been also used to obtain composite materials [40, 139-144]. The words "composite" or "hybrid" are used to describe systems where the monomer is polymerized in the presence of polymeric counterions (e.g., polyanions), [145] or when the polymer is used as a matrix for metals deposition [139-144].

The incorporation of different components like metals nanoparticles [139-144], enzymes [146], photochemically active compounds [147], silicomolybdate [148], nickel hexacyanoferrate [149], nucleotides [150], etc., results in composite materials with new and advantageous properties. In many cases the enhanced of catalytic activity, or of capacity, etc., are due to the increased of active area. In other cases the interaction between the conducting polymer and the other constituents results in a novel material that can be used for specific applications [151-154].

### 1.6.1 Metal deposition on conducting polymers

Recently CPs have been used as matrix for metals deposition [14-38]. Due to the presence of metal nanoparticles these hybrid materials have better conductivity and catalytic activities. Therefore they are perfect candidates for

application in sensors field. Au-PEDOT composite layers have been used for detecting dopamine, uric acid and ascorbic acid [142, 155-158], or DNA [159]. The composite layers of conducting polymers with metal particles are mainly obtained electrochemically. Three different ways are known for incorporating the metal particles in a conducting polymer matrix. One method is electroless deposition of the metals on top of the previously deposited polymer layer [29, 160-167]. If one brings the PEDOT layer into its reduced state, metal ions can be reduced on the polymer film, and as a final effect, a metallic layer will be obtained on the polymer surface. A second way to deposit the metal particles is electrochemically, by applying a current or voltage to the system, in a solution containing metal ions [168-174]. The third way is the co-deposition of both polymer and metal particles at the same time, from electrolyte that contain the monomer, the colloidal solution of metal nanoparticles which will be incorporated during the electropolymerization and some ligands that allow the formation of the colloidal suspension of nanoparticles (trisodium citrate was used in this work for gold nanoparticles suspension, see 2.2.1) [175, 176].

1.6.2 Electroless Deposition of Metals in Conducting Polymers

Smith et al suggested a chemical method for depositing nanoparticles in CPs, namely electroless precipitation, as follows (Eqs. 17, 18) [177, 178]:

$$Me^{n+} + ne^- \rightarrow Me^0 \hspace{3cm} \text{Eq. 17}$$

$$CP^{m+} \rightarrow CP^{(m+n)+} + ne^- \hspace{2.5cm} \text{Eq. 18}$$
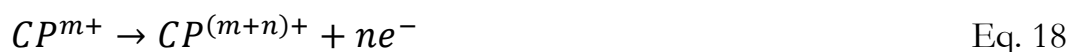
In Eqs. 17 and 18 n is the number of electrons exchanged for reducing a metal ion and m denotes the extent of initial oxidation of the CP material [177].

The electroless precipitation process is influenced by several factors like [156, 157]:

26

Initial redox state of the CP layers. The initial redox state of the CP layers, can be modified using electrochemical pretreatment in the absence of metal ions, as it was performed in this work the polymer was first reduced at a defined potential (see 3.3.2). Several studies regarding the electroless metal precipitation in reduced CPs like PEDOT, PPY and PANI have been made [177-191]. In this case, the precipitation process was determined by the larger potential difference between the open circuit potential, OCP, at initial dipping and the equilibrium potential of the metal used as metal ion in plating solution. This method makes possible the formation of homogeneously distributed metal nanoparticles on the polymer surface during several minutes. It has been shown that the reduction charge of the polymer layer and the immersion time of the reduced polymer into metal ions containing solution are the right parameters to manipulate the amount of precipitated metal according with the specific requirements for further applications of these hybrid materials [156, 157, 166].

Role of the surface morphology. The influence of the polymer surface morphology was studied by Mourato et al. [192]. They have studied in their work electroless deposition of Pd on PANI layers with different surface morphology. It was found that for compact PANI layer, Pd clusters with the size of 20 nm but also larger clusters with size distribution between 80–200 nm were formed. For porous PANI layers, smaller clusters, approx.15 nm size, with very narrow size distribution together with larger clusters between 100 and 200 nm size range were observed also [156, 157, 192].

Concentration of the metal ions. The concentration of the metal ions influences the rate-determining step of the precipitation reaction between transport limitations of the metal ions in the solution, for low concentrations, and CP based kinetic limitations, for high concentrations [156, 157, 183]. This effect was described by Tsakova et al. [193] for PANI/Ag system [163].

The advantage of metal electroless deposition is the possibility to eliminate the role of structural microdefects in the CP layer, as Skompska et al. presented in [28]. The most favorable sites for metal particles precipitation are those where the polymer structure becomes easily oxidized [28, 156, 157].

1.7 Neurotransmitters

Neurotransmitters are an important class of molecules, which act as chemical messengers that transport information between biological cells [194–203]. Direct measurement of the concentration of these neurotransmitters provides a way of understanding regarding their role in biological systems. Indeed, many studies aimed a group of biogenic amines, cathecholamines, including dopamine (DA) [204], epinephrine (also known as adrenalin, EP) [205], serotonin (5-hydroxytryptamine, 5-HT) [204], histamine. All of these are electroactive and can be easily oxidized at an electrode surface [204]. Due to the electroactive nature of these biogenic amines, electrochemical methods have been developed for their quantitative detection [204-210].

The detection of catecholamines in the human body has been of great interest to neuroscientists, because dopamine, epinephrine and serotonin (Fig. 7) play important roles in various biological, pharmacological, and physical processes. They are distributed in the mammalian central nervous system and they co-exist in biological medium [204-210]. Their concentrations in biological systems are between 100 nM and 1 μM for DA, between 40 nM and 1.33 μM for 5-HT, between 100 μM and 500 μM for ascorbic acid (AA). These values reflect the activity of the sympathoadrenal system [204-210].

Some major problems are often found in the determination of neurotransmitters. One is the interference of AA, which has similar oxidation potential and in vivo it is present in concentrations 100 to 1000 times higher

than the concentrations of other catecholamines. Another problem is the interference of voltammetric responses of analytes one with each other. These problems were successfully resolved in this work (see 3.4).

Dopamine plays a very important role in the functioning of several systems as central nervous, renal, hormonal, and cardiovascular systems are. Thus, a loss of neurons which produce DA can determine neurological ailment such as Parkinson's and schizophrenia [204]. Parkinson's disease is often correlated to a decrease in dopamine level in the substantia nigra of the brain and drugs prescribed to patients with Parkinson's disease are aimed to increase the dopamine level. By contrast one factor responsible for schizophrenia is the excess of dopamine or an oversensitivity of certain dopamine receptors therefore tranquillizers are used to treat this disease because they block and reduce the effects of dopamine [204].
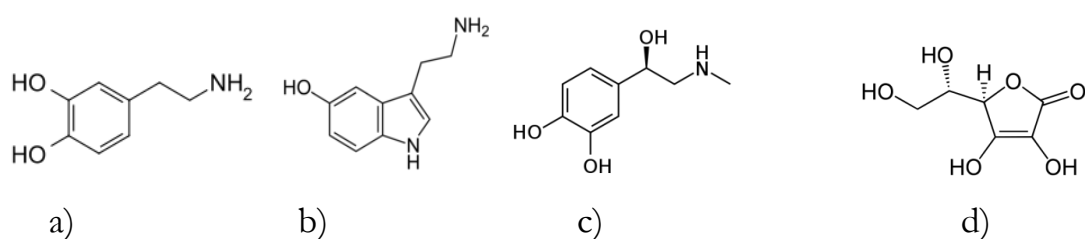

a)   b)   c)   d)

Fig. 7 Chemical structure of the neurotransmitters: dopamine a), serotonin b), epinephrine c), ascorbic acid d) [196]

Serotonin is a very important neurotransmitter because control the emotions by regulating mood and sleep [204, 206]. It has been found that patients suffering depression have abnormally lower levels of serotonin [204].Therefore, the selective detection and measurement of serotonin levels is of great value and can aid in understanding its role in depression and other neurological disorders.

Theoretical Background

Epinephrine controls the activity of sympathetic system associated with the excitement of the fight-or-flight response. Increased of epinephrine secretion above the physiological concentration can cause hypoglycemia, myocardial infarction [205, 210]. Low, or absent, concentration of epinephrine, may lead to neurological disorders such as Addison's disease [205].

Ascorbic acid, AA, vitamin C, is a hydrosoluble vitamin. The excess of AAA can lead to gastric irritation, and one of its metabolites, oxalic acid, causes renal problems [211].

The oxidation mechanism of catecholamines has been studied. It proceeds always via an o-quinone intermediate [204-211]. Oxidation of dopamine to dopamine-o-quinone, is followed by cyclisation and further oxidation (Fig. 8).The mechanism is defined as an ECE mechanism which involves an electrochemical step, followed by a chemical step and terminates in an electrochemical step [212].
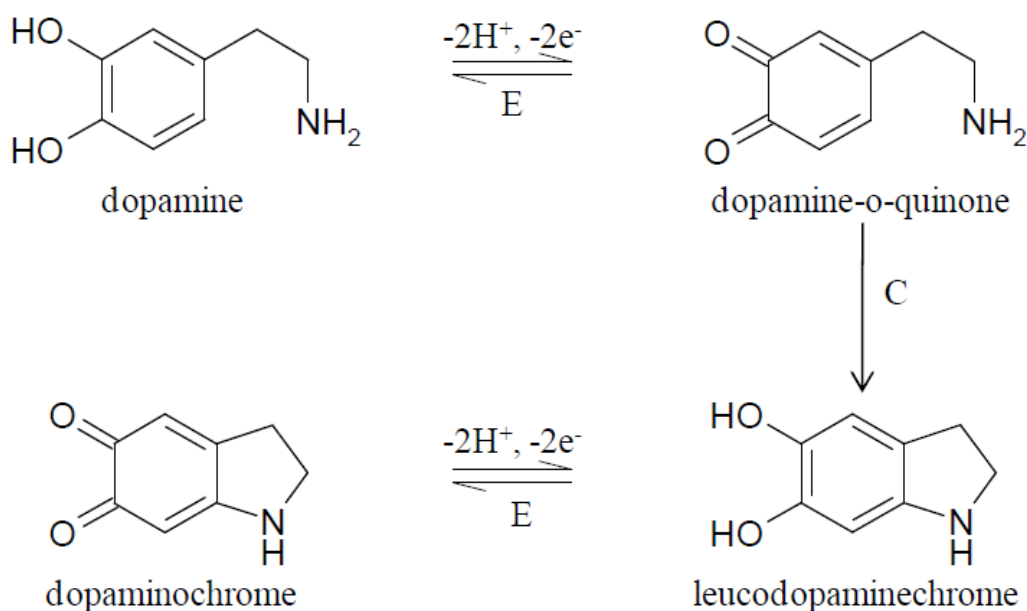

Fig. 8 Mechanism of DA oxidation [212]

A similar mechanism applies to epinephrine and serotonin [212].

Many biological studies were possible because the electrochemical methods provided quantitative information about neurotransmitter concentrations [204-211]. The surface of the electrode used for detection is usually large compared to the site of neurotransmitter release at synapse level, thus the detection of neurotransmitters in conditions able to reproduce the biological system has not been achieved [211].

Nanocomposite materials were synthesized in this work. A conductive polymer, PEDOT, with gold nanoparticles (AuNPs), were obtained. The hybrid polymer, PEDOT/AuNPs has a very good sensitivity and selectivity for catecholamine detection (see 3.4). The electropolymerization mechanism of PEDOT was studied using different techniques for electrodeposition, including pulse potentiostatic technique (see 3.2). For the last one the proper parameters were determined using EQCM technique (see 3.2.3) and a new model was proposed (3.3.2.1) in order to calculate the mass of deposited metal layer.

The synthesized PEDOT/AuNPs modified electrode shows a high selectivity and sensitivity especially for serotonin detection (3.4.4.1).

2 Experimental Details

The electrolyte composition (see 2.1), experimental setup (2.3) are described in this chapter. The preparation (2.2) and characterization of gold nanoparticles (2.7), regarding size, shape, surface charge is required in order to gain insight in the composite film formation. The particular techniques used are described in 2.5 and 2.6.

2.1 Electrolyte Composition

The electrolyte used in electropolymerization experiments consisted of an aqueous solution containing 8 mM 3,4-ethylenedioxythiophene, EDOT, (Alfa Aesar), 1 mM sodium dodecyl sulfate (SDS) (Alfa Aesar), and 0.2 M $LiClO_4$ (Alfa Aesar). The EDOT was used as functional monomer, $LiClO_4$, as supporting electrolyte and SDS as surfactant.

Due to the low solubility of the EDOT monomer in water (2.1 g L^{-1} at 20°C), an efficient oligomerization in aqueous solutions can be achieved by the addition of surfactants [213]. Characteristic for all surfactants is the fact that the current density during electrooxidation increases due to the formation of micelles [213]. Lacaze has shown that the oxidation potential in anionic micellar solutions, like SDS; is lowered whereas no significant changes occur in cationic as well nonionic aqueous media [213]. This is explained by Lacaze et al. that during the first step of the polymerization no repulsive interactions occured between cationic or nonionic surfactants and the radical cations [86]. The variation of the oxidation potential in anionic micellar solutions shows the interactions between anionic surfactants and the radical cations [213].

The salt used in this work as supporting electrolyte is 0.2 M $LiClO_4$. The supporting electrolyte and its concentration should be chosen, so that the transport numbers of the electroactive species is zero [213].

In order to increase the solubility of EDOT in water the solution was stirred using a magnetic stirrer for 1 h in a covered beaker. The pH of aqueous electrolyte used in this work was 4.2.

Voltammetric measurements for electroanalytical detection of neurotransmitters were performed in phosphate-buffered solution (PBS). Dopamine, serotonin and ascorbic acid were purchased from Alfa Aesar and dissolved in PBS.

The PBS consists of 0.1 M K_2HPO_4 and 0.1 M KH_2PO_4 and the pH was 6.9.

For layer characterization potentiodynamic experiments were performed in 0.5 M H_2SO_4 at pH 0.9.

2.2 Particle Preparation

In order to improve the electroanalytical properties of PEDOT layers gold nanaoparticles, AuNPs, were used. AuNPs were produced following the Turkevich method [214].

At the beginning 10 ml of 1mM $HAuCl_4$ *$3H_2O$ aqueous solution (purchased from Alfa Aesar) was heated to boiling in a 50 ml two-neck round-bottom flask under reflux and stirring. When the solution started to boil 0.5 ml of 2% (w/w) trisodium citrate aqueous solution was quickly injected. The solution was left to boiling under continue stirring until a typically red color appeared (Fig. 9). Then the heater was stopped, but the colloidal solution was kept stirred until cooled slowly to the room temperature in order to prevent the conglomeration of particles and to have a uniform distribution of particles size. The colloidal

suspension prepared in this way had a mean particle size of around 19.2 ± 1.4 nm, determined with a Zetasizer Nano device from Malvern.

Fig. 9 The colloidal solution of gold nanoparticles prepared by means of Turkevich technique

2.3 Electrodes and Electrochemical Set-up

Two different types of working electrodes, WE, were used: AT-cut quartz crystals from Vectron International, Germany, with gold electrodes on each surface and glassy carbon electrodes from BioAnalytical System.

Two gold electrodes, with 100 nm thickness, were deposited on the opposite faces of a quartz crystal, on a 5-10 nm chromium adhesion layer. The quartz resonators have approximately 15 mm the diameter and 165 µm the thickness.

The active surface areas of gold electrodes are 0.2213 cm², respectively 0.0706 cm² for glassy carbon electrodes.

The electrochemical set up involved a three-electrodes cell. The counter electrode was a platinum foil of approximately 3.7 cm² surface area and 0.2 mm thickness. All potentials were reported vs. an Ag/AgCl reference electrode. All measurements were performed at room temperature. Prior to all experiments, the solutions were purged with argon, for more than 30 minutes,

and an argon blanket was maintained above the solutions during the measurements.

The electrochemical cell was a homemade Teflon cylindrical cell with 3.6 cm inner diameter and 4.2 cm height.

All experiments were performed with an EG&G Versastat II potentiostat/galvanostat controlled by a lab-made software. The direct current (DC) deposition was performed at 0.9 V and the total plating charge was between 5.6 mC/cm² and 56.2 mC/cm². The corresponding thicknesses for these charges are between 100 nm and 1 μm. During the potentiostatic pulse (PP) experiments the pulse frequency, f_P, [*i.e. $f_P = 1 / (t_{on} + t_{off})$*] and the duty cycle, θ, [*i.e. $θ = t_{on} / (t_{on} + t_{off})$*] of the pulses were consecutively varied in order to find the suitable parameters for the aim of this work .

The pulse on-time (t_{on}) which is the anodic pulse duration (t_a), was kept constant at 0.5 s and the pulse pause (t_{off}), meaning the cathodic pulse duration (t_c), was varied between 0.2 s and 0.9 s respectively, as it is shown in Table 2. All the pulse experiments were performed for an anodic potential (deposition potential, E_a) of 0.9 V. After the cathodic pulse duration was fixed at 0.7 s, the cathodic potential (relaxation potential, E_c), was varied between -0.3 V and 0.5 V.

Table 2 Applied potentiostatic pulse plating programs. The cathodic potential was 0.3 V and the anodic potential 0.9 V respectively

t_{off} (t_c) / s	t_{on} (t_a) / s	f_P / Hz	θ / %
0.2	0.5	1.4	71.4
0.3	0.5	1.3	62.5
0.4	0.5	1.1	55.6
0.5	0.5	1	50
0.6	0.5	0.9	45.5
0.7	0.5	0.83	41.7
0.8	0.5	0.77	38.5
0.9	0.5	0.7	35.7

2.4 Substrate Preparation

Before each measurement the gold quartz crystal were cleaned in concentrated nitric acid for several minutes. The glassy carbon electrode was also polished with suspensions of alumina nanoparticles (Buehler, 0.06 and 0.013 µm) on polishing pads (Struers type MD) to a mirror finish. Afterward the working electrode was rinsed with doubly distilled water, dried with clean pressurized air and immersed immediately into the electrolyte.

2.5 Electrochemical Quartz Crystal Microbalance (EQCM)

The resonance frequency, f_0, of the unloaded quartz crystals was approx. 10 MHz, and it was measured with an Advantest R3753BH network analyzer (Advantest, Tokyo, Japan) in the reflection mode. The quartz crystal was

placed at one end of the cell, and fixed between an o-ring (Viton, solution side) and a silicone gasket on the air side.

The network analyzer records the admittance spectra of the resonator near its resonance frequency. The admittance spectra were transferred to a computer via a GPIB card and fitted with a Lorentzian [96, 101]. The connection between the electrochemical cell and the network analyzer was made by a pi network adapter (PIC-001, Advantest, Japan) and a decoupling device consisting of a capacity, $C = 0.1\,\mu F$, and an inductance, $L = 1\,mH$, to decouple the high and the low frequency signals of the quartz [96, 101]. The device provides information on the resonance frequency of the quartz crystal and on its damping, which is expressed as the value of the full width at half maximum (FWHM) of the resonance curve.

The shift of frequency gives informations about the mass deposited on the quartz, while the FWHM shift provides informations about the damping of the quartz [96, 101] and also about the surface roughness of the deposited layer. Since the adsorption of oligomers might determine porous layers, a accurate monitoring of the damping of the quartz is necessary. An interpretation of the EQCM data by means of Eq. 6 is meaningful only if the frequency shift is higher than the FHWM [131].

The damping shift, dw, during electrodeposition was some hundreds of Hz while frequency shift was some tens of KHz. These results allow us to apply Eq. 6.

2.6 Layer characterization

In order to characterize the PEDOT pristine layers and PEDOT/AuNPs nanocomposite layers deposited onto solid substrates, different surface characterization techniques, were used in this work.

2.6.1 Scanning Electron Microscopy (SEM / EDX)

Scanning electron microscopy with energy dispersive X-ray spectroscopy (SEM/EDX) is a familiarly and extensively used technique for surface analysis. The images for surface morphology have high resolution and excellent depth of field and are obtained using a highly-focused, scanning (primary) electron beam. The primary electrons penetrate the surface with an energy of 0.5 – 30 kV generating secondary electrons. The intensity of these secondary electrons is ruled by the surface topography of the sample. Thus the image of the surface can be obtained by measuring secondary electron intensity as a function depending on the position of the scanning primary electron beam. High resolution can be achieved because it is possible to focus the primary electron beam to a very small spot, smaller than 10 nm. High sensitivity to the components smaller than 5 nm, as nanoparticles can be, is achieved by using primary electron beam with an energy of < 1 kV.

SEM combined with by X-ray analysis, is a fast, cheap, and non-destructive technique for surface characterization. More details regarding the SEM technique were already reported in literature [215].

In the present study a SEM model Hitachi S-4800 , was used because is capable of imaging surfaces of metals, dielectrics, resists and other polymers, PEDOT, PEDOT/AuNPs, in the present work.

2.6.2 Glow Discharge Optical Emission Spectroscopy (GD-OES)

The Glow Discharge Optical Emission Spectroscopy (GD-OES) analysis has been performed with a GDA 750 system from SPEC-TRUMA ANALYTIK GmbH, in order to check the distribution of the Au film deposited on the PEDOT layer. For these measurements, PEDOT/AuNPs nanocomposite layers were deposited on glassy carbon electrodes, under the same experimental condition as those used for the EQCM experiments. For depth profiling was used an anod RF-source with 2.5 mm diameter, in constant potential–current mode at550 V and 60 mA respectively [29].

2.6.3 Laser profilometer

The topography of polymer layer was measured my means of laser profilometry (UBM, type UBC 14, UBM Messtechnik GmbH) in order to quantify the surface roughness. Using a raster scan, the Profilometer can give 2D and 3D data about the sample surface. The platform has a video microscope which extends the profilometer applications into the realm of surface microscopy.

The PEDOT layers for profilometer analyses were deposited on gold electrodes used on EQCM experiments.

2.7 Particle-Characterization

2.7.1 Zeta Potential Measurement

The zeta potential (ζ) of the gold nanoparticles was determined by measuring the mobility of charged particles from colloidal solution under the influence of the gradient of the electric field [216, 217]. ζ potential is defined as the

difference of potential between the medium where the particles are dispersed and the layer of liquid nearest to the particles surfaces. [217].

The zeta potential values indicate the stability of colloidal dispersions, the degree of electrostatic repulsion between charged particles from the solution. For high zeta potential the small particles are stable and remain dispersed in the solution. When the potential is small, attractive forces can become stronger than the repulsion one and in this case the colloidal particles flocculate. It can be concluded that colloids with high zeta potential are stable while colloids with low zeta potentials can easily coagulate or flocculate as it is presented in the Table 3 [217].

Table 3 The stability of particles with respect of zeta potential values [217]

Zeta potential / mV	Stability behavior of the colloidal solutions
from 0 to ±5,	Rapid coagulation or flocculation
from ±10 to ±30	Incipient instability
from ±30 to ±40	Moderate stability
from ±40 to ±60	Good stability
more than ±61	Excellent stability

The instrument used in this work is to measure the ζ potential and size of nanoparticles is a Zetasizer Nano (Malvern Instruments, Herrenberg), with a 633 nm laser which is used to illuminate the particles from colloidal solution. Any movement of particles during the measurement will cause a fluctuation of the scattered light, called Doppler frequency shift. This shift of frequency, Doppler shift, is used to calculate the mobility of the particles under the

influence of an applied electric field. The mobility is determined by comparing the shift of frequency between the scattered light and the incident light, which is the reference beam [217]. If the studied particles are not electrical conductive, but with a double layer comparable with the diameter of particles, than the Smoluchowski formula can be used to calculate the ζ-potential [217]. The Smoluchowski formula applies to colloidal solutions for particles with any shape and any concentration [217].

The ζ-potential and zeta size of the gold nanoparticles were determined in diluted electrolyte in the pH range between 2 and 9. The pH was adjusted with HCl or NaOH. This dilution procedure is necessary to adjust the ionic strength of the solution to the requirements of the zeta potential measurement (see 3.1.1).

2.7.2 Transmission electron microscopy (TEM)

TEM is a technique that uses a beam of electrons which interact with the specimen as it passes through. Due to this interaction an image of analyzed sample can be obtained. This image is magnified and focused onto a fluorescent screen [218]. TEM device are able of imaging at a higher resolution than light microscopes, due to the de Broglie wavelength of electrons. This technique give us the possibility to analyze details like single column of atoms which is thousands of time smaller than the smallest object studied with a light microscope [218].

Electrons are generated in an electron microscope by a filament, which usually is a tungsten filament, during a process named thermionic emission [218]. The formed electrons are then accelerated in an electric field by applying a constant

potential and focused onto the sample by the electrostatic and electromagnetic lenses [218].

TEM technique was used to determine the size of AuNPs (see 3.1.1).

2.7.3 Differential Centrifugal Sedimentation (DCS)

DCS or analytical centrifugation is suitable for high resolution particle size characterization from 0.002 μm to 50 μm, depending on the density of particles. The particles size distribution is measured using a spinning disc with a sucrose gradient to separate particles according to their size, and the system can easily separate particles with a difference in size at least 2-5%. Sedimentation of particles in a fluid is used to characterize the particles size distribution. Stokes' law (Eq. 19) is used to determine an unknown distribution of spherical particle sizes by measuring the moving time required for the particles to traverse a known distance in a fluid with a known viscosity and density [219].

$$D = \sqrt{\frac{18\eta ln(R_f/R_i)}{(\rho_p - \rho_f)\omega^2 t}}$$
Eq. 19

In Eq. 19 D is the particle diameter, η is the fluid viscosity, R_f is the final radius of rotation, R_i is the initial radius of rotation, ϱ_p is particle density, ϱ_f is the fluid density ω is the rotational velocity, t is the time required to sediment from R_i to R_f.

Detailed description of the DCS can be found in [219].

2.7.4 UV-Vis spectroscopy

UV-Vis spectroscopy is another method used to characterize nanoparticles. Nanoparticles have optical properties that are sensitive to size, shape, agglomeration, and concentration changes of particles. These interesting optical

properties of metal nanoparticles are due to the oscillations of electrons from the conduction band [220]. The changes which appear in optical properties influence the refractive index near the surface of nanoparticles, making possible to characterize nanomaterials using UV-Vis spectroscopy technique. UV-Vis spectroscopy is a fast and easy technique for particles characterization from colloidal suspensions (see 3.1.1) [220].

Molecules that contain π-electrons or free electrons are able to absorb the ultraviolet or visible light therefore the absorbed energy will excite the electrons [220]. The excitation of electrons is proportional with the wavelength of absorbed light, the longer the wavelength of light which it can be absorbed, the higher excitation of electrons.

The spectroscopy method is often used in a quantitative way to determine concentrations of an absorbing species in solution, using the Beer-Lambert law (Eq. 20) [220]:

$$A = log_{10}(I_0/I) = \varepsilon c L \qquad \text{Eq. 20}$$

In Eq. 20 A is the measured absorbance, in Absorbance Units (AU), I_0 is the intensity of the incident light , I is the transmitted intensity, ε is the molar absorptivity, with the unit $1/M * cm$, c is the concentration of the absorbing species and L is the path length through the sample [220].

3 Results and Discussions

This section is dedicated to PEDOT and PEDOT nanocomposite layers electrodeposition from 8 mM EDOT+1 mM SDS++0.2 M LiClO$_4$ aqueous solution. The synthesized gold nanoparticles (see 2.2) were characterized using different techniques (3.1.1). PEDOT layers were obtained using several methods: potentiodynamic (see 3.2.1) potentiostatic (3.2.2), and potentiostatic pulse (3.2.3), in order to compare the morphology and layers properties, as electrocatalytic activity for neurotransmitter detection. Afterwards these polymers were used as matrix to deposit gold nanoparticles (AuNPs) by electroless deposition (see 3.3.2). The aim was to synthesize a PEDOT/AuNP nanocomposite layers with very good electrocatalytic properties for electroanalytical application as biosensors (see 3.4).

3.1 Synthesis and characterization of gold nanoparticles

The Au nanoparticles, AuNPs, with a diameter of ca. 20 nm were prepared according to Turkevich method (see 2.2) (Fig. 10) [214].
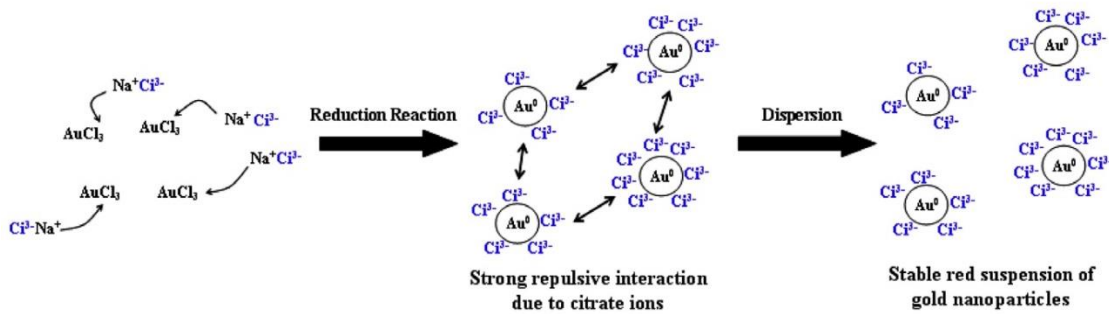
Fig. 10 Schematic synthesis of gold colloids with a diameter 20 nm [214]

44

3.1.1 Techniques to characterize gold nanoparticles

Transmission electron microscopy was used to characterize the prepared gold nanoparticles. The size distribution of the AuNPs was approx. 20 nm (Fig. 11, Fig. 12).
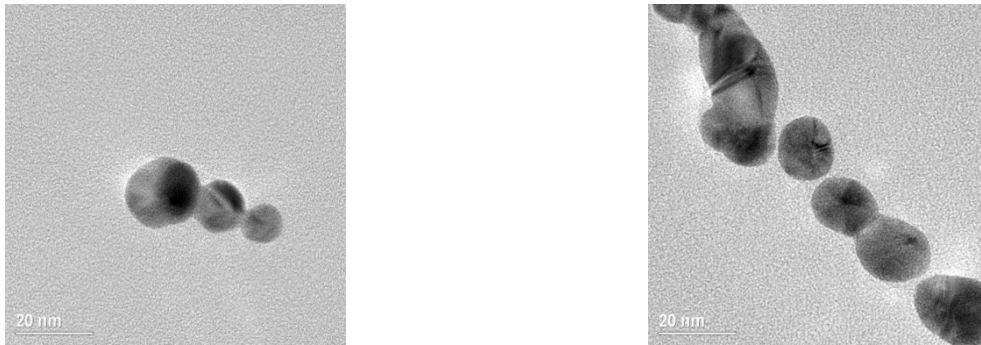
Fig. 11 TEM images of AuNPs
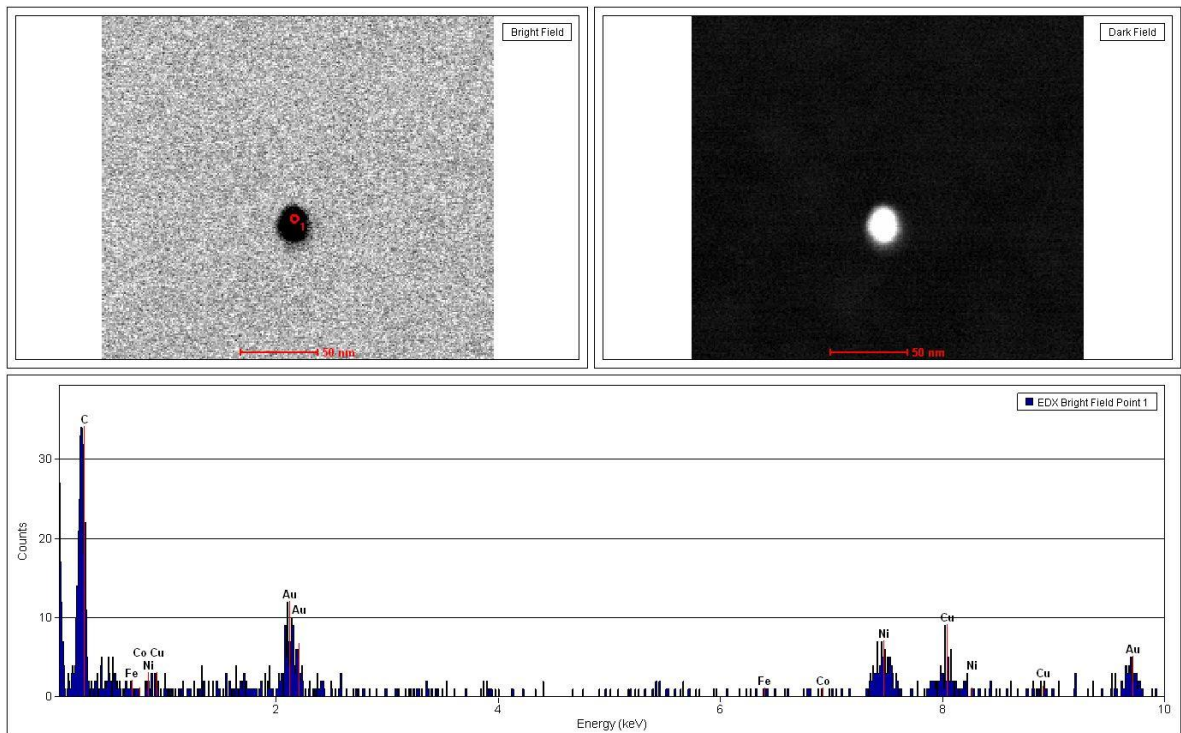
Fig. 12 TEM and EDX analysis of AuNPs

Results and Discussions

Differential Centrifugal Sedimentation data confirm that for the colloidal solution used in this work the particles diameter was approx. 19.2 nm (Fig. 13).
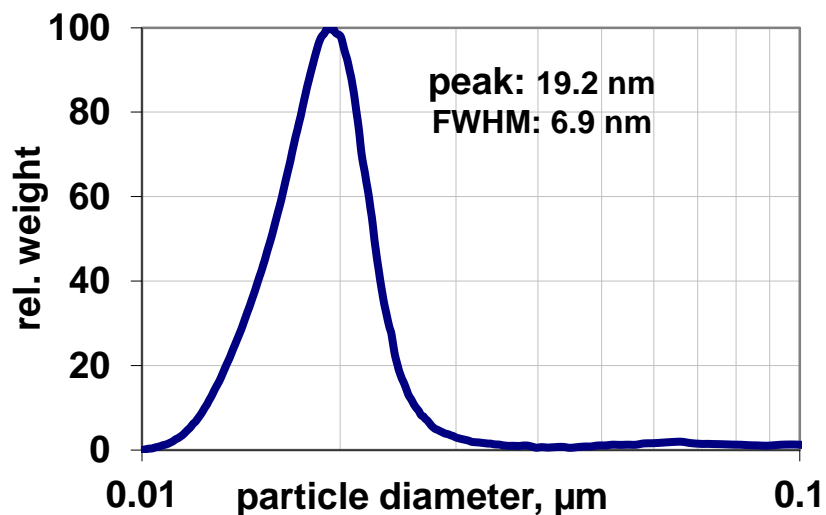
Fig. 13 The size of AuNPs, using DCS measurement

UV-Vis spectroscopy was also used to characterize nanoparticles due to their optical properties. It can be seen that the maximum absorption wavelength increases with increasing size of the AuNPs. In diluted solution the particles are better dispersed and they have smaller size compared to those in concentrated solution in which the particles form clusters (Fig. 14). The position of absorption peak of gold nanoparticles from colloidal solution does not give any quantitative information about the size of nanoparticles, because it is not possible to observe distinguished peaks according to the sizes of particles from colloidal solution.

UV/Vis spectra of Au NP
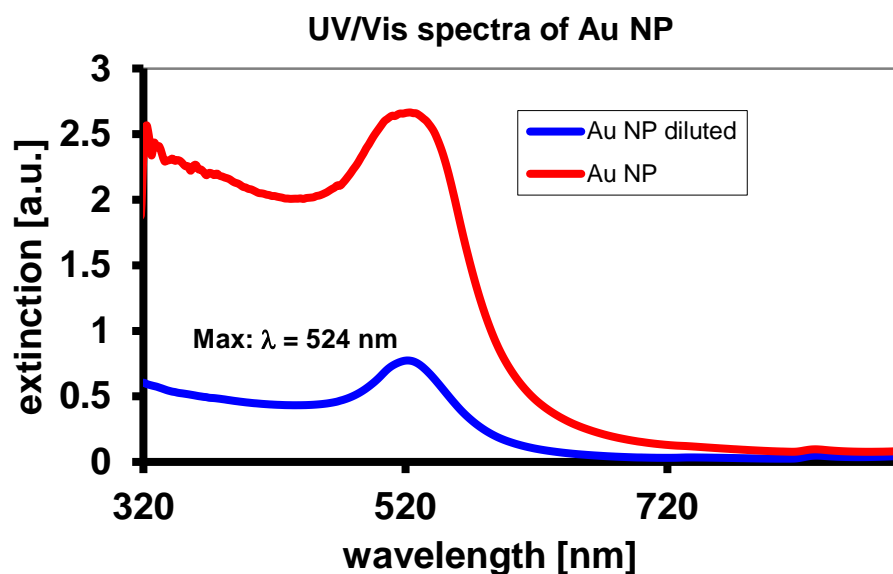
Fig. 14 UV-Vis absorption spectrum of gold colloidal solution

Dynamic light scattering (DLS) was another technique used to verify the results from TEM and DCS. This method can be applied to measure narrow particle size distributions especially in the range of 2–500 nm. Before the measurement, the colloid was diluted (1/30, v/v in water). The sample was loaded into a quartz microcuvette, and five measurements were performed, for which the mean result was recorded (Fig. 15 a). The obtained data are similar with DCS measurements and a narrow distribution around 20 nm was measured.

With the same device *ζ-potential measurements* of the diluted AuNPs solution were carried out in solutions with different acidity (Fig. 15 b). The pH of the solutions was adjusted by 0.25 mol/L HCl or 0.25 mol/L NaOH. It is found that at pH >6 the AuNPs have a constant negative ζ -potential value close to −36 mV and thus a moderate stability should be expected in neutral solutions. The negative ζ-potential is due to the adsorption of negative citrate ions to the gold surface [216].
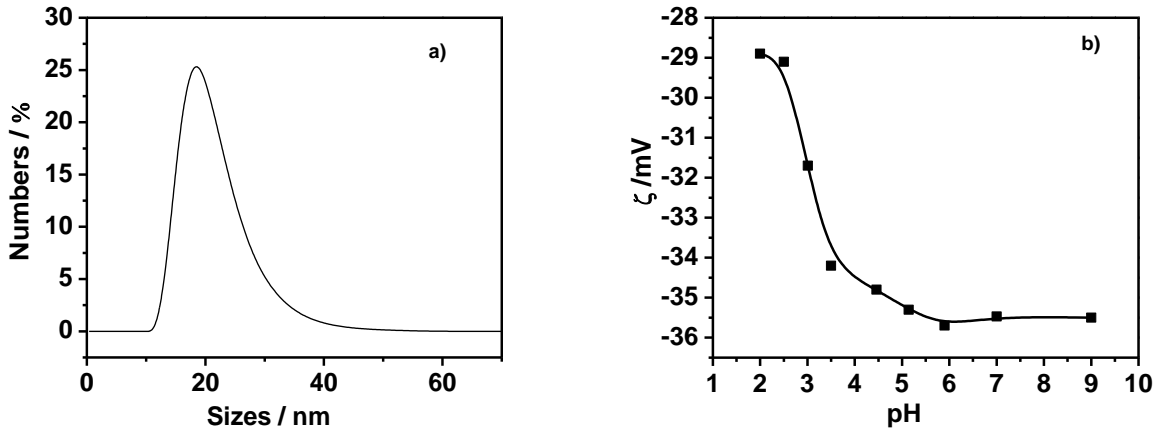
Fig. 15 The dynamic light scattering measurements for size (a) and ζ –potential (b)

The values of the ζ –potential for a pH >6 are properly to determine repulsive interaction between particles avoiding clusters formation. For a solution prepared by 24 h before to be used, with the pH < 5.0, the gold nanoparticles agglomerate due to an adsorption of H^+ on their surface and the attractive van der Waals interaction enhance (Fig. 16).
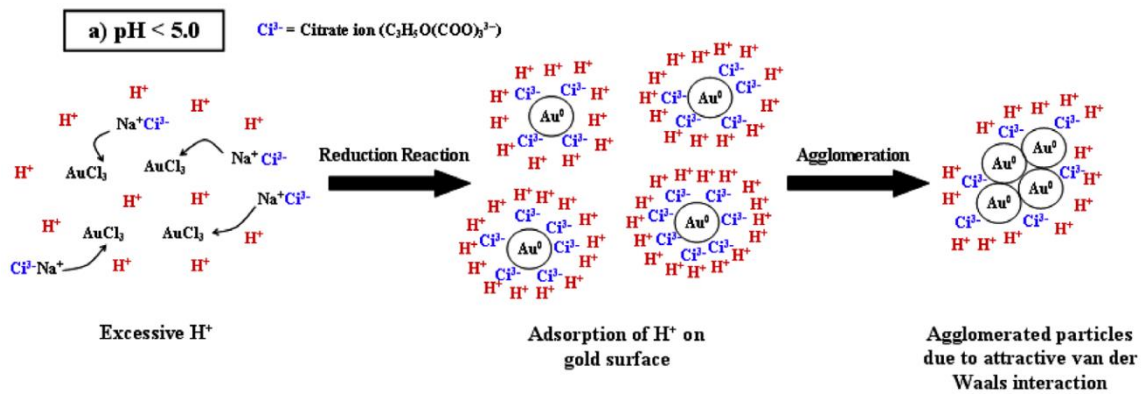
Fig. 16 The pH influence on AuNP stability [216]

The measurements were repeated after six month and confirmed the stability of gold colloidal solution. The old AuNPs solution had the same characteristics as a fresh one.

3.2 Electrochemical deposition of PEDOT layer

Different electrochemical techniques were used to deposit polymer layers in order to find the proper one for the aim of this work.

3.2.1 Potentiodynamic Deposition

Cyclic voltammograms were recorded between -0.3 and 1.3 V vs. Ag/AgCl in aqueous solution which contains 1 mM SDS as surfactant (Fig. 17). One can see that the current density increases strongly above approximately 0.8 V, a fact that indicates the oxidation of the monomer. The current density further increased with increasing cycle number. This is due to the increase of the active area of the electrode and the increase of layer thickness, with increasing cycle number

(Fig. 17). The increase of layer thickness is correlated with the mass increase, which can be calculated using the QCM (Fig. 18). The cathodic branch does not present significant variations, a capacitive behavior has been seen in the potential range from -0.3 V to ca. 0.8 V. The deposited mass at the beginning of the experiment has zero value as one can see in Fig. 18 proving that at that point no mass was deposited on crystal surface. After the first cycle a thin layer was formed on electrode surface and due to this the second cycle started from the point which corresponds to an already deposited mass value by 13.5 $\mu g/cm^2$. During the EQCM deposition the damping variation, Δw, was approx. 450 Hz, showing a uniform layer.
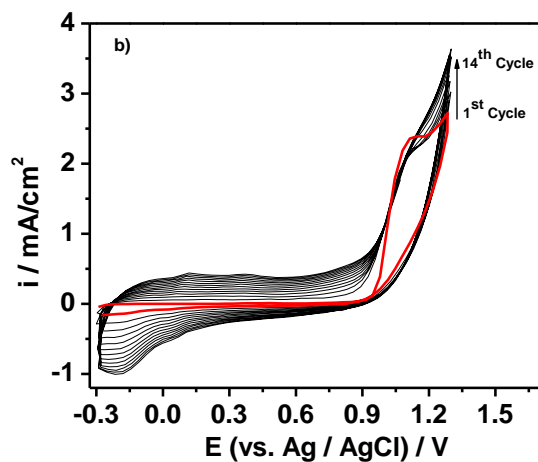
Fig. 17 Potentiodynamic deposition of PEDOT layer, from aqueous solution / 8 mM EDOT+1 mM SDS+0.2 M $LiClO_4$, ν=50 mV/s, at room temperature
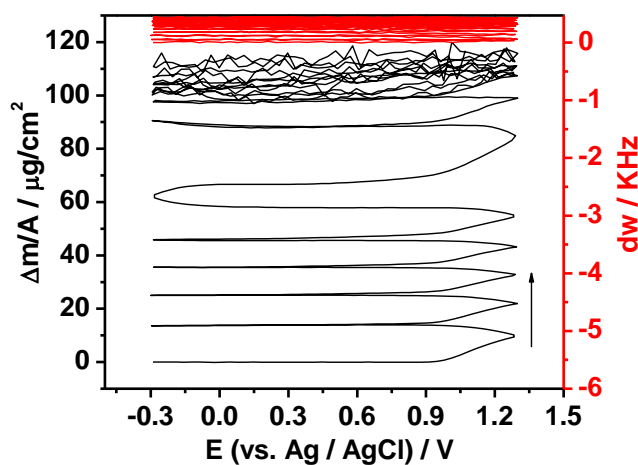
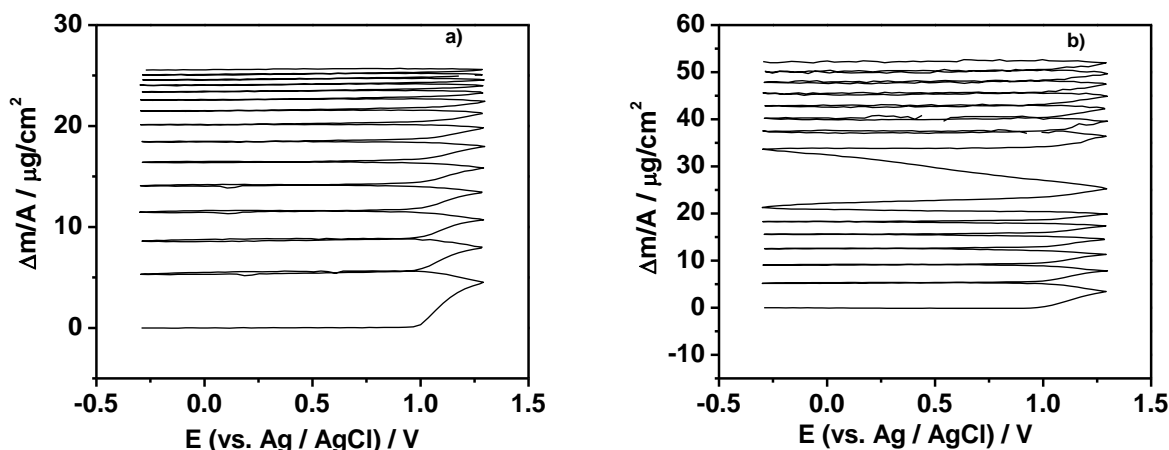Fig. 18 The areal mass density and damping changes during cyclic voltammetry, for PEDOT deposition using EQCM technique, from aqueous solution / 8 mM EDOT+1 mM SDS+0.2 M $LiClO_4$, ν=50 mV/s, at room temperature

After the polymerization starts, the next step is the deposition, which includes nucleation and growth. For linear growth of polymer, the relative growth rate per cycle, v_g, can be calculated according to Eq. 21 [111]:

$$v_g = k \frac{i_{pa}^{pol}}{(n-1)}$$
<div align="right">Eq. 21</div>

In Eq. 21 k is the proportionality constant, i_{pa}^{pol} is the anodic peak current of the polymer oxidation and n is the the cycle number

A typical phenomenon observed during the first voltammetric cycle of an electropolymerization experiment is so-called "nucleation loop". It was first described by Pletcher and it is characterized by a maximum for current value before the switch of potential [15]. (Fig. 17) This loop involves a crossing effect that appears in all voltammograms on the reverse sweep of the first electropolymerization cycle, if this scan reversal lies closely behind the peak potential [221]. This has been considered as the beginning of the nucleation process of the polymer. A strong argument for this assumption is the fact that this effect always appears in voltammetric experiments with freshly polished electrodes and only in the reverse sweep of the first cycle [221].

Heinze et, all have studied also this phenomenon [221]. The electrochemical data proved that the loop effect is based on a homogeneous reaction from an intermediate Oligo^{n+} with the starting monomer Mon to $\text{Oligo}^{(n-1)+}$ and Mon^+ (Fig. 19) [111, 221]. Heinze explained that it is an autocatalytic mechanism, which helps the oxidation of the monomer at the beginning of the process. The charged oligomers, Oligo^{n+}, of thiophene are generated during the first anodic oxidation cycle. They act as a redox mediator for the starting monomer [111, 221].
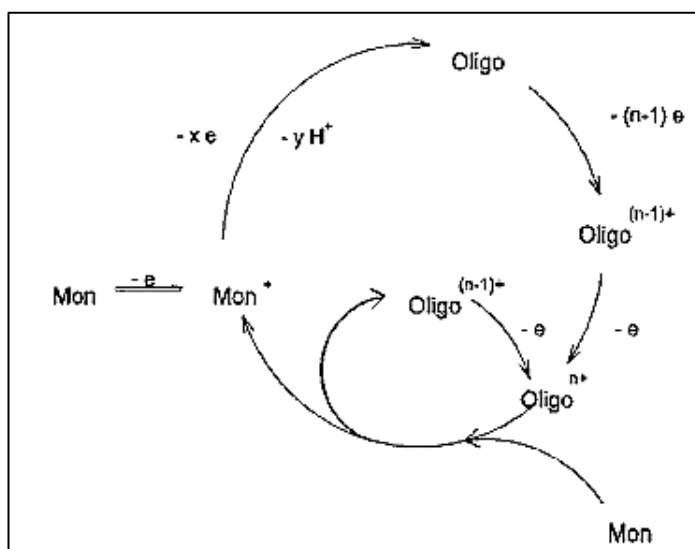
Fig. 19 General reaction scheme of the autocatalytic oxidation of EDOT during potentiodynamic polymerization [111, 221]

The oxidation potential of EDOT monomer in acetonitrile, according with literature [111], was found at 1.08 V, with approx. 0.28 V higher than in aqueous solution. This significant decrease of potential in aqueous medium relative to organic solution can be attributed to the anionic surfactant, SDS, which creates hydrophobic and hydrophilic regions at the metal/ solution interface, determining an electrocatalytic effect [213].

First were performed potentiodynamic experiments using EQCM technique from electrolytes with different SDS concentration: 1 mM, 4 mM and 2 mM (Fig. 18, Fig. 20).

Fig. 20 The changes of mass density during cyclic voltammetry, for PEDOT deposition using EQCM technique: a) from aqueous solution / 8 mM EDOT+4 mM SDS+0.2 M LiClO$_4$ and b) from aqueous solution / 8 mM EDOT+2 mM SDS+0.2 M LiClO$_4$. The experiments were performed at a scan rate of 50 mV/s, at room temperature

An explanation for the decrease of polymerization rate of EDOT with the increase of concentration of SDS in solution can be the hydrophobic interactions between the dodecyl aliphatic tails and already polymerized PEDOT chains that partially obstruct the effective doping and further growth of PEDOT [213]. We performed several experiments from electrolytes with concentration of SDS above and under the critical micellar concentration (2 mM in 0.1 M LiClO$_4$ aqueous solution).

The data for the frequency shift and the normalized frequency obtained during the polymerization from electrolytes with different concentration of SDS are shown in Fig. 21.

The polymerization process is characterized by a sharp decrease in the frequency shift with increasing of polymerization charge, Q$_{poly}$. For all three types of layers the polymerization is characterized by an almost constant

frequency shift per polymerization charge indicating a homogeneous growth and the incorporation of one and the same amount of dopant species and solvent molecules in this stage of polymer's growth.
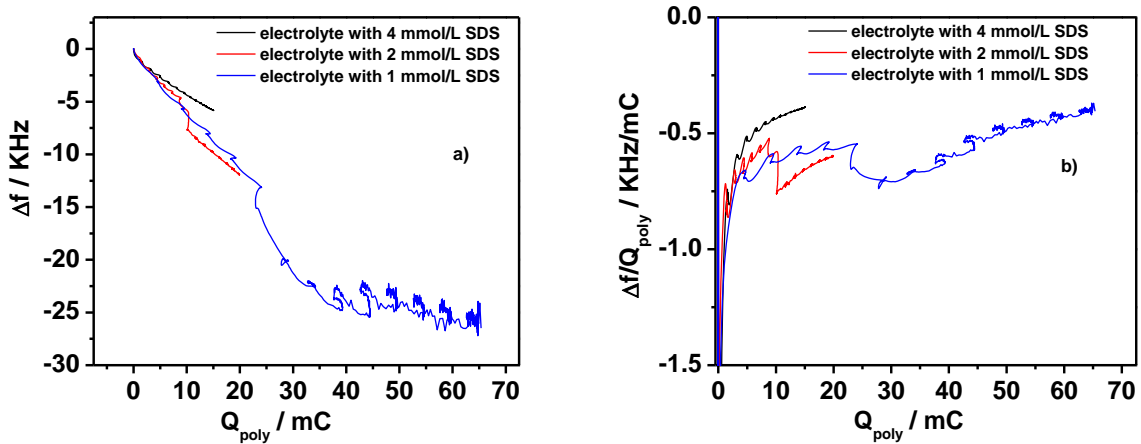
Fig. 21 Frequency change (a) and normalized frequency change (b) in dependence of the polymerization charge for PEDOT layers obtained in aqueous solution containing 4, 2 and 1 mmol/L SDS.

The Δf/Q_{poly} constant values were calculated and compared as follows: 4 mM SDS (0.44 kHz/mC) < 2 mM (5.55 kHz/mC) < 1 mM (0.62 kHz/mC). The normalized frequency to polymerization charge for a deposition from an electrolyte containing micellar SDS was lower than from solution containing submicellar SDS concentration (1 mM SDS).

The data for the damping show high differences in the rigidity of the PEDOT layers synthesized in the presence of different concentrations of SDS (Fig. 22). For a PEDOT layer synthesized from submicellar solution (1 mM SDS) the w_0/w values is above 0.90 during the entire polymerization process this indicating a high rigidity of polymer layer. However the PEDOT layers synthesized from micellar solutions (2 mM SDS and 4 mM SDS) are

characterized by a rapid and strong decrease in the normalized damping showing strong viscoelastic properties.
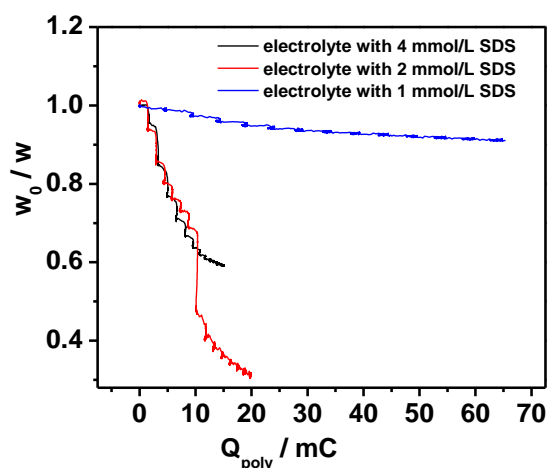
Fig. 22 Normalized damping in dependence of the polymerization charge for PEDOT layers obtained in aqueous solutions containing 1, 2, 4, mmol/L SDS.

A porous PEDOT film was obtained after 14 cycles which grew steadily with the number of cycles, as one can see from SEM images (Fig. 23).
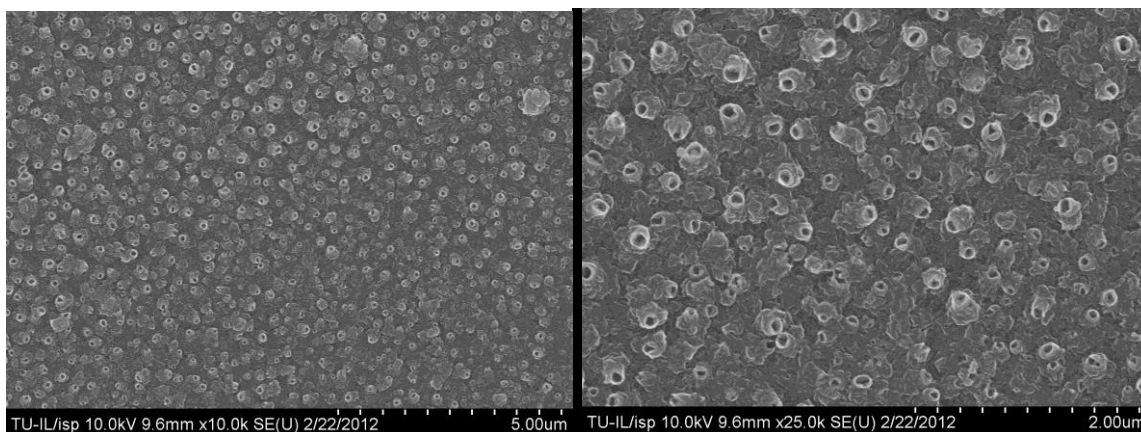
Fig. 23 SEM images of pristine PEDOT films surface obtained by potentiodynamic synthesis, after 14 cycles between -0.3 V and 1.3 V (vs. Ag/AgCl). The electrolyte consists of: 8 mM EDOT+1 mM SDS+0.2 M LiClO$_4$, at room temperature.

Based on the results obtained in the potentiodynamic experiments, the potential for the direct plating (potentiostatic deposition) (3.2.2), as well as the anodic and the cathodic potentials of the pulse sequences were chosen (see 3.2.3). All experiments from 3.2.2 and 3.2.3 were performed from aqueous electrolytes which contain SDS in submicellar concentration (1 mM SDS).

3.2.2 Potentiostatic deposition

Using potentiostatic technique, PEDOT was deposited at 0.9 V in order to avoid the polymer overoxidation (Fig. 24) [111]. The initial spike of current corresponds to the charging of the double layer, as in the beginning a lower potential was applied (0.1 V, for 30 s) and this potential is not enough for monomer oxidation [111]. After the charging of double layer, the current density decreases and also during this period monomers diffuse from the solution to the electrode surface. After the oxidation, the monomers return to the solution where both the coupling with radical cations and the oligomerization process take place [111]. When the oligomers are formed in front of the electrode, oligomer clusters start to deposit onto the electrode surface generating the first polymer nuclei. Thereafter, it was a slow increase of current corresponding to the formation of PEDOT nuclei followed by the growth of the polymer. The relationship between current and time depends on electrocrystallization mechanisms is in accordance with literature reports [111].
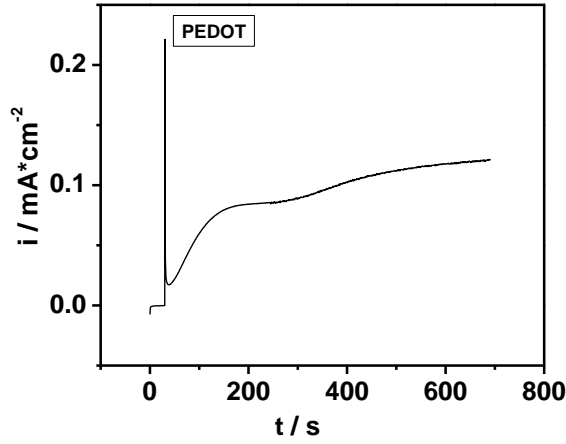
Fig. 24 Formation of PEDOT layer using the potentiostatic method at 0.9 V, from the electrolyte: 8 mM EDOT+1 mM SDS+0.2 M LiClO$_4$, at room temperature.

The influence of polymerization potential is presented in Fig. 25 where the changes of current during the polymerization to 0.82–0.98 V are shown. After a short rise, the current decreases to a constant value at which polymerization proceeds. Fig. 26 shows the deposited mass calculated from the current according to following equation (Eq. 22) [138]:

$$m(t) = \frac{M_{mono} + \gamma m_{ClO_4}}{(2+\gamma)F} \int_0^t I(\xi) d\xi \qquad \text{Eq. 22}$$

In Eq. 22 it is assumed that the addition of one molar equivalent of monomer, with a mass M_{mono}=140 g mol^{-1}, released two electron equivalents after each covalent bond is formed and it is followed by addition of γ molar equivalents of doping anion ClO_4^- with molar mass m_{ClO_4}. According to literature the doping level of PEDOT films obtain from aqueous solution is γ=0.3 [138].
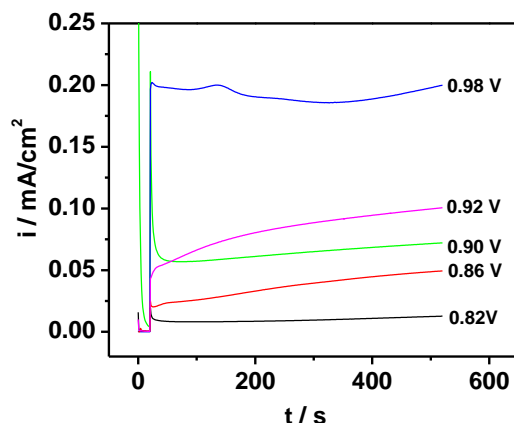
Fig. 25 Electropolymerization current density versus time. The electrolyte consists of: 8 mM EDOT+1 mM SDS+0.2 M LiClO$_4$, at room temperature.
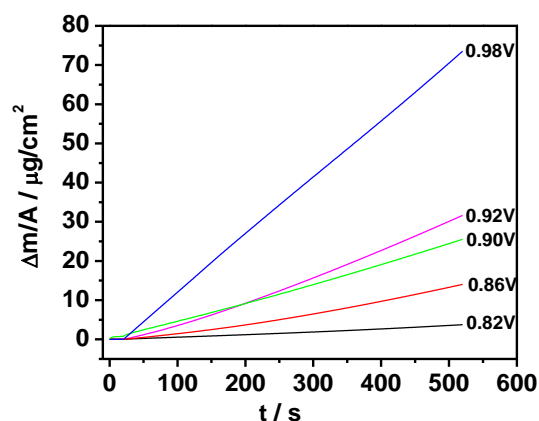
Fig. 26 Polymer deposited mass per unit of surface versus time. The data were calculated according to Eq. 22

Fig. 26 shows that for a low polymerization potential, 0.82 V, the deposited mass is very small because at low potentials, the oligomers are weakly charged, and consequently, the electropolymerization may end at an oligomeric level. The high oxidation potentials involve the formation of highly charged and reactive oligomers which lead to defects and to the formation of cross-linked materials [111].
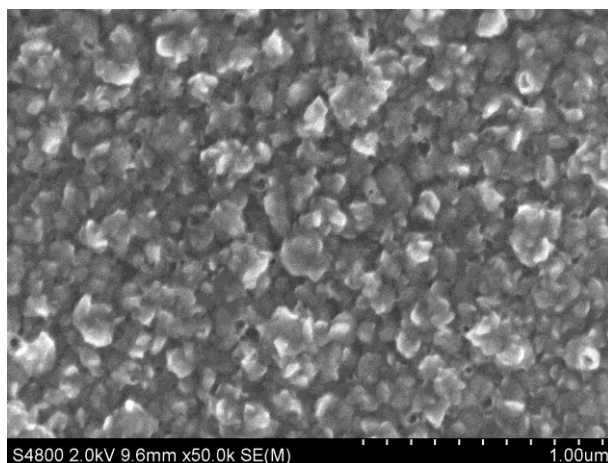
Fig. 27 SEM images of PEDOT layer using the potentiostatic method at 0.9 V (vs. Ag / AgCl), from the electrolyte consists of: 8 mM EDOT+1 mM SDS+0.2 M $LiClO_4$, at room temperature.

The SEM image for a polymer synthesized at 0.9 V shows a compact layer with a rough surface (Fig. 27). The damping variation for QCM data was approx. 400 Hz (Fig. 28).
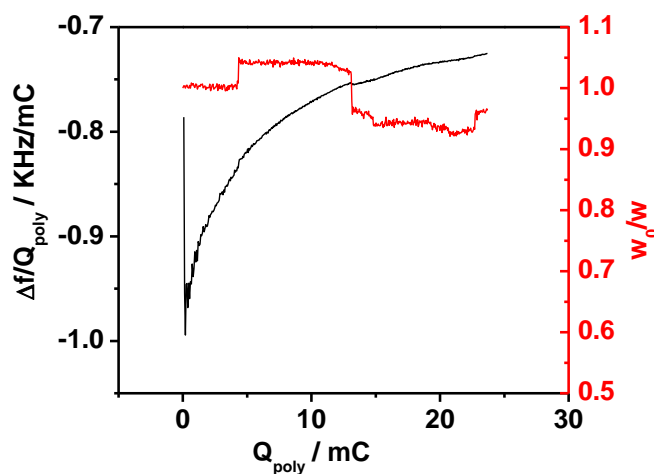
Fig. 28 The normalized frequency change and the normalized damping in dependence of the polymerization charge for PEDOT layers obtained in aqueous solution 8 mM EDOT+1 mM SDS+0.2 M $LiClO_4$, at room temperature. The polymerization potential was 0.9 V (vs. Ag / AgCl).

The QCM data for a pristine layer polymerized at 0.9 V show a rigid layer because the value for normalized damping is above 0.9 (Fig. 28). One explanation can be that SDS acts as dopant competing with ClO_4^- anions. The incorporation of SDS anions increases the rigidity but makes the PEDOT layer to act as a membrane with selectivity for cations (see 3.4).

3.2.3 Potentiostatic pulse deposition

In the pulse plating experiments, the anodic and the cathodic pulses were varied so that duty cycles between 20 and 60% were obtained (see 2.3, Table 2). The duty cycle is defined by the ratio between the duration of the "on" pulse (which corresponds to the time when the deposits grow due to an applied anodic potenial) and the total duration of a pulse sequence. The total number of "on" pulses was chosen such that a growth time equivalent of 400 s was reached. The following pulse parameters were chosen after some preliminary tests: pulse "on" time, which is the anodic pulse duration (t_a) where the oxidation of the monomer and larger formation occur, was 0.5 s (see 3.2.3.1). Pulse "off" time, cathodic pulse duration (t_c), where the reduction of the layer occurs, was 0.7 s (see 3.2.3.2), at the cathodic potential, E_c=0.3 V (see 3.2.3.3). The total number of pulses was 800.

After synthesis, the polymer-coated electrodes were transferred to 0.5 M H_2SO_4 (pH=0.8) aqueous solution for measuring their voltammetric behavior in the potential window from −0.4 to 0.8 V at a scan rate of 100 mV s^{-1} (see 3.2.3.1). The film morphology was studied by SEM (3.2.4.4).

3.2.3.1 The influence of anodic potential, E_a, on electrodeposition

Different PEDOT layers were prepared for these experiments, where the duty cycle and the anodic potential pulse were varied. The cathodic potential, E_c,

60

was constant at 0.3 V. Two values of the anodic potential, E_a, were investigated: 0.9 V and 1 V (Fig. 29). The reduction charge of the films, Q_{red}, was calculated from the CV data in 0.5 M H_2SO_4 solution between -0.3 V and 0.8 V, with a scan rate of 100 mV/s: the integration of the reduction part yields the charge (Fig. 30). One can notice in Fig. 29 that when E_a was 1.0 V, no significant variations of the reduction charges of the CP with the duty cycle were observed. However, for a polymerization potential by 0.9 V, a clear decreasing tendency of the reduction charge with decreasing anodic pulse duration was observed. The charge can be correlated with the quantity of electropolymerized material [213]. Thus it can be concluded that more material is electropolymerized when the anodic potential limit was 1.0 V (Fig. 29). However, when high anodic potentials are chosen, the film can be easily over-oxidized. In order to avoid this, in the following measurements an anodic potential of 0.9 V and an anodic duration of 0.5 s were chosen.
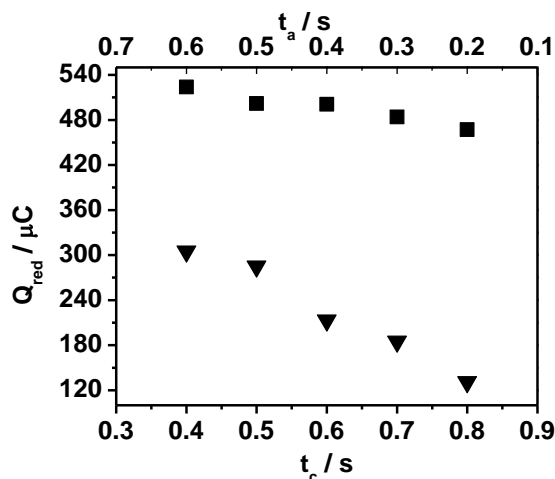
Fig. 29 Redox charges of PEDOT films grown by the pulse potentiostatic method with $E_a = 1$ V (■) and $E_a = 0.9$ V (▼), for $E_c = 0.3$ V, and different pulses durations, t_c-cathodic time and t_a-anodic time. The electrolyte consists of: 8 mM EDOT+1 mM SDS+0.2 M $LiClO_4$, at room temperature.
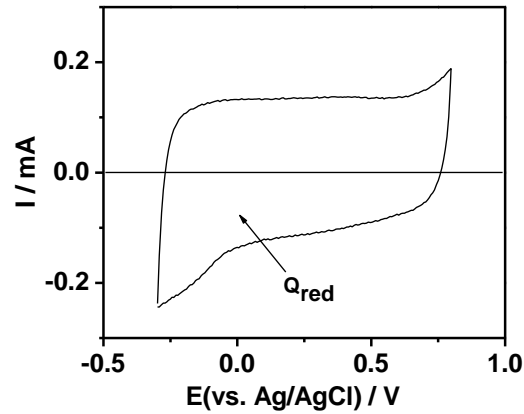
Fig. 30 The CV recorded for 0.5 M H$_2$SO$_4$ after polymer synthesis at a scan rate of 100mV/s at room temperature. The integration of the reduction part yields the charge, Q$_{red}$.

3.2.3.2 The influence of the cathodic time, t_c, on electrodeposition

The effect of the cathodic time, t_c, on the polymer layer growth was studied (Figs. 31, 32). In the experiments presented in Fig. 31 and Fig. 32 only the cathodic time duration was varied. The cathodic and anodic potentials of the pulse, as well as the anodic pulse time were kept constant at the following values: E_c = 0.3 V, E_a = 0.9 V and t_a = 0.5 s, for N=800, the total number of pulses for each experiment.

As it can be seen in Fig. 31 the ratio between Q_{ox} and Q_{pol} is highest if t_c was 0.7 s.

Q_{ox} is the sum between the oxidation charge of monomer and EDOT species which diffuse close to the electrode surface, like dimers or oligomers [2] and the oxidation charge of the already formed PEDOT film [2].

The oxidation potential of the monomer is always higher than the potential necessary for charging of oligomers or for the resulting polymer, due to that the polymer formation and oxidation take place simultaneously [2].

Q_{pol} is the polymerzation charge of PEDOT layer and it was determined by integration over all 800 pulses, which are represented by the currents versus time when the pulse potential is applied (Fig. 33).
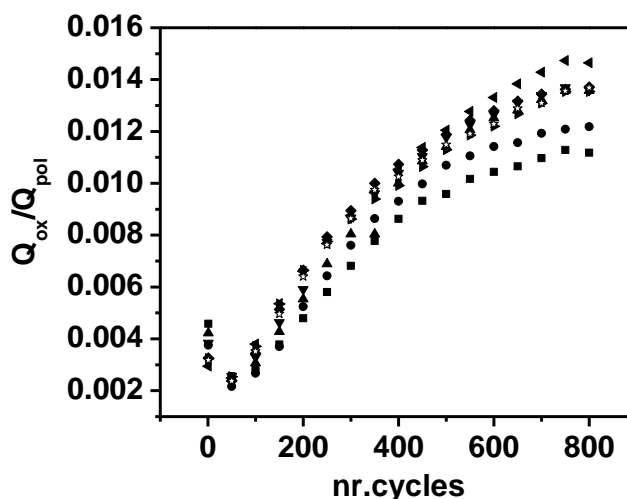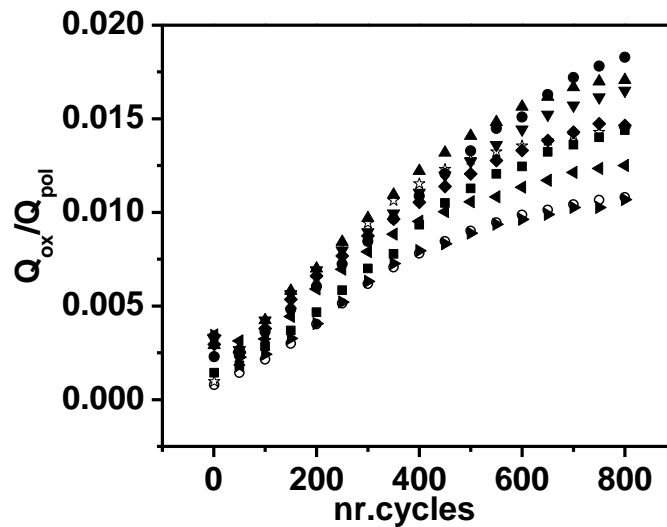

Fig. 31 The oxidation charge normalized to the polymerization charge for PEDOT layer, at E_a =0.9 V, t_a=0.5 s, E_c =0.3 V for different duration of cathodic potential [(■), t_c=0.2 s; (●) t_c=0.3 s; (▲) t_c=0.4 s; (▼) t_c=0.5 s; (◆) t_c=0.6 s; (◀) t_c=0.7 s; (▶) t_c=0.8 s; (☆) t_c=0.9 s].
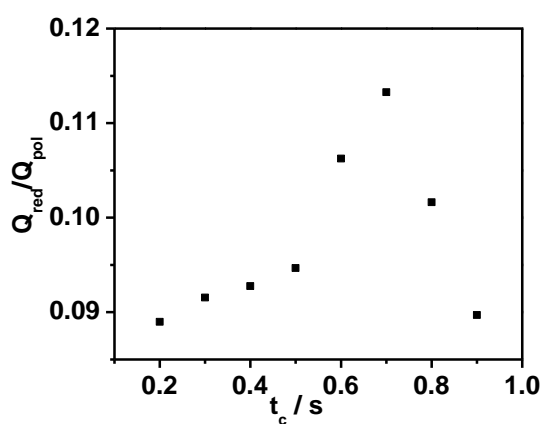
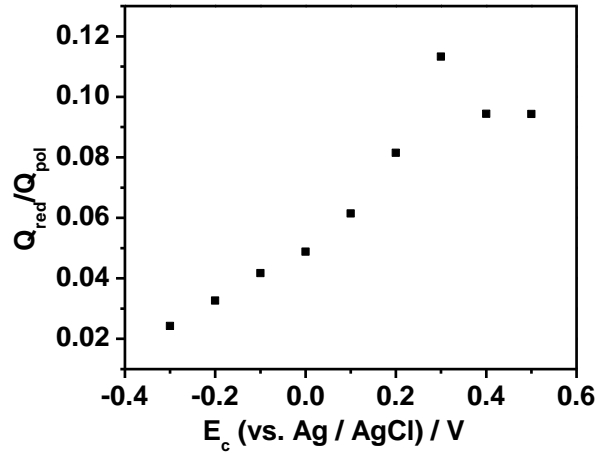Fig. 32 The ratio of the redox charges vs. the polymerization charges of PEDOT films grown by the pulse potentiostatic method with E_a = 0.9 V, t_a=0.5 s, E_c = 0.3 s and different cathodic pulse time, t_c

Results and Discussions

As it can be seen in Fig. 32 that the ratio between the reduction charge and the charge needed for electropolymerization (Q_{red}/Q_{pol}), which represents the redox activity of the PEDOT layers, was also maximal for t_c =0.7 s. The ratio Q_{red}/Q_{pol} increase sharply with the cathodic time up to 0.7 s and after words decreases with the increase of applied pulse time.
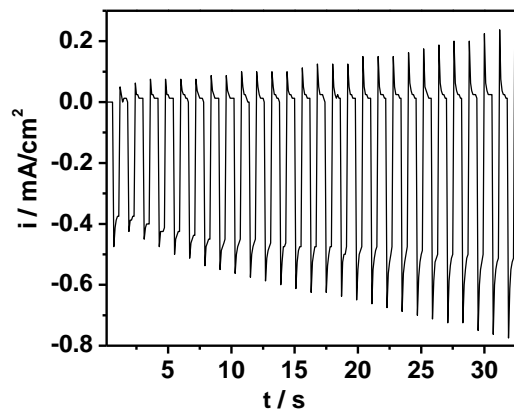
Fig. 33 Current density versus time for a sequence of potentiostatic pulse deposition of PEDOT at E_a =0.9 V, t_a=0.5 s, E_c =0.3 V, t_c=0.7 s. The integration of all the applied pulses during the deposition will give the polymerization charge, Q_{pol}. The integration of graph region which corresponds to the anodic current, when the anodic potential pulse is applied, will give the oxidation charge, Q_{ox}. The electrolyte consists of 8 mM EDOT+1 mM SDS+0.2 M LiClO$_4$, at room temperature.

Due to the intercalation of anions, the redox activity is always much smaller than unity, because some amount of anions remain trapped inside the polymer. The periodic reduction of the polymer film during the cathodic pulses creates favorable conditions for the overall growth process.

It is obvious from these results that a relatively long cathodic time is required in order to allow the relaxation of the polymer layer for the next growth step.

However, further increase of t_c above a critical limit seems to produce the opposite effect and consequently the ratio of oxidation charge to the polymerization charge decreases with further increasing of the cathodic time (Fig. 33).

3.2.3.3 The influence of cathodic potential on electrodeposition

The growth of the polymer for different cathodic potentials, but at fixed E_a (0.9 V), t_a (0.5 s) and t_c (0.7 s) was also studied. From obtained data, the corresponding electrical oxidation charge was calculated, and normalized to the polymerization charge, in order to obtain a parameter which allows us to compare the obtained results (Fig. 34).

Fig. 34 The oxidation charge normalized at polymerization charge for PEDOT layer, at E_a=0.9 V, t_a=0.5 s, t_c=0.7 s for different cathodic potentials. (O) E_c=-0.3 V; (☆) E_c=-0.2 V (■) E_c=-0.1 V; (●) E_c=0.0 V; (▲) E_c=0.1 V; (▼) E_c=0.2 V; (◆) E_c=0.3 V; (◄) E_c=0.4 V; (►) E_c=0.5 V. The electrolyte consists of: 8 mM EDOT+1 mM SDS+0.2 M LiClO$_4$, at room temperature.

Results and Discussions

According to ESCR Model, by Otero at al. [117, 118], presented in 1.4.1 it can assumed that application of an anodic overpotential to a neutral conjugated polymer provokes an expansion of the closed polymeric structure. In this case, partial oxidation takes place and anions from the solution move into the polymer. During reduction reverse processes take place. The positive charges on the polymer are neutralized and anions are expelled. Reverse conformational changes determine the shrinking of the polymer. Diffusion of the anions becomes harder if the structure closes. The compaction of the polymeric structure depends on the applied cathodic potential. This effect is stronger at more negative potentials. The closer and more packed the initial state is, the higher is the potential necessary to open the structure allowing the oxidation to begin [2].

One can notice in Fig. 34 that for the highest values of the cathodic pulses, the oxidation charge during the polymerization increases slowly with time. During the cathodic potential the polymer is reduced only for the most negatively values and in these cases in order to be again in the oxidized state, when the anodic potential is applied, more time is needed. However, in all the experiments the same anodic duration was used (t_a = 0.5 s). For the highest values of cathodic potential (0.4 V, 0.5 V) it has been found a reduced activity of polymer layers. This can be explained with the fact that the polymers remain in the oxidized state. These results prove that an intermediate relaxation period is necessary for an enhanced of polymer growth.

Fig. 35 Redox charges of PEDOT films grown by the pulse potentiostatic method with E_a=0.9 V, t_a=0.5 s, t_c=0.7 s and different cathodic pulse, E_c. The electrolyte consists of 8 mM EDOT+1 mM SDS+0.2 M LiClO$_4$, at room temperature.

Fig. 35 presents the redox activity of the PEDOT layers which has a maximum value for E_c=0.3V where upon slowly decrease with the increase of potential. According to the presented data in 3.2.3.1-3.2.3.3, the following parameters for potentiostatic pulse deposition were chosen: E_a=0.9 V, t_a=0.5 s, E_c=0.3 V t_c=0.7 s.

3.2.3.4 Electropolymerization mechanism for pulse PEDOT deposition proposed by Pandey
The potentiostatic pulse electrodeposition of PEDOT produces a layer with highly porous and fibrous morphology (see 3.3.2). According to Pandey the t_c, for the pulse technique influences the nucleation, the structure and the process of attachment of the PEDOT polymeric chains on the substrate giving it a particular morphology [222].

The growth mechanism is initiated with the formation of radicals cations [EDOT]$^{+\bullet}$ [222]. The doped state of PEDOT is obtained by anions (ClO$_4^-$ and

67

SDS⁻) and they are associated within the growing of polymer network due to presence of positive charge in π bonds of the chain. The short potential pulses influence the polymerization mechanism and the anions association process steps in the PEDOT film growth (Fig. 36) [222].
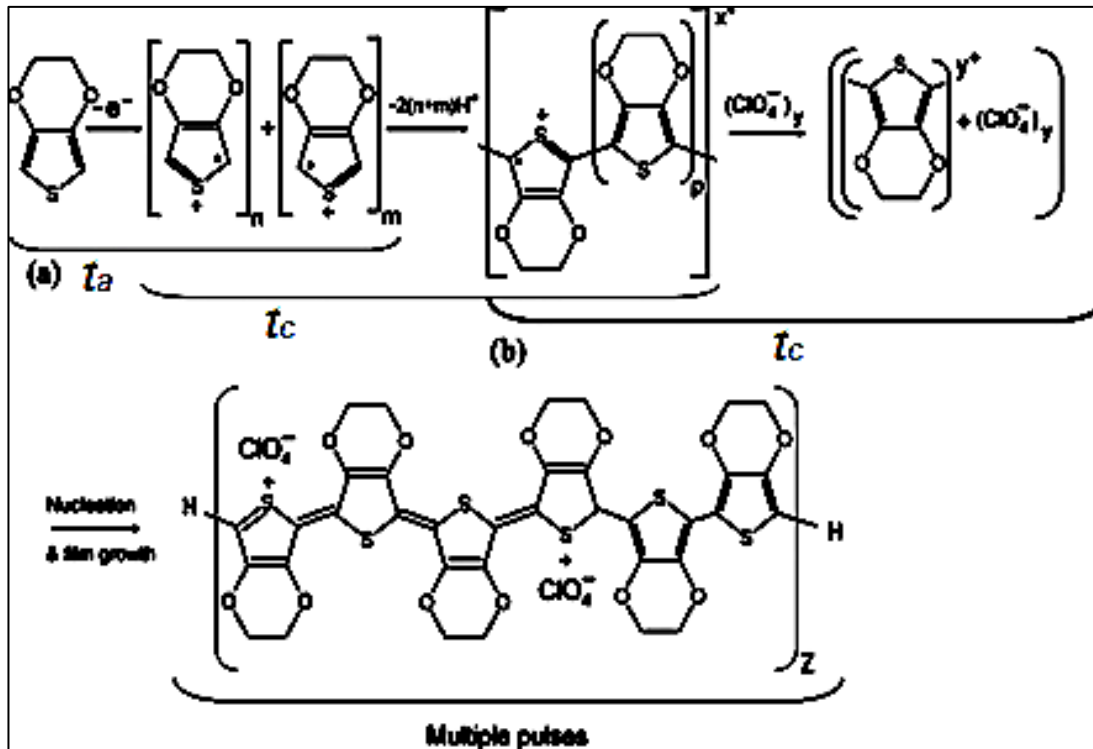
Fig. 36 Schematic presentation of mechanism for PEDOT film growth during galvanic pulse polymerization, proposed by Pandey [222].

The PEDOT oligomer chain growth is limited by the number of cation radicals formed in the anodic time because no new radicals are generated during the cathodic potential period, t_c [222]. By applying short pulses, the formed polymer has short chain oligomers which give also the specific morphology, which has been seen on SEM (3.2.4.4).

Pandey [222] calculated the radical cations life time between two consecutive pulses, assuming 100% efficiency of cations radicals at the film formation.

According to his work the life time of radical cations is approx. 2 s (Eq. 23) [222]:

$$\frac{1}{[R]_{pulse}^{+\cdot}} - \frac{1}{[R]_1^{+\cdot}} = -\alpha_\tau t \qquad \text{Eq. 23}$$

In Eq. 23 $[R]_1^{+\cdot}$ is the number of cation radicals created initially when an anodic pulse is applied, α_τ is the rate constant for radical cations formation. According to Pandey model, since life time is higher than the cathodic pulse time, $t_c = 0.7s$ in this study, a continuous growth of the PEDOT oligomer occurred. Furthermore, the PEDOT film growth in the pulse polymerization is not limited by monomer diffusion process, forming ordered growth of PEDOT short chain oligomers and realize their concurrent conjugation without to obstruct the oxidation reaction processes [222].

3.2.4 Electrochemical characterization of PEDOT layer

3.2.4.1 The enhancement factor, EF

In order to characterize the polymer growth under pulse conditions, the enhancement factor (*EF*), was introduced, Eq. 24 [223].

$$EF = \frac{Q_{red}(t_a, N)}{Q_{red}^0(\tau)} \qquad \text{Eq. 24}$$

All the polymer layers after synthesis were characterized by potentiodynamic cycling in 0.5 M H_2SO_4, between -0.3 V and 0.8 V, with a scan rate of 100 mv/s (3.2.3.1, Fig. 30). The reduction charge, Q_{red} of each polymer was compared with the reduction charge, Q^0_{red}, of PEDOT layers synthesized under potentiostatic conditions at the same E_a for the same total polymerization time (τ), $\tau = N * t_a$. One can notice that for the same anodic potential and for the same total polymerization time, the polymerization charge, Q_{pol}, was the same

(Q_{pol}=142.8 mC/cm²) for a polymer synthesized potentiostatically and for the polymer obtained by pulsed deposition with the following parameters,

E_a=0.9 V, E_c=0.3 V, t_a=0.5 s, t_c=0.7 s, but the reduction charge was higher for the PEDOT layer obtained by potentiostatic pulse, as it can be seen in Fig. 37 and Fig. 38. Due to this we defined the enhancement factor as a function of reduction charge [223]:
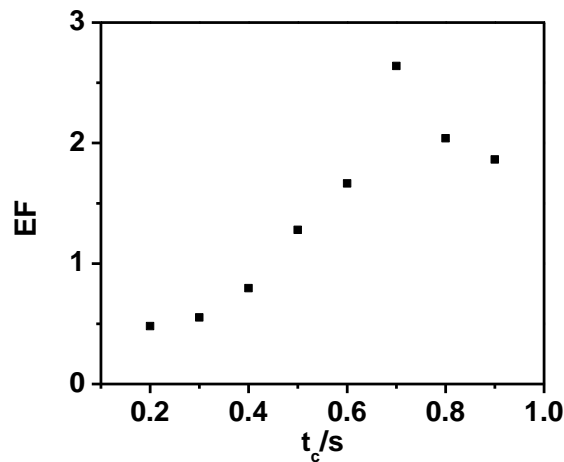
Fig. 37 Enhancement factor, *EF*, as a function of the polymerization cathodic time for PEDOT layers synthesized by pulse potentiostatic method for following parameters: E_a=0.9 V, t_a=0.5 s, E_c=0.3 V. The electrolyte consists of 8 mM EDOT+1 mM SDS+0.2 M LiClO$_4$, at room temperature.
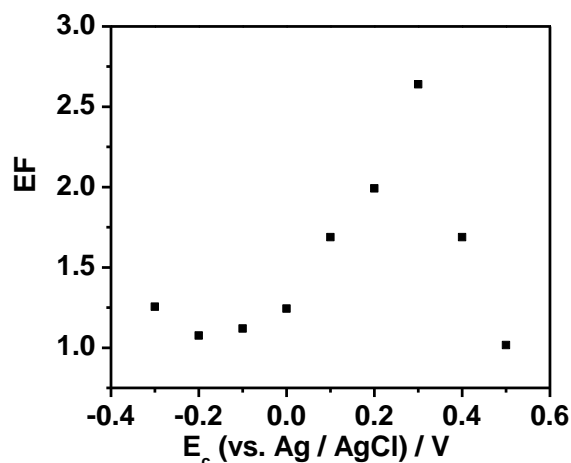
Fig. 38 Enhancement factor, *EF*, as a function of the cathodic potential for PEDOT layers synthesized by pulse potentiostatic method for following parameters: E_a=0.9 V, t_a=0.5 s, t_c=0.7 s. The electrolyte consists of 8 mM EDOT+1 mM SDS+0.2 M LiClO$_4$, at room temperature.

It must be mentioned that an *EF* value higher than 1 indicates an enhancement of the polymerization rate while *EF* value less than 1 shows an inhibition of the polymer growth during pulse deposition. Both E_c and t_c are important for accelerating the polymer growth. The possible reason for the enhanced growth under pulse conditions can be explained in terms of the relaxation of the concentration profile in the vicinity of the working electrode during the reduction pulse. At these circumstances a fresh solution containing higher monomer concentration arrives at the growing interface of the CP layer during the cathodic relaxation time, a fact that facilitates the following growth of the film during the consecutive on time.

For the experimental conditions it was observed in this study that the polymerization rate is reduced when the cathodic pulses duration is smaller than 0.4 s (Fig. 37). Obviously in this case the cathodic time is not enough for

properly relaxation of the polymer. Values of *EF* higher than unity were obtained when t_c was larger than 0.5 s (Fig. 37). The highest *EF* value was obtained for $t_c = 0.7$ s.

Studying the influence of cathodic potential on polymerization process an inhibition of the polymer growth was noticed for the highest values, between -0.3 V and 0.0 V (Fig. 38). A possible explanation is that on these high cathodic potential the polymer is reduced and to reach again the oxidize state during anodic pulse, a longer time is required. For the cathodic pulses larger than 0.3V the polymerization process was also inhibited. This it can be explained by the fact that the polymerization process was inhibited since the polymer remains in its oxidized state (Fig. 38).

3.2.4.2 The doping level, γ

The redox activity of a polymer layer can be also described by the doping level, γ, which represents the fraction of mobile counterions. The doping level can be calculated by means of Eq. 25 [223, 224]:

$$\frac{Q_{red}}{Q_{pol}} = \frac{\gamma}{\gamma+2} \qquad \text{Eq. 25}$$

According to Stromberg et al. [223] this measure for the redox activity of the PEDOT film is available only in the case when the polymerization is 100% [223].
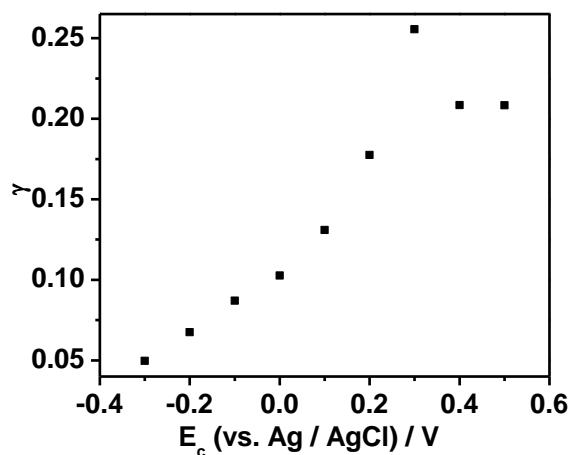
Fig. 39 Apparent doping degree γ of PEDOT layers as a function of the cathodic potential, E_c, for PEDOT layers synthesized by pulse potentiostatic method for following parameters: $E_a=0.9$ V, $t_a=0.5$ s, $t_c=0.7$ s. The electrolyte consists of 8 mM EDOT+1 mM SDS+0.2 M LiClO$_4$, at room temperature.
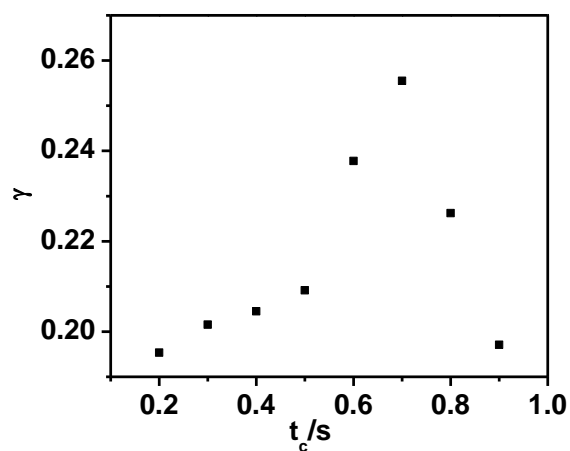
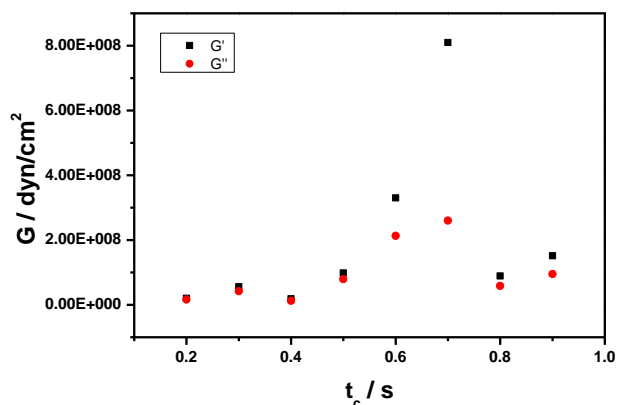Fig. 40 Apparent doping degree γ of PEDOT layers in dependence on the cathodic potential duration for PEDOT layers synthesized by pulse potentiostatic method for following parameters: $E_a=0.9$ V, $t_a=0.5$ s, $E_c=0.3$ V. The electrolyte consists of 8 mM EDOT+1 mM SDS+0.2 M LiClO$_4$, at room temperature.

Depending on the synthesis potential and polymerization charge a doping level, γ, between 0.08 and 0.26 (Fig. 39 and Fig. 40) was found, which is in agreement with other literature reports for PEDOT film electropolymerized from aqueous solution [223, 224]. The data from literature demonstrate that PEDOT films prepared from micellar surfactant solutions present a compact structure and low ions mobility compared to those obtained in organic media [225].

3.2.4.3 QCM investigation

QCM technique was used to investigate if the results presented in 3.2.3 are due to the variation of polymerization charge or due to the structural modification. PEDOT layers were synthesized for different cathodic time and different cathodic potential at the same parameters presented in 3.2.3.1 and 3.2.3.2, but for the same frequency shift, $df = 18\,KHz$. It has been shown that the EQCM is a powerful method to investigate the electropolymerisation process, viscoelastic properties, the oxidation/reduction, (doping/dedoping), of conducting polymers [221].

When an acoustic wave propagates across a thin viscoelastic layer deposited on a quartz electrode, results a complex frequency shift, Δf^*, (1.5.1, Eq. 8) [133]. The acoustic impedance, Z^*, of a quartz resonator which has on top a viscoelastic film characterized by a finite thickness h_f and density, ρ_f, in a solution with density, ρ_L, and viscosity, η_L, is usually modeled by the following Eq. 26 [29, 107]:

$$Z^* = i\omega\rho_s + Z_p \left[\frac{Z_L \cosh(\gamma h_f) + Z_p \sinh(\gamma h_f)}{Z_p \cosh(\gamma h_f) + Z_L \sinh(\gamma h_f)}\right] \qquad \text{Eq. 26}$$

In Eq. 26 γ is the shear wave propagation constant of the layer. The mechanical properties of the polymer can be specified by the shear modulus G. Under sinusoidal deformation, it is represented as complex quantity, Eq. 27 [29, 107]:

$$G = G' + jG'' \qquad \text{Eq. 27}$$

The real part of G, G', called *storage moduli*, represents the component of energy storage in the film. The imaginary part, G'', represents the power dissipation in the film and is called *loss moduli* [29, 107].

$$\gamma = i\omega \left(\frac{\rho_f}{G}\right)^{1/2} \qquad \text{Eq. 28}$$

$$Z_p = \left(\rho_f G\right)^{1/2} \qquad \text{Eq. 29}$$

$$Z_L = (i\eta_L \rho_L \omega)^{1/2} \qquad \text{Eq. 30}$$

In this work the *storages moduli* and *losses moduli* G' and G'' were calculated numerically resolving the Eq. 27, for PEDOT layers synthesized at different cathodic time, respectively at different cathodic potential (Fig. 41, Fig. 42).
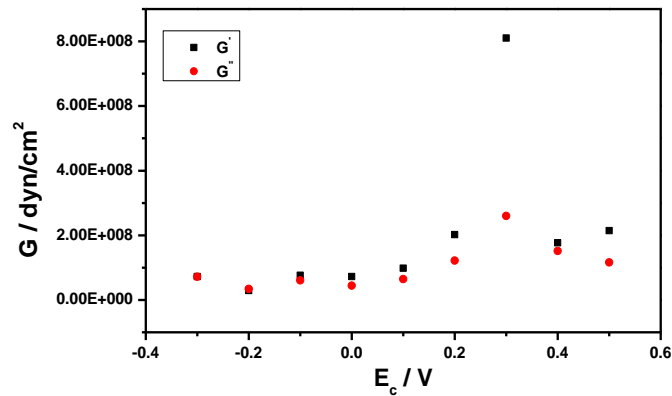
Fig. 41 The shear storage and losses moduli, G' and G'', for different cathodic potential for PEDOT layers synthesized by pulse potentiostatic method for following parameters: E_a=0.9 V, t_a=0.5 s, t_c=0.7 s. The electrolyte consists of 8 mM EDOT+1 mM SDS+0.2 M LiClO$_4$, at room temperature.

Fig. 42 The shear storage and losses moduli G' and G'' for different cathodic duration for PEDOT layers synthesized by pulse potentiostatic method for following parameters: E_a=0.9 V, t_a=0.5 s, E_c=0.3 V. The electrolyte consists of 8 mM EDOT+1 mM SDS+0.2 M LiClO$_4$, at room temperature.

The results show that for t_c=0.7 s and E_c=0.3 V the polymer has an ordered structure, a denser film with longer conjugation length can be obtained, therefore for layer with higher G less mass exchange occur (Fig. 43).
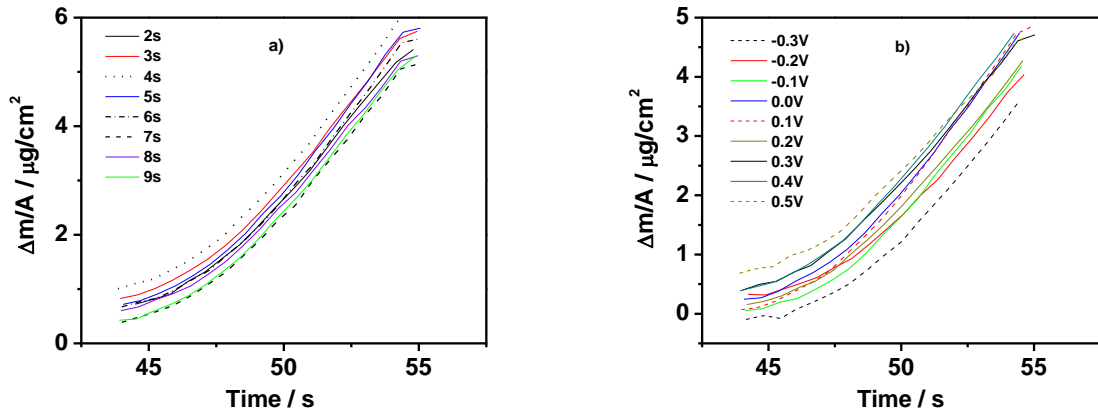
Fig. 43 The mass changes during the polymers oxidation in 0.5 M H$_2$SO$_4$. The CV measurements were performed between -0.3 V and 0.8 V for a scan rate of 100 mV/s. The data from graph a) are for polymer layers synthesized under different cathodic time. The graph b) presents data for polymer layers synthesized under different cathodic potential.

The correlation between the reduction charge (Fig. 32, Fig. 35, see 3.2.3.2 and 3.2.3.3) and elastic moduli G (Fig. 41 and Fig. 42) can be rationalized in terms of Rouse-Zimm model [226] for G moduli of a polymer. In this model G' is proportional to the squared relaxation time τ^2, which according to Stokes-Einstein formula is inversely proportional to the mobility of charged chain segments. Mobility of charged species decreases when ionic strength of the solvent increases [226-229, 232-234]. Totally this leads to the increase of G according to the formula for shift of storage modulus G' relative to its value G_0' in the absence of charges (Eq. 31) [227]:

$$\frac{G' - G_0'}{G_0'} = \frac{4\sqrt{\pi}e^3 \sqrt{\sum_i N_i z_i^2}\, q}{3(\varepsilon kT)^{3/2}(1+\sqrt{q})} \qquad \text{Eq. 31}$$

In Eq. 31 N_i is volume concentration of ions with charge z_i in the solvent inside the polymer, $e,\ k,\ T,\ \varepsilon,\ q$ are the electron charge, Boltzmann constant,

temperature, dielectric permittivity and ion transport number respectively. Assuming that charges of one sign are fixed on polymer chains and the opposite are in mobile phase it can be concluded that the elastic modulus increases as $Q^{1/2}$, where $Q = Q_{red}$. A rough estimation which is possible in this case gives $\frac{\delta G}{G} = 0.3$, for $\varepsilon = 10$ and $N_i = 10^{20}$ cm^{-3}. Similar formula can be derived for loss modulus. Thus the observed correlation between increase of doping level and G values at certain parameters of cathodic part of pulse finds its explanation.

In all experiments the QCM data for pristine layers polymerized at different parameters have the value for normalized damping above 0.9. The synthesized layers from submicellar solution with pulse technique have a high rigidity due to SDS anions incorporation, as was presented before in 3.2.1, 3.2.2 for potentiodynamic and potentiostatic methods also.

3.2.4.4 Surface analysis

The surface of polymer layers was analysed by profilometer technique for two polymers obtained by potentiostatic and potentiostatic pulse. Both polymers were synthesized on an Au electrode of a quartz crystal from an EQCM technique, for the same shift of frequency, $df = 16KHz$. According to profilometer data the PEDOT layer obtained by pulse method, is rougher and thicker compared to PEDOT layer synthesized by direct current technique (Fig. 44).
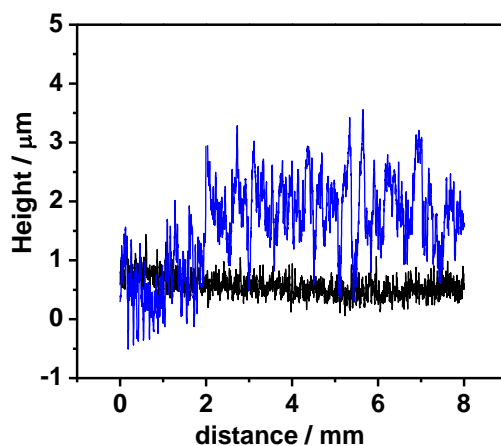
Fig. 44 Profilometer data for surface analysis of PEDOT layers obtained by pulse (blue line) and by potentiostatic technique (black line)

The data from Fig. 44 were confirmed by QCM technique (Fig. 45). The thickest layer was obtained by potentiostatic pulse technique proving that the relaxation time, t_c, it is essential for an enhancement of polymer growth.
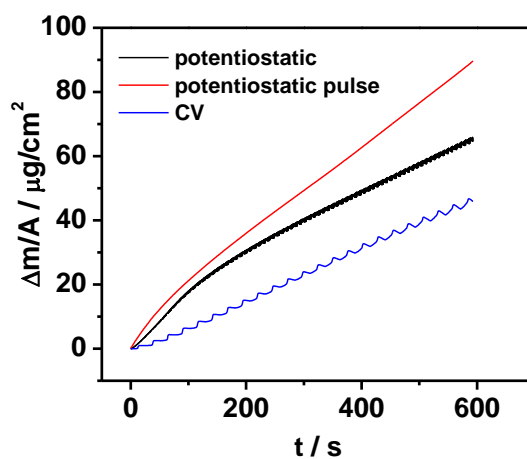
Fig. 45 Polymer deposited mass per unit of surface versus time. The data were calculated according to Eq. 6. The electrodeposition conditions were described in 3.2.1, 3.2.2 and 3.2.3.
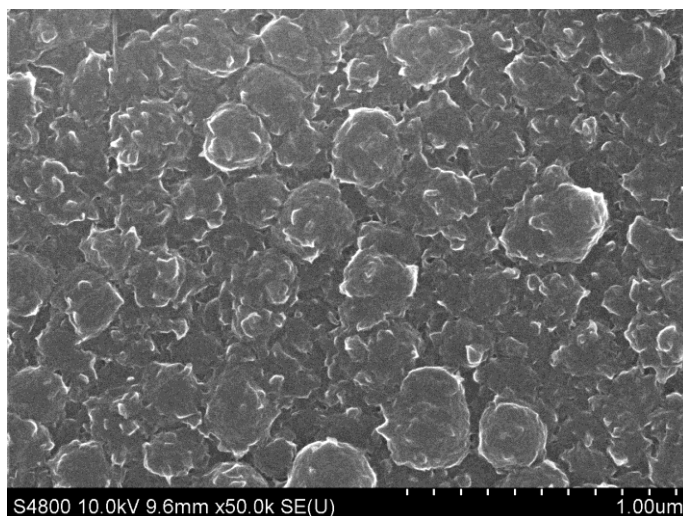
Fig. 46 SEM analysis of PEDOT layer synthesized by potentiostatic pulse method (3.2.3) from submicellar solution (1 mM SDS) at room temperature.

More porous layers were obtained by potentiostatic pulse method compared to those synthesized by potentiodynamic (3.2.1) and potentiostatic methods (3.2.2).

3.3. PEDOT/gold nanoparticles composite layers

Nanocomposite layers were obtained by two routes (3.3.1 and 3.3.2). The aim was to incorporate gold nanoparticles as much as possible for bioanalytical applications (3.4).

3.3.1 Electrochemical co-deposition of PEDOT layer and presynthesized gold nanoparticles

After synthesis of gold nanoparticles, AuNPs, (see 3.1) the colloidal solution and monomer electrolyte (8 mM EDOT+1 mM SDS+0.2 M LiClO$_4$) were mixed in ratio 1:4. The first electrodeposition experiments were performed using potentiodynamic method, in potential window (-0.3 V; 1.3 V) at the scan rate of 50 mV/s (Fig. 47 a, b). Nanocomposite layers were also deposited

potentiostatically at 0.9 V (Fig. 48 a) and by potentiostatic pulse at the already established parameters (3.2.3) (Fig. 48 b).
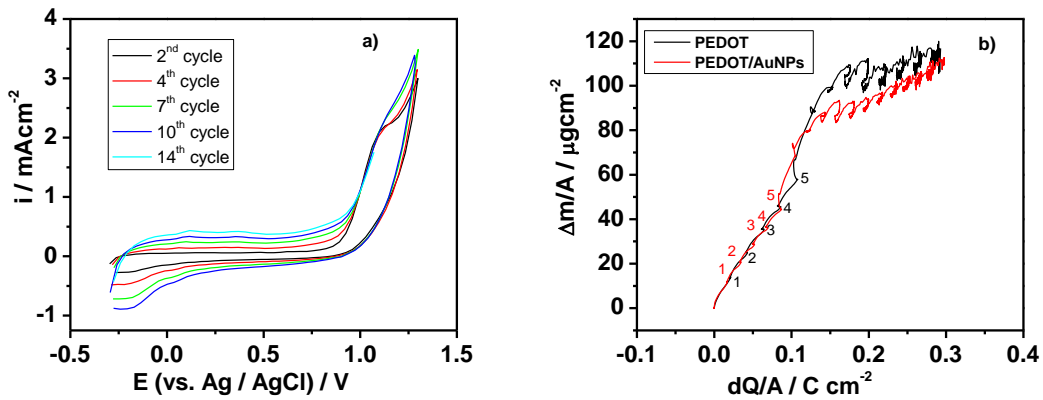
Fig. 47 CV recorded for co-deposition of PEDOT/AuNPs (a) and compared data for mass variation during nanocomposite and pristine layers synthesis using EQCM technique (b)
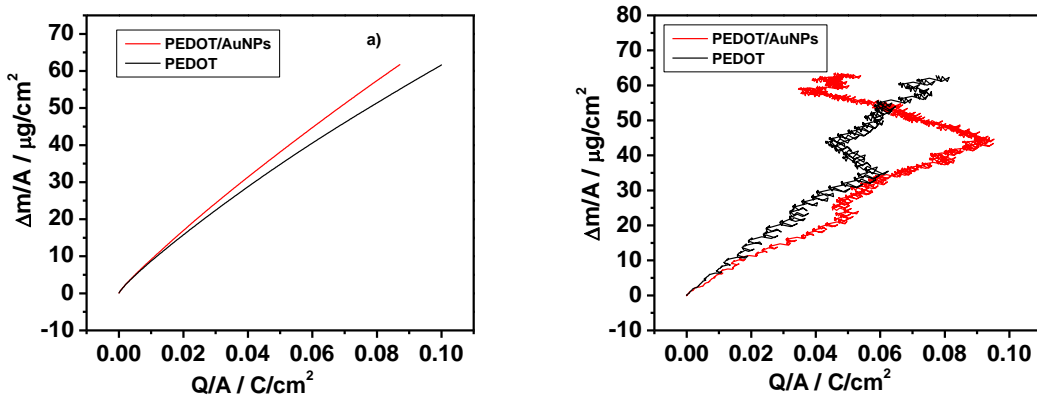
Fig. 48 The mass variation during nanocomposite and pristine layers synthesis for potentiostatic a) and potentiostatic pulse method b) using EQCM technique

From the data presented in Fig. 47 b and Fig. 48 b one can notice an inhibition of mass increase during co-deposition of nanoparticles. One possible explanation is the adsorption of trisodium citrate, which was used to reduce the

gold salt, on gold quartz electrode surface. When potentiostatic method is used the deposited mass increases due to the presence of gold nanoparticles on polymer surface. As it can be seen in SEM image shown in Fig. 49 a the nanoparticles are not uniformly distributed on the PEDOT surface.

a. b.
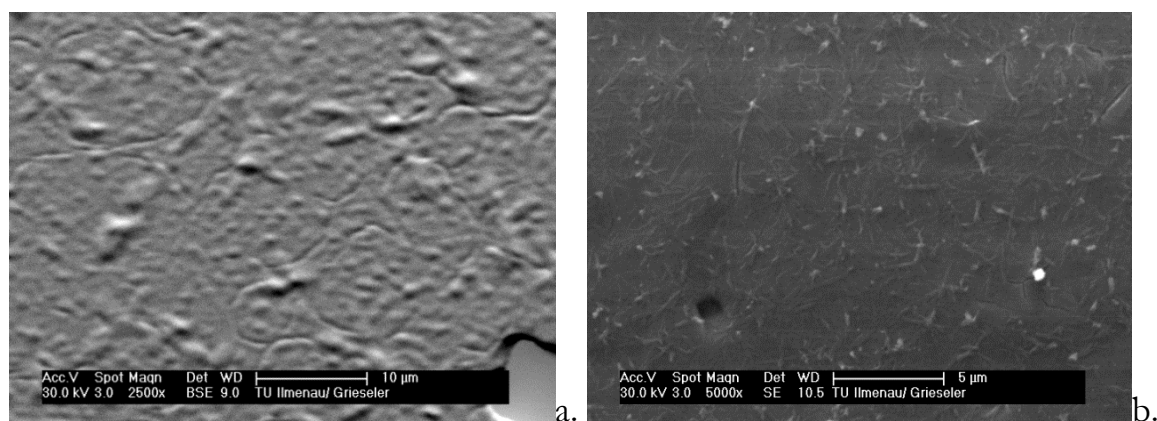
Fig. 49 SEM image of PEDOT/AuNPs nanocomposite layers synthesized by potentiostatic a) and potentiodynamic b) method

The amount of deposited gold is very small and from SEM image (Fig. 49) it can be seen that only a few nanoparticles are on the surface. The presence of AuNPs on the film was also proved by EDX measurements (Fig. 50).
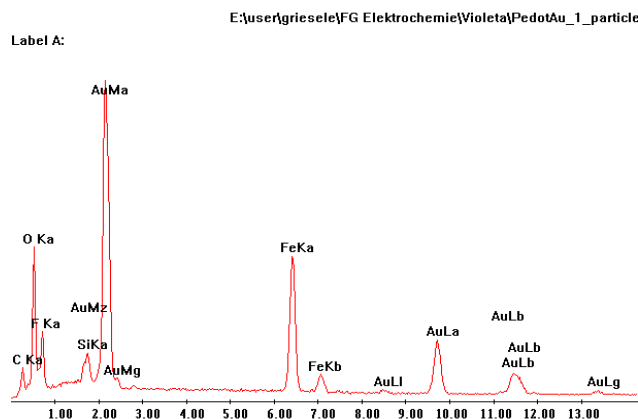
Fig. 50 EDX spectra for PEDOT/AuNPs nanocomposite layer co-deposited on glassy carbon electrode by potentiodynamic method

3.3.2 Electroless deposition of gold on PEDOT layer

The next step in this work was to increase to amount of Au nanoparticles on polymer surface. The used method was electroless deposition of Au from 1 mM solutions of $HAuCl_4$. First the pristine PEDOT layer was electrodeposited on two ways: potentiostatic at 0.9 V, the anodic polymerization potential and potentiostatic pulse at 0.3 V cathodic potential, E_c, 0.7 s cathodic pulse duration, t_c, 0.9 V anodic deposition potential, E_a, 0.5 s anodic pulse duration, t_a. The reason why these parameters were chosen was already explained in 3.2.3. Both polymers were synthesized on an Au electrode of a quartz crystal, for the same shift of frequency, $df = 16\ KHz$. Electroless precipitation of gold on PEDOT was carried out after reducing the PEDOT layers at E=−0.5 V for 600 s in 0.5 M H_2SO_4 solution [29, 235], into 1mM hydrogen tetrachloroaurate (III) trihydrate solution.

The morphology and the composition of the deposits were analyzed by SEM and EDX with a Hitachi S-4800 device (Fig. 51, Fig. 52). The SEM

measurements, as one can see in 3.2.4.4 Fig. 46, showed that pulse technique provide porous layer which is a better reduction agent for gold salt.
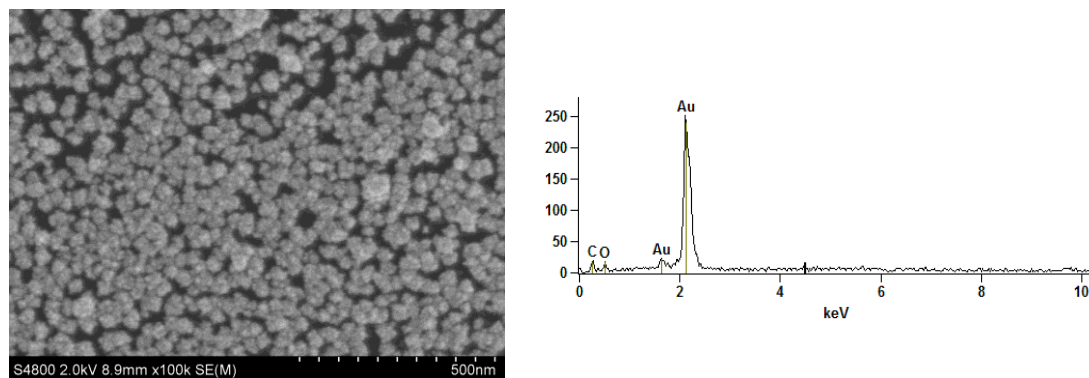
Fig. 51 SEM image and EDX analysis of PEDOT/AuNPs layer on glassy carbon electrode. The pristine layer was synthesized by potentiostatic pulse technique and gold nanoparticles by electroless method.
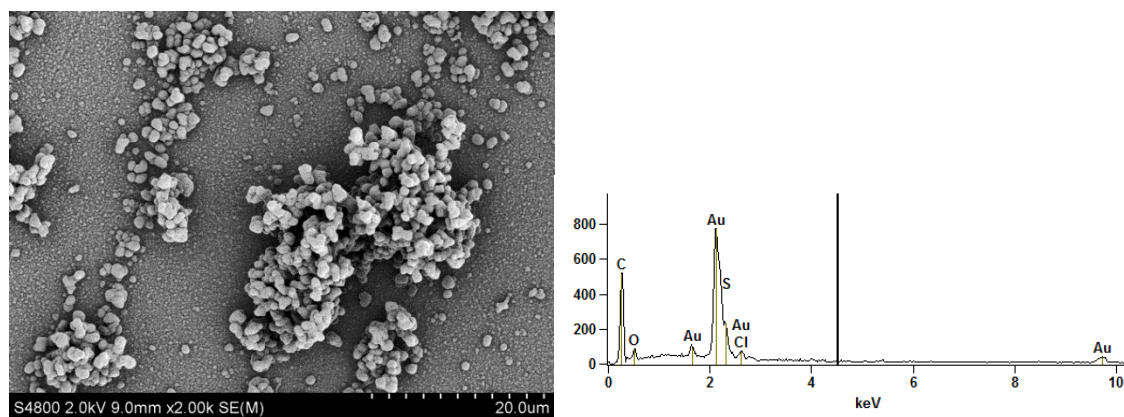
Fig. 52 SEM image and EDX analysis of PEDOT/AuNPs layer on glassy carbon electrode. The pristine layer was synthesized by potentiostatic technique and gold nanoparticles by electroless method.
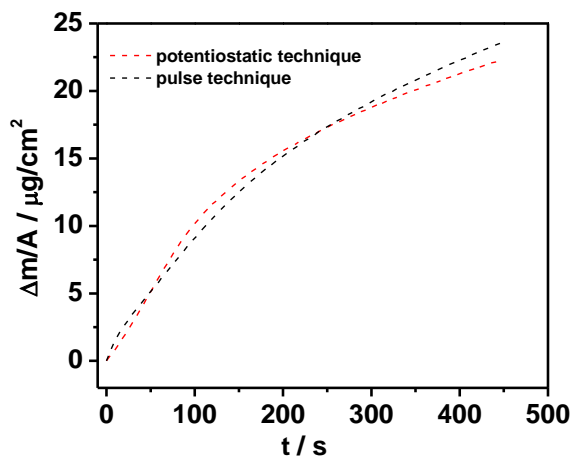
Fig. 53 EQCM data for the mass variation versus time during electrodeposition, using potentiostatic technique (red dots), pulse technique (black dots).

Even if EQCM data show similar results regarding deposited gold mass on polymer surface (Fig. 53), SEM image (Fig. 51) showed a uniform distribution of AuNPs on the polymer surface obtained by potentiostatic pulse technique. Due to this reason the pulse procedure was chosen for this work to synthesize pristine layer.

It was established from EDX data that the gold clusters are present only on the outer surface of polymer films but not in the pores. The data for the analysis of the dark region of the film, where only polymer exists, demonstrate that is no gold signal (Fig. 54).
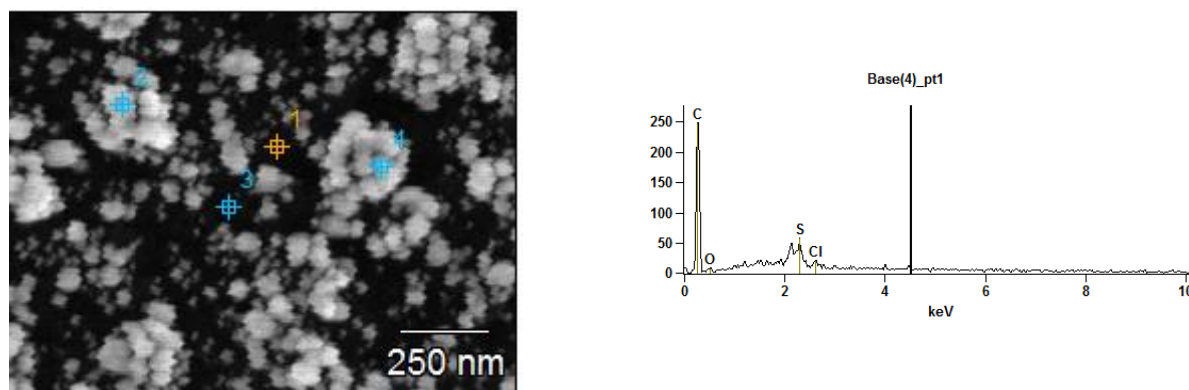
Fig. 54 SEM and EDX data for PEDOT/AuNPs layer on glassy carbon working electrode. The pristine layer was synthesizes by potentiostatic technique and gold nanoparticles by electroless method.

Similar results were obtained for nanocomposite materials when pulse technique was used to synthesize the pristine layer.

The cluster sizes depend on the time of exposition of a PEDOT layer in solutions of Au(III) ions and the concentration of these ions. Comparing the data regarding the layers characterization for pristine PEDOT films and nanocomposites, cyclic voltammograms (CVs) of nanocomposite layers show in the presence of chloride ions additional redox peaks due to the oxidation of gold. On the reversal of the potential scan direction takes place the reduction of the product [29, 235].

3.3.2.1 The proposed model for electroless deposition of gold nanoparticles from aqueous electrolyte, using EQCM technique

To control the mass of AuNPs deposited by electroless method, the EQCM technique was used. The mass changes detected by this technique start from few ng/cm². The presence of a viscoelastic substrate makes determination of deposited mass more complicated than just the traditional calculation from

Sauerbrey equation (Eq. 6) used for thin and rigid layers. The amplitude of oscillations decreases on the interface between the film and liquid due to the energy losses in the film. The resonance frequency shifts because of deposited mass, viscosity of liquid, losses in the film, and mass of the film. All values are of the same order of magnitude, and due to the presence of a reflected acoustic wave in the film, their contributions cannot be summed [29].

A model for resolving this problem was reported in literature [29] and can be applied on PEDOT/AuNPs layers in aqueous electrolyte, where gold is deposited by electroless method on top of a PEDOT film.

To include a mass of metal nanoparticles added on top of polymer film it is enough to consider it as a structure formed from two layers, where the metal layer has a finite thickness h_d, density ρ_d, shear modulus G_d and wave number $\gamma_d = i\omega(\rho_d/G)^{1/2}$. If it takes a limit of small h_d and large G_d, the term $Z_d\ tanh(\gamma_d\,h_d) \approx i\omega\rho_d h_d$, from Eq. 26 is altered as follows, Eq. 32 [29]:

$$Z = i\omega\rho_s + Z_P\left(\frac{\left(Z_L + i\omega\rho_d h_d\right)\cosh(\gamma h_f) + Z_P\sinh(\gamma h_f)}{Z_P\cosh(\gamma h_f) + \left(Z_L + i\omega\rho_d h_d\right)\sinh(\gamma h_f)}\right) \qquad \text{Eq. 32}$$

The effect of rigid layer deposited on top of viscoelastic layer is reduced to the correction of liquid impedance by the impendance of deposited mass.

Eq. 32 was used to determinate the deposited mass (term $\rho_d h_d$) of metal layer following the next two steps: first, acoustic impedance is measured for polymer film which has a known thickness h_f in liquid and its G', G'' are determined as roots of Eq. 26. Second, acoustic impedance is measured during electroless deposition of metal. Since it does not affect the property of underlying film, the G', G'' of polymer remain the same, as were found from Eq. 26. Then G',

G'' are used to resolved Eq. 32 with respect to $\varrho_d h_d$. In practice, it is easier to determine G', G'' from Eq. 32 because the only varying parameter is $\varrho_d h_d$. When these roots from Eq. 32 are equal to the roots from Eq. 26 then the value of parameter $\varrho_d h_d$ is the right one [29].

Electrochemical reduction of pristine layers in the absence of metal ions and dipped after that in the metal-plating solution have done by several researchers [21, 192, 193, 237]. In this study AuNPs were electroless precipitated on PEDOT, this approach providing the opportunity for the formation of homogeneously distributed metal nanoparticles on the polymer surface. It was shown that the reduction charge of the polymer layer and the dipping time are suitable parameters to control the amount of precipitated metal [21, 156, 157]. During electroless deposition of AuNPs open circuit potential and acoustic admittance were simultaneously measurements (Fig. 55) [29].
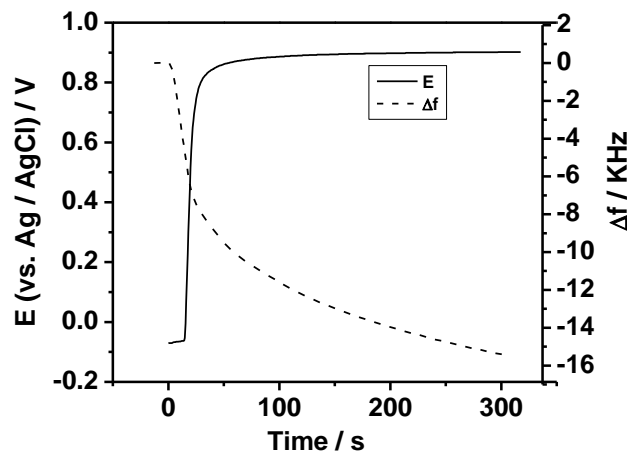
Fig. 55 OCP measurements during electroless deposition of Au from 1 mM hydrogen tetrachloroaurate (III) trihydrate solution on top of a PEDOT layer of ca 450 nm the thickness, for a dipping time of 320 s [29].

As it can be seen in Fig. 55 the decrease of the resonance frequency of the quartz crystal during the dipping time indicates the electroless deposition of AuNPs on polymer surface. At the same time, the open circuit potential of the system increases rapidly in the first seconds, due to the oxidation of the polymer during AuNPs deposition, and it reaches a plateau at 0.9 V after approximately 2 minutes from the immersion.

The obtained PEDOT/AuNPs bi-layer was transferred to an aqueous 0.5 M H_2SO_4 solution, and potentiodynamically measurements have been performed (Fig. 56). The CVs data present in anodic region up to 1.2 V the oxidation peak and in cathodic region, approx. at 0.47 V the reduction peak of gold, Fig. 56. Poguyaichenko et al. [235] showed that if the potentiodynamic experiments are performed with an anodic limit up to +1 V, then only one oxidation and one reduction peak of Au appear. If the anodic region will be increased then two oxidation peaks and two reduction peaks for Au are present. This is possible if Cl^- ions are also involved. These peaks can be attributed to the irreversibility of the redox process that implies both Au^{3+} and Cl^- ions. The gold oxidation can be associated to the formation of Au_2O_3 oxide at potentials above 1.2 V, whereas the reduction of the Au occurs at ca. +0.9 V. The second Au reduction peak that appears at ca. 0.47 V is due to the presence of Cl^- ions. In the present measurements, the occurrence of the double peaks in the CVs (Fig. 56) can also be attributed to the presence of the Cl^- ions because Cl^- ions could diffuse into the electrolyte from the reference electrode [29].
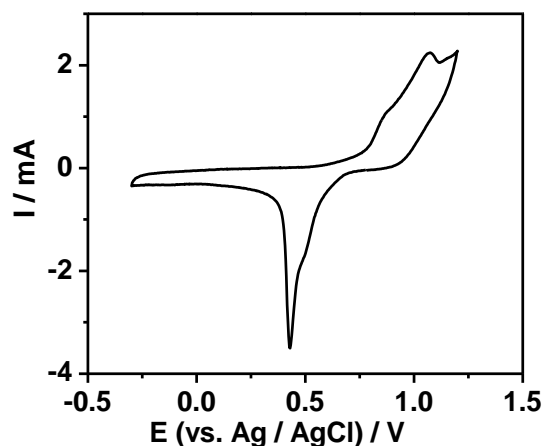
Fig. 56 CV recorded for 0.5 M H$_2$SO$_4$ solution on a PEDOT/AuNPs bi-layer working electrode, at the scan rate of 50 mV/s, at room temperature [29].

Another used technique to determine the distribution of the Au film deposited on the PEDOT layer is GD-OES. The results are plotted as intensity over sputter time, due to a missing calibration for high carbon contents (Fig. 57) [29].
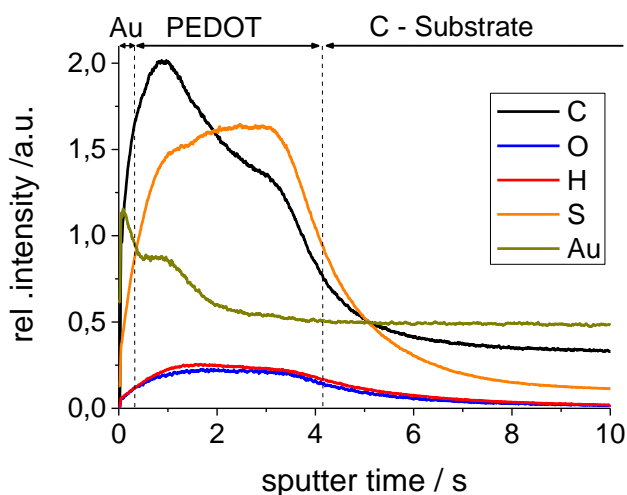
Fig. 57 GD-OES measurements on thin PEDOT/AuNPs bi-layer obtained onto glassy carbon electrodes under the same experimental conditions as those used for the EQCM experiments [29].

Ex-situ GD-OES analysis proved that a thin Au layer covers the surface of PEDOT film (Fig. 57). The depth profile also established that below Au, are present only the components of PEDOT (C, S, H and O). The Au and S signals within the substrate come from the spectral background of these element lines and the low C signal can be explained by the lower sputtering rate of the glassy carbon substrate compared to the PEDOT layer [29].

The thickness of PEDOT films were approximately 0.51 μm and 0.9 μm respectively. The values for both films $G'=6\bullet10^8$ and $G''=3\bullet10^8$ dyn/cm^2 have been calculated from Eq. 26. For the thin and for the thick pristine PEDOT layer have been obtained the same G value. After reduction in H_2SO_4 the PEDOT layers were immersed into Au deposition bath. Immediately it starts the electroless deposition of AuNPs, during which resonance frequency decreased and acoustic resistance increased with time. The acoustic spectra have been used to calculate the mass according to Eq. 32 [29]. For each spectrum the fitting has been done by varying surface density $\varrho_d b_d$ in Eq. 32 until the roots G', G'' reached the values found for PEDOT film deposition. The best close values were found to be exactly the same, $G'=6\bullet10^8$ and $G''=3\bullet10^8$ dyn/cm^2, as for PEDOT deposition. This finding demonstrates that the main supposition of the model, that gold layer is located on top of PEDOT layer without considerable penetration, is the correct one [29]. The data regarding the surface mass density as a function of time calculated in this way are presented in Fig. 58 a and b for PEDOT layers with different thickness, 0.51 and 0.9 μm. For both layers the mass of deposited Au was calculated and it is approximately the same, as it was expected for similar electrochemical conditions. In the same figure mass calculated from Sauerbrey equation using

frequency shift is shown as well. This mass is ca. 40-50% larger than mass calculated from admittance curve fitting [29].
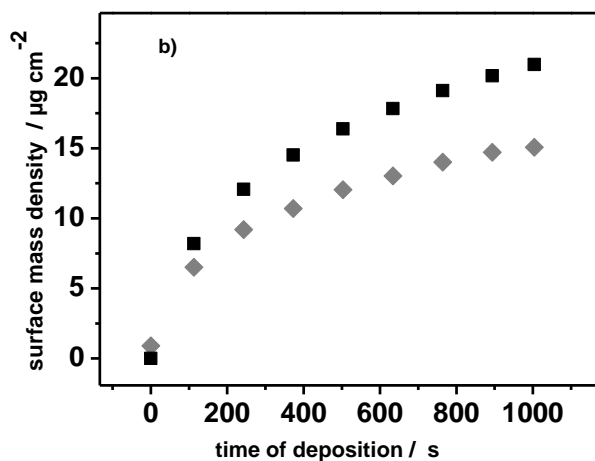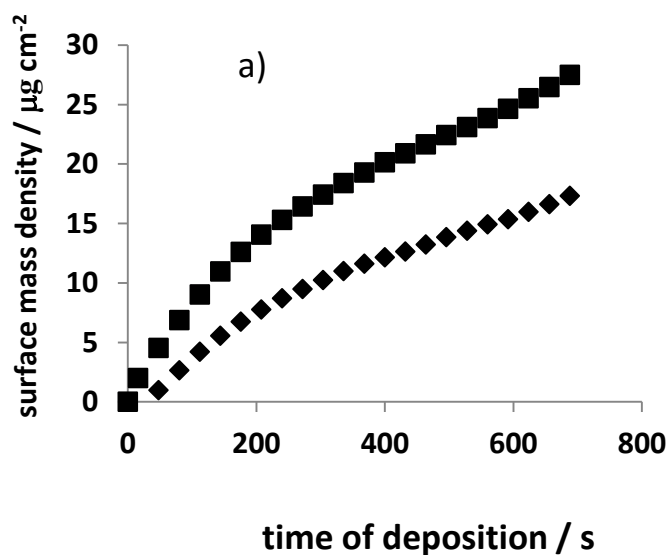
Fig. 58 Electroless deposition of Au on top of 0.51 (a) and 0.90 (b) μm PEDOT layer as a function of time. The surface mass density was calculated using Eq. 32 (rhombs), and from Sauerbrey equation (squares) [29].

The results showed that direct use of Sauerbrey equation significantly overestimates the deposited mass of nanoparticles. The method can be applied to wide range of multilayered sensors, which include alternating viscoelastic polymer and metal elements [29].

3.4 Electroanalytical detection of neurotransmitters

Recent activities in electroanalytical chemistry were focused on development of nanoparticles and particularly gold nanoparticles which have potential applications in the biosensor field due to their good stability and biocompatibility in biomolecule detection [41, 142, 158, 207,238, 239]. A polymer with a good stability in aqueous electrolytes and biocompatibility with biological media has been chosen in this work. Gold nanoparticles have been grown on the PEDOT surface by chemical routes, electroless deposition, as was presented in 3.3.2.

Catecholamines are a class of neurotransmitters which include epinephrine (E) [205], dopamine (DA) [204], and serotonin (5-hydroxytryptamine, 5-HT) [204] (see 1.7). Dopamine and serotonin were investigated in this work.
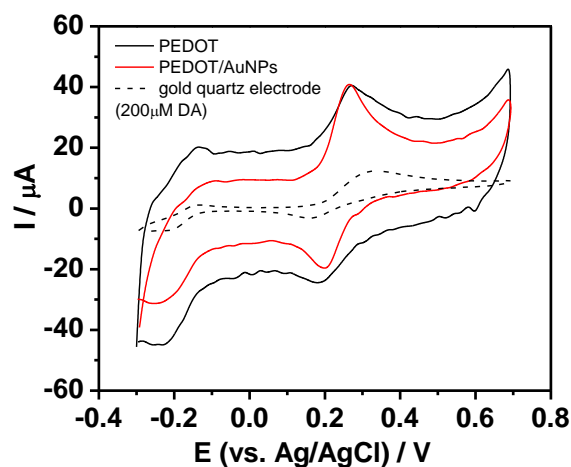
Fig. 59 CV recorded for 0.1 M phosphate buffer solution for electroanalytical detection of 200 μM DA using QCM technique, between -0.3 V and 0.7 V, at the scan rate of 50 mV/s, at room temperature.

The electroanalytic experiments were carried out with glassy carbon electrodes in order to avoid possible influence in the electrocatalytic reactions of the otherwise used gold electrode for the first experiments (Fig. 59). It is known that glassy carbon electrodes have a low sensitivity for the oxidation reactions of dopamine [41].

All electroanalytical detections were performed in 0.1 M phosphate buffer solution (PBS) consisting of 0.1 M K_2HPO_4 and 0.1 M KH_2PO_4, (pH=7.0).

The parameters relevant for a sensor were considered:

- *reproducibility*, this is the capability of a sensor to reiterate a measurement when it is placed again in the same environment. It is frequently directly associates to accuracy, but a sensor can be inaccurate, even though is repeatable in making observations.

- *sensitivity*, is defined as the change of measured signal with respect of the concentration unit of the analyte, i.e., the slope of a calibration graph.

94

- *selectivity*, represents the characteristics that establish if a sensor can respond to a group of analytes or individual to a single analyte only.

- *stability*, is the competence of a sensor to give reproducible results for a certain duration, preserving the selectivity, sensitivity, response, and recovery time.

- *detection limit* is the lowest concentration of an analyte that can be detected by the sensor. The detection limits used in this work (signal/noise) [S/N] was 3, according with the literature [41].

- *dynamic range* is the range of concentration of analyte between the detection limit and the highest limiting concentration where the detection is still possible.

- *linearity* is the relative deviation of an calibration graph which was experimentally determined, from an ideal straight line.

- *resolution* is the lowest concentration at which the sensor can give a distinguished response.

- *response time* is the time needed for sensor to respond to a change of concentration from zero to a particular concentration value.

- *recovery time* is the necessary time for the signal of a sensor to comeback to its initial value, which corresponds to zero concentration, after a step concentration took place.

3.4.1 Influence of the polymer layer thickness

The role of the PEDOT layer thickness has been investigated for both DA and 5-HT oxidation in order to identify the optimal conditions for the performance of the PEDOT and the PEDOT/AuNPs system (Fig. 60) [156, 157].
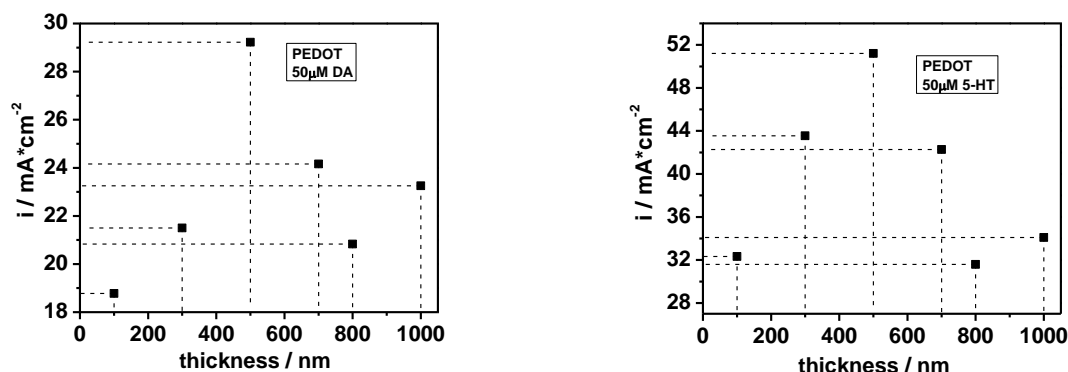
Fig. 60 Data regarding voltammetric oxidation peaks on PEDOT modified glassy carbon electrode for DA and 5-HT in 0.1 M PBS, at room temperature. All the experiments were performed at the scan rate of 20 mV/s.

In Fig. 60 DA and 5-HT oxidations were separately studied by using PEDOT coated electrodes with different thickness of the polymer layer ranging from 0.1 μm to about 1 μm. The comparison of the electrochemical response due to DA and 5-HT oxidation respectively is made by subtracting from each voltammetric curve measured in the presence of the analyte (DA or 5-HT), the reference curve (for the corresponding PEDOT layer) measured in buffer solution without analytes. The subtraction method provides the opportunity to follow only the voltammetric waves due to the oxidation of the analytes without interference of the intrinsic pseudocapacitive currents of PEDOT. The data from Fig. 60 shows that the oxidation currents of both DA and 5-HT depend on the thickness of the PEDOT layers. Using thick PEDOT layers for the DA and 5-HT oxidation it is noticed a strong inhibition of the response with increasing the polymer thickness. Due to this a compromise thickness of 500 nm (corresponding to a charge density by 120 mC/cm^2) of PEDOT layer was used in all the experiments.

3.4.2 Oxidation of ascorbic acid on PEDOT and PEDOT/AuNPs composite layer

3.4.2.1 Electrochemical detection of ascorbic acid

The electrochemical behavior of AA on a PEDOT and PEDOT/AuNPs modified glassy carbon electrode in phosphate buffer solution were investigated. The electroanalytical detection in micromolar range was investigated because in biological medium AA concentration is between 100 and 500 μM, which is between 100 and 1000 time higher than the concentrations of catecholamines investigated in this study.

The used technique for these measurements was differential pulse voltammetry, DPV. The first DPV measurements in 0.1 M phosphate buffer solution (PBS) were carried out for all polymers or polymer/AuNPs modified electrodes in buffer solution without the analytes to be present. These are the reference measurements and they were necessary to evaluate the contribution of the current due to the intrinsic electroactivity of the PEDOT, or PEDOT/AuNPs layers in the buffer solution. All the voltammetric curves were measured with following parameters: modulation time 0.05 s, step potential 5 mV, and modulation amplitude 20 mV, scan rate 20 mV/s. The electrodes were pre-conditioned at −0.1 V for 30 s before each DPV run [156, 157].

The modified electrode showed good electrocatalytic activity for the oxidation of ascorbic acid at approx. -5.4 mV on PEDOT (Fig. 61 a) and at -39 mV on PEDOT/AuNPs layers (Fig. 62 a) indicating a cathodic shift of approx. 33.6 mV. Furthermore, a sharper oxidation peak was obtained for PEDOT/AuNPs electrode (Fig. 62 a).
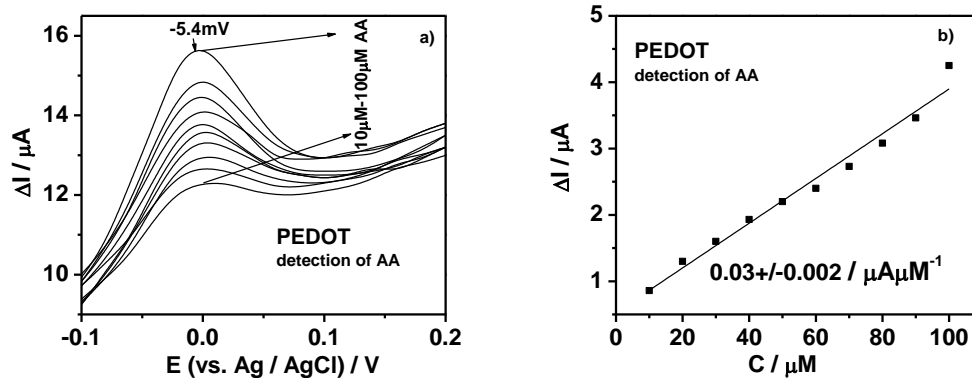
Fig. 61 DPV recorded in PBS with different concentrations of AA in the range from 10 to 100 µM on PEDOT layers a) and concentration dependence of the AA oxidation peak b)
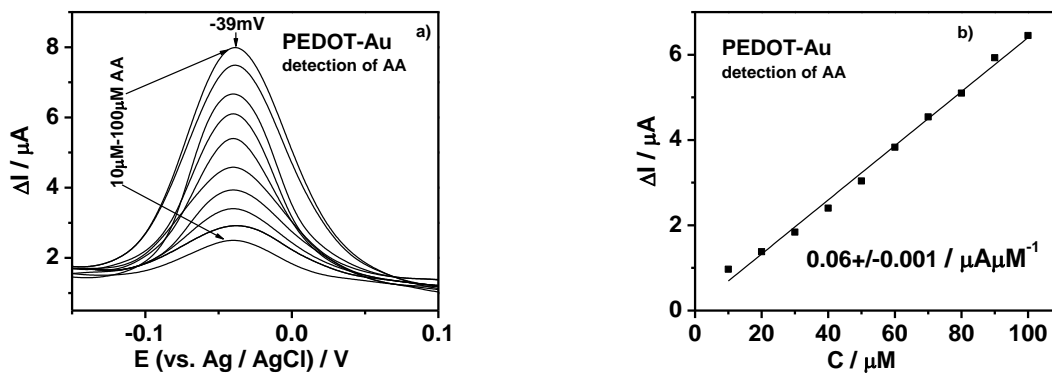
Fig. 62 DPV recorded in PBS with different concentrations of AA in the range from 10 to 100 µM on PEDOT/AuNPs layers a) and concentration dependence of the AA oxidation peak b)

The low oxidation potential and the enhanced of oxidation current peaks were attributed to electrostatic interactions between the functional groups of the coated electrode and the analyte. The cationic PEDOT and PEDOT/AuNPs layers interacted with the negatively charged ascorbate resulting in an analyte detection at a less anodic value [240].

The development of an electrochemical sensor based on modified glassy carbon electrode with incorporation of gold nanoparticles on PEDOT layer has as result a strongly electrocatalytic oxidation of AA [141].

The sensitivity increased two times for AA detection on nanocomposite layer, making it a suitable candidate for sensor applications.

3.4.3 Oxidation of dopamine on PEDOT and PEDOT/AuNPs composite layer

3.4.3.1 The individual oxidation behavior of dopamine on modified electrode

The concentration range used for electroanalytical detection of DA was for micromolar range between 5 µM—20 µM (Figs. 63, 64) and for nanomolar range between 50 nM-500 nM (Fig. 65). The electroanalytical detection in nanomolar range was possible only for PEDOT/AuNP nanocomposite layers proving the catalytic activity of gold nanoparticles. Besides, it was also found that, once immersed in a buffer solution which contains DA, the pristine PEDOT or nanocomposite layers showed afterwards additional electroactivity when they are transferred again in PBS without DA. This is very probably due to the irreversible adsorption of electroactive intermediates or products. The initial state of the PEDOT electrode was partially recovered by continuously cycling of the electrode in PBS solution only. Because of this, after each measurement in DA containing solution, the electrode was transferred back in PBS, without DA, in order to recover its initial state. Even in this way, the problem with the irreversible inhibition of the surface of the PEDOT layers could be only partially resolved for the studied concentration range of DA.

The electrochemical oxidation of DA in an aqueous solution is shown in Fig. 8, in 1.7. Two electrons are exchanged resulting dopamine-o-quinone (DOQ) [212]. This molecule can undergo an intermolecular addition, which results in a cyclization reaction generating leucodopaminechrome which, in turn, is

oxidized further via another two electron transfer to dopaminochrome [212]. The dopaminochrome can be further oxidized to indolic-o-quinone for a lower anodic potential comparative with potential for the first oxidation reaction, and to generate an insoluble melanin, which poisons the electrode surface [212]. Due to this these experiments were performed in a potential range which is proper only for the redox process of dopamine, without to have this poisoning in the electrochemical sensing but as mentioned before this cannot be completely avoided.
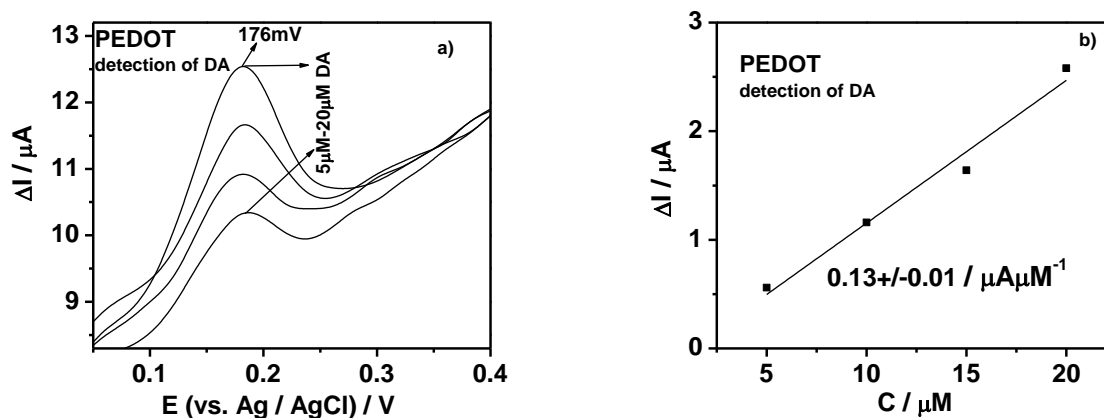
Fig. 63 DPV recorded in PBS with different concentrations of DA in the range from 5 to 20 μM on PEDOT layer a) and concentration dependence of the DA oxidation peak b)
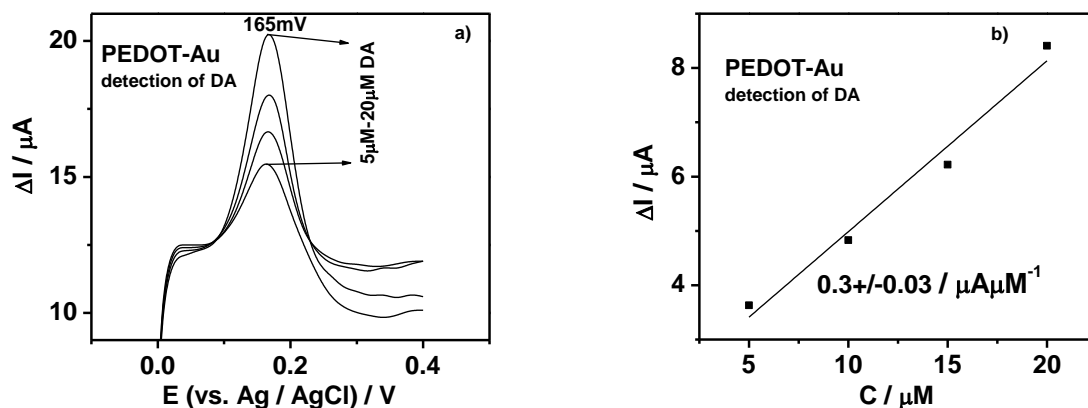
Fig. 64 DPV recorded in PBS with different concentrations of DA in the range from 5 to 20 μM PEDOT/AuNPs layers a) and concentration dependence of the DA oxidation peak b)
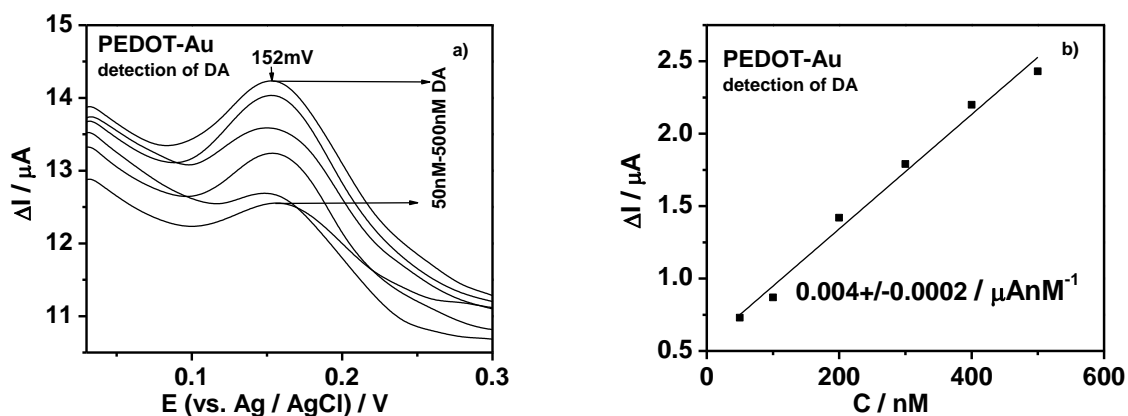
Fig. 65 DPV curves measured in PBS at different concentrations of DA from 50 to 500 nM PEDOT/AuNPs layers a) and concentration dependence of the DA oxidation peak b)

The oxidation behavior of dopamine on PEDOT and the PEDOT/AuNPs modified glassy carbon electrode is shown in Figs. 63-65. Oxidation of DA

occurs at 0.176 V on pristine PEDOT layer (Fig. 63) and at 0.165 V on nanocomposite layer (Fig. 64). The decrease of oxidation potential with 0.011 V but also the increase in oxidation current on hybrid polymer electrodes with approx. 50% clearly indicates catalytic oxidation of DA on nanocomposite layers. The increase in oxidation current in the presence of Au nanoparticles is attributed to the weak adsorption of DA cations on gold particles [158]. The weak adsorption of DA on the Au surface may be because of the fact that dopamine self-assembles on gold surfaces through the interaction between – NH_2 group from DA structure and Au [158]. Interestingly, the reversibility of DA oxidation is also greatly enhanced on the PEDOT/AuNPs electrode, which may have been favoured by the PEDOT polymer film which has a rich electron cloud and acts as an electron mediator. In addition, a hydrophobic environment seems to advantage reversible oxidation of dopamine [158].

The concentration dependence of the peak current shows a sensitive linear response in the 5 to 20 µM DA concentration interval (Fig. 63 b and Fig. 64 b). The sensitivity response increases in nanomolar concentration range, between 50 nM to 500 nM (Fig. 65 b). The slopes obtained for these concentrations ranges correspond to the sensitivity for DA determination. In this work the nanocomposite layer had a higher sensitivity for DA detection (0.3+/-0.03 / $\mu A \mu M^{-1}$) than the PEDOT layer (0.13+/-0.01 / $\mu A \mu M^{-1}$) values which are in accordance to literature reports [40]. The second linear region found in the 50 nM to 500 nM range (Fig. 65 b) shows a higher slope (0.04+/-0.0002 / $\mu A n M^{-1}$) corresponding to a higher sensitivity for DA determination in the nanomolar concentration range. The sensitivity for DA detection in nanomolar range is approx. by tenfold higher than in micromolar range.

3.4.3.2 The oxidation behavior of dopamine on modified electrode in the presence of ascorbic acid

Another aim of this work was the determination of DA in the presence of excess of AA because that is a challenging task in electroanalytical research field. To develop a sensor the sensitivity and selectivity are equally important. Simultaneous detection of DA and AA has been reported on electrodes coated with substituted PANIs and PPys, which help separation of the voltammetric peaks from oxidation of DA and AA [40,140, 156, 157]. It is well known that for both DA and AA the oxidation process occurs at approximately the same potential and appears as a single broad peak on a glassy carbon electrode [40, 140]. However they are clearly separated on a PEDOT electrode (Fig. 66) and as well on PEDOT/AuNPs modified glassy carbon electrode (Fig. 67).
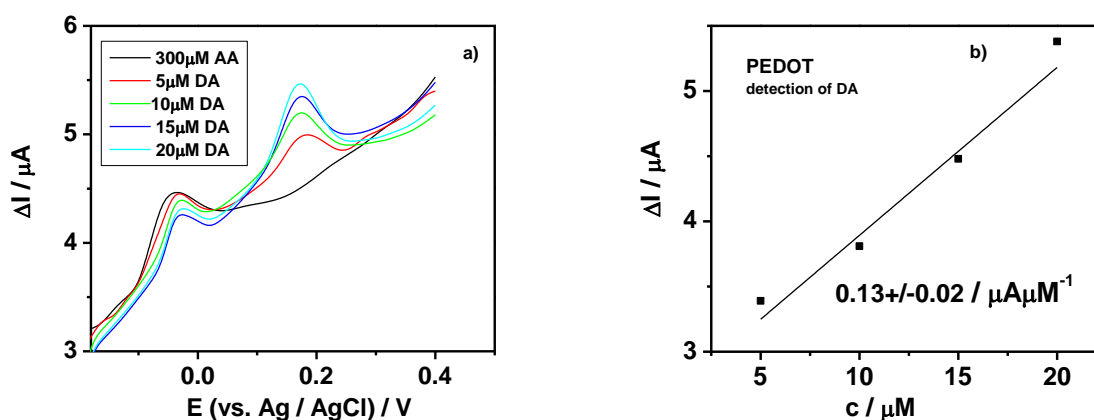
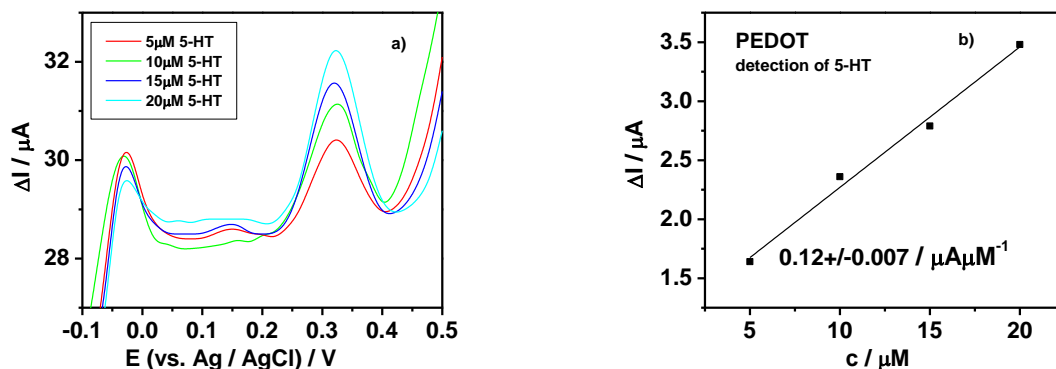Fig. 66 The DPV recorded in PBS with different concentrations of DA in the range from 5 to 20 µM on PEDOT layers in the presence of 300 µM AA a) and concentration dependence of the DA oxidation peak b)
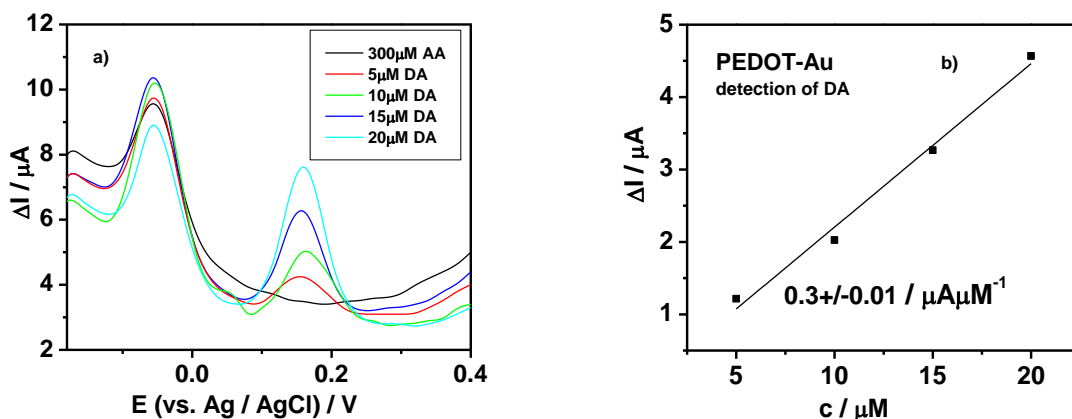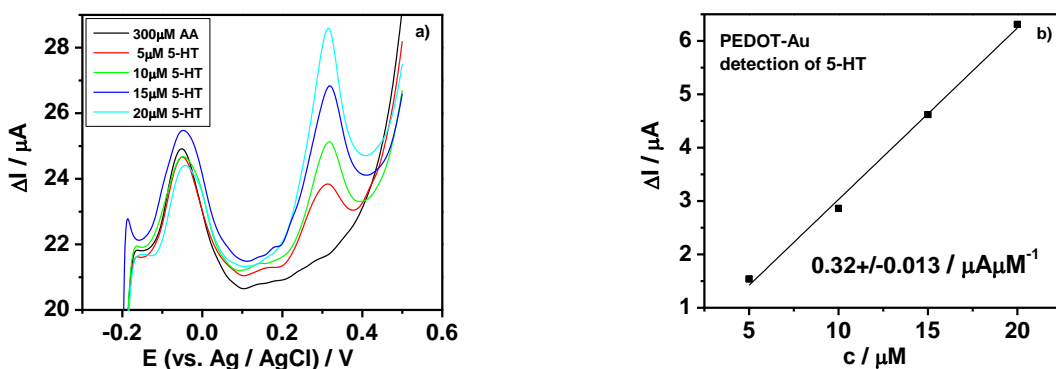
Fig. 67 DPV recorded in PBS with different concentrations of DA in the range from 5 to 20 µM on PEDOT/AuNPs layers in the presence of 300 µM AA a) and concentration dependence of the DA oxidation peak b)

According to Fig. 66 and Fig. 67 there is a separation peak between AA and DA oxidation about 0.173 V on PEDOT electrode and 0.161 V on PEDOT/AuNPs electrode.

As can be seen from Fig. 67 the peak current of DA is enhanced in the case of the PEDOT/AuNPs electrode compared to pristine PEDOT electrode, even in the presence of AA. This clearly shows the synergism between the polymer matrix and gold nanoparticles.

The sensitivity for DA detection in the presence of excess of AA has similar values as for only DA detection in the absence of AA. It was established through voltammetric studies that the PEDOT film favours the separation of the voltammetric peaks of DA and AA by hydrophobic and non-specific interactions [241]. It is established that the conducting polymer films, as polypyrrole, coated on the different electrodes have reduced and oxidized regions which are present in the entire structure [40, 242]. The reduced regions are more hydrophobic than the oxidized ones [241] and the same situation is

expected to be present in the case of PEDOT electrode, too. That result could be also due to the fact that DA is more hydrophobic than AA and it is more probably that DA interacts with the reduced regions of PEDOT whereas AA does not. This fact confirms that the selective determination of DA is possible on the presence of AA in excess concentration without visible interferences. Another argument is the voltammetric peak current of AA oxidation which remains unchanged, whereas the oxidation current of DA increases linearly with the increase of the bulk concentration of DA. This further confirms that the oxidation of DA and AA on a PEDOT film take place independently.

3.4.4. Oxidation of serotonin on PEDOT and PEDOT/AuNPs composite layer
3.4.4.1 The individual oxidation behavior of serotonin on modified electrode

The selective and quantitative detection of 5-HT levels is relevant for understanding the role played by serotonin in depression and other neurological disorders.

The first DPV measurements, the references measurements, on PEDOT and respectively for PEDOT/AuNP modified electrodes were performed in buffer solution only. These reference measurements were used to subtract the contribution of the current due to the intrinsic electroactivity of the PEDOT, or PEDOT/AuNPs layers in the buffer solution. All the voltammetric curves were measured at the same parameters presented before (see 3.4.2). The concentration range used for electroanalytical detection of 5-HT was in micromolar range between 5 µM—20 µM (Fig. 68, Fig. 69) and respectively in nanomolar range between 50 nM-500 nM (Fig. 70).
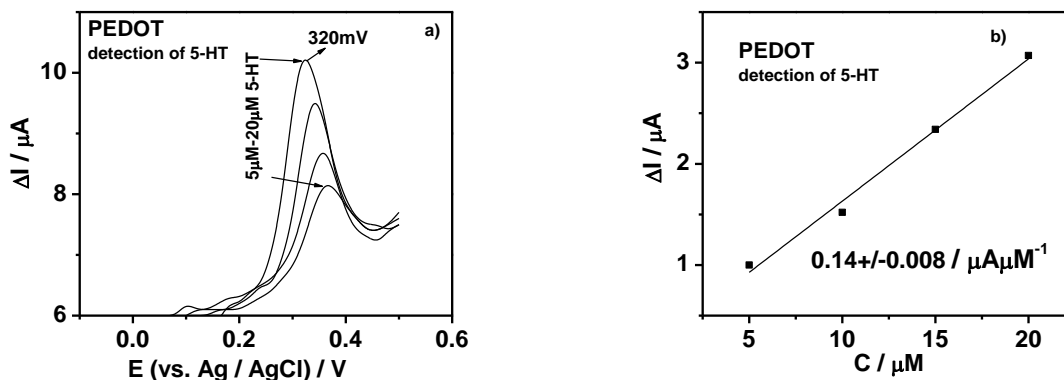
Fig. 68 DPV recorded in PBS with different concentrations of 5-HT in the range from 5 to 20 μM on PEDOT layer a) and concentration dependence of the 5-HT oxidation peak b)
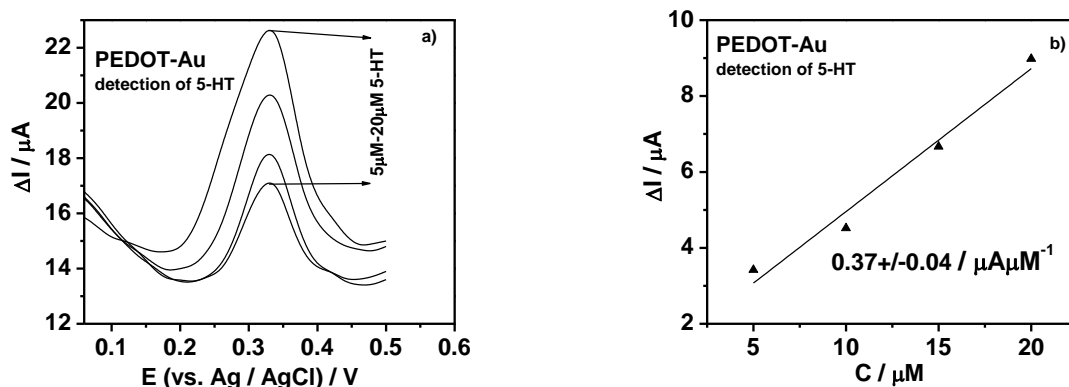
Fig. 69 DPV recorded in PBS with different concentrations of 5-HT in the range from 5 to 20 μM on PEDOT/AuNPs layer a) and concentration dependence of the 5-HT oxidation peak b)
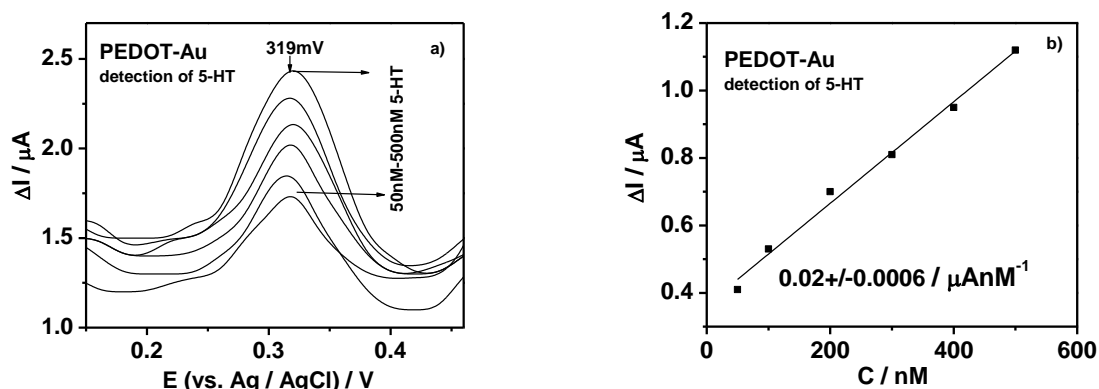
Fig. 70 DPV recorded in PBS with different concentrations of 5-HT in the range from 50 to 500 nM on PEDOT/AuNPs layer a) and concentration dependence of the 5-HT oxidation peak b)

The detection of serotonin using current methods has a couple of methodological provocation due to the interference of other neurotransmitters, such as DA. These neurotransmitters have similar redox potentials on glassy carbon, which pose a challenge to distinguish response signals using electrochemical methods. In this study could be proved that the analytes (DA, 5-HT) have distinguished oxidation peaks on PEDOT and PEDOT/AuNPs electrode. The oxidation potential for 5-HT is 0.32 V on PEDOT and PEDOT/AuNPs layers but the increase in the oxidation current on hybrid polymer electrodes with approx. 70% clearly indicates catalytic oxidation effect of 5-HT on the nanocomposite layers. The synergic effect of this catalytic system can be defined as the accumulation ability of the PEDOT layers which is enhanced by the nano-size effect of gold particles. The higher sensitivity for 5-HT detection (0.4+/-0.04 / $\mu A\mu M^{-1}$) was obtained for PEDOT/AuNPs layer. Comparing with the data for PEDOT layer (0.13+/-0.004 / $\mu A\mu M^{-1}$) the values were threefold higher. These values are according with the literature [243]. A second higher sensitive linear region was obtained for the

107

concentration range between 50 nM to 500 nM, only for nanocomposite layers (Fig. 70). The sensitivity for 5-HT detection on nanocomposite electrode increases in nanomolar range by a hundred times.

PEDOT electrode has not a good sensitivity in nanomolar range.

Besides, a similar situation as for DA was noticed, the irreversible absorption of electroactive reaction intermediates or products of 5-HT on the pristine PEDOT and nanocomposite layers. Due to these on electrode surface an additional electroactivity in PBS without analyte appear. The initial state of the PEDOT electrode could be partially recovered by continuously cycling in PBS solution.

3.4.4.2 The oxidation behavior of serotonin on modified electrode in the presence of ascorbic acid

It is relevant to investigate the electrochemical response of 5-HT in the presence of AA because they co-exist in biological medium, as mentioned before. The DPV technique was used to investigate the interference of 300 μM AA, constant concentration, on serotonin detection. The concentration of 5-HT was linear increased in the range 5-20μM for pristine PEDOT (Fig. 71) and nanocomposite layers (Fig. 72).

The peak current value of AA oxidation was at potential -0.034 V and for 5-HT at 0.32 V. However, with the addition of 5-HT, the signal increased linearly while AA current response remained constant.

Fig. 71 DPV recorded in PBS eith different concentrations of 5-HTin the range from 5 to 20 µM on PEDOT layers in the presence of 300 µM AA a) and concentration dependence of the 5-HT oxidation peak b)

Fig. 72 DPV recorded in PBS with different concentrations of 5-HT in the range from 5 to 20 µM on PEDOT/AuNPs layers in the presence of 300 µM AA a) and concentration dependence of the 5-HT oxidation peak b)

The sensitivity of serotonin detection in the presence of AA was comparable with the values obtained in the absence of AA. The value of sensitivity obtained on PEDOT electrode was $0.12+/-0.007$ / $\mu A \mu M^{-1}$ and $0.3+/-0.01$ / $\mu A \mu M^{-1}$ for PEDOT/AuNPs electrode.

Results and Discussions

Based to the presented data one can mention that a concentration of AA 100-1000 time higher than the concentration of DA or 5-HT did not interfere with the response of analytes.

All discussed above data are summarized in Table 4 for sensitivity and in Table 5 for oxidation potentials.

Table 4 Sensitivity of analytes detection on PEDOT and PEDOT/AuNPs glassy carbon modified electrodes

Analyte		PEDOT sensitivity	PEDOT/AuNPs sensitivity
AA	5-100 µM	$0.03+/-0.002$ µA µM^{-1}	$0.06+/-0.002$ µA µM^{-1}
DA	5-20 µM	$0.13+/-0.01$ µA µM^{-1}	$0.3+/-0.03$ µA µM^{-1}
	5-500 nM	negligible	$0.004+/-0.0002$ µA nM^{-1}
5-HT	5-20 µM	$0.14+/-0.008$ µA µM^{-1}	$0.4+/-0.04$ µA µM^{-1}
	5-500 nM	negligible	$0.02+/-0.0006$ µA nM^{-1}

Table 5 Oxidation potential of analytes on PEDOT and PEDOT/AuNPs glassy carbon modified electrodes

Analyte		Oxidation potential on PEDOT	Oxidation potential on PEDOT/AuNPs
AA	5-100 µM	-5.4 mV	-39 mV
DA	5-20 µM	176 mV	165 mV
	5-500 nM	n.a.	152 mV
5-HT	5-20 µM	320 mV	320 mV
	5-500 nM	n.a.	319 mV

The data show different mechanisms of electron transfer in PEDOT/AuNP construct for AA on one hand and dopamine, serotonin on the other. Redox potential for AA shifts by -44 mV between PEDOT and PEDOT/AuNP electrodes and the slope corresponding to the sensitivity increases two times. Therefore is no adsorption steps involved for AA reaction and slow stage is electron transfer from AA to the surface. Situation with neurotransmitters is different: there is no significant shift of potential of oxidation peak (Table 5), whereas the current is increasing by threefold for the both studied molecules in micromolar range and by tenfold in nanomolar range (Table 4). This means that slow step is chemical binding to the surface followed by electron transfer through PEDOT layer. The increase in oxidation current in the presence of gold nanoparticles is attributed to the favourable weak adsorption of dopamine / serotonin cations on gold particles. The reversibility of oxidation process is also enhanced on the PEDOT/AuNPs electrode, which may have been favoured by the PEDOT polymer film which has a rich electron cloud and acts as an electron mediator. A hydrophobic environment appears to favour reversible oxidation of dopamine and serotonin [158]. The increase of serotonin sensitivity on PEDOT/AuNP glassy carbon modified electrode compared to dopamine is presumably due to a large conjugated structure of serotonin, which has the possibility to intercalate into the PEDOT/AuNP film [158]. Another reason can be the presence of $-NH_2$ and $-NH$ groups in serotonin, which increase the positive charge density and the interaction with gold nanoparticles.

4 Summary and Outlook

The aim of this work was to synthesize a nanocomposite layer, PEDOT/gold nanoparticles with application in biosensors domain. Firstly a porous polymer with a large active area was electrochemically obtained which has been used as a matrix for gold nanoparticles deposition. The colloidal solution of gold nanoparticles was synthesized (see 2.2) and characterized (3.1.1) by different techniques which proved a narrow distribution of 20 nm size and a very good stability in time (more than six months).

EQCM technique has been used for electrochemical deposition and characterization of pristine and PEDOT/AuNPs composite layers. This is a suitable technique to control the deposited mass. The suitable parameters for deposition of pristine PEDOT layers were found, using the potentiostatic pulse method and EQCM technique (see 3.2.3). In order to characterize the polymer growth under pulse conditions, the enhancement factor (*EF*), was introduced (3.2.4.1). Acoustic impedance data was recorded and converted into shear elastic moduli for storage *G'* and losses *G''* (3.2.4.3). One can observes that at optimal parameters of the pulse sequence, where EF reached maxima, elastic moduli reached maxima as well.

Polymers electroplated by three different routes were compared. For the same deposition mass, the polymer deposited by potentiostatic pulse method (3.2.3) had a higher thickness therefore a porous morphology comparing with PEDOT layers obtained by direct current techniques, potentiostatic (3.2.2) and potentiodynamic (3.2.1).

The synthesized polymer by potentiostatic pulse technique was used as matrix for gold nanoparticles deposition using the chemical method (3.3.2). The reduced polymer acted as a reduction agent for gold salt. The reduction time

for polymer and also the immersion time of polymer electrode in gold containing solution are important parameters to control the Au clusters growth. After several experiments these parameters were fixed in order to obtain AuNP with 20 nm size. The nanocomposite layer was analyzed by SEM, EDX and GDOES which confirmed the uniform distribution of AuNPs on polymer surface. These data were used to develop a novel model which can be applied for polymers/metal nanocomposite layers (3.3.2.1). This model is successfully applied for viscoelastic polymers to calculate the deposited metal mass on top of polymer layer.

The obtained nanocomposite layer was used as amperometric sensor for electroanalytical detection of AA (3.4.2) and neurotransmitters such as dopamine (3.4.3) and serotonin (3.4.4) in 0.1 M phosphate buffer solution. The influence of layer thickness on analyte response was also studied (3.4.1) and a compromise thickness of 500 nm was chosen for this work. The polymer electrode and also the nanocomposite glassy carbon modified electrode showed distinguished oxidation peaks, at -0.005 V for AA, 0.176 V for dopamine and 0.32 V for serotonin on PEDOT electrode and -0.039 V, 0.165 V and 0.319 V on PEDOT/AuNP electrode (Table 4). The sensitivity for analytes detection on nanocomposite layer increased by threefold comparing with the data on pristine PEDOT layer (Table 3). In nanomolar range the sensitivity increased by tenfold for dopamine detection (3.4.3.1) and one hundred times for serotonin (3.4.4.1).

The increase of serotonin sensitivity on PEDOT/AuNP glassy carbon modified electrode compared to dopamine is presumably due the presence of –NH_2 and –NH groups in serotonin, which increase the positive charge density and also the interaction with gold nanoparticles.

Summary and Outlook

During electroanalytical procedure the electroactive reaction products were adsorbed on polymer surface poisoning the active area. The initial state of the PEDOT electrode was partially recovered by continuously cycling the electrode in PBS solution. For that reason, after each measurement in DA or 5-HT containing solution, the electrode was transferred back to PBS, without DA / 5-HT, in order to recover its initial state. Even in this way, the problem with the irreversible inhibition of the surface of the PEDOT layers could not be overcome completely for the concentrations of studied analytes.

Neurotransmitters coexist in biological medium with AA which is in concentration between 100-1000 times higher than the concentration of studied neurotransmitters. From this reason it was verified if it is any interference of AA in dopamine and serotonin detection. However, with the addition of dopamine and serotonin, the responses were increase linearly with the concentration while the current response for AA remained constant (3.4.3.2 and 3.4.4.2). Due to this one can mention that the high concentration of AA did not interfere with the response of analytes. Therefore it could be proofed that PEDOT/AuNPs electrode fulfill all the properties to become a proper candidate for an amperometric sensor.

4.1 Outlook

It has been shown in this work that a uniform distribution of gold nanoparticles on top of PEDOT layer can be obtained. Using the proposed model the deposited metal mass can be accurately calculated. To improve the electrocatalytic properties the co-deposition of carbon nanotubes and gold nanoparticles on PEDOT layer are planned. In order to develop a model for a better understanding of the oxidation mechanism of neurotransmitters more experiments in situ will be performed.

Conductive polymers are a real solution for developing very good biosensors.

5 References

[1] C. C. K. Shirakawa, H. Macdiarmid, Phys. Rev. Lett. 39, no. (1977) 1101.

[2] T.A. Skotheim, Handbook of Conducting Polymers, second ed., New York, 1998.

[3] M. Delamar,P. C. Lacaze, J. S. Dumousseau, J. E. Dubois, J. E. Electrochim. Acta 27 (1982) 61.

[4] G. E. Wnek, J. C. Chien, F. E Karasz, C. P. Lillya, Polymer 20 (1979) 1441.

[5] A. F. Diaz, K. K. Kanazawa, G. P. Gardini, J. Chem. Soc., Chem. Commun. (1979) 635.

[6] A. F. Diaz, Chem. Scr. 17 (1981) 142.

[7] G. Tourillon, F. Garnier, J. Electroanal. Chem. 135 (1982) 173.

[8] A. F. Diaz, J. A. Logan, J. Electroanal. Chem. 111 (1980) 111.

[9] R. Noufi, A. J. Nozi, J. White, J. F. Warren, J. Electrochem. Soc. 129 (1981) 2261

[10] I. Winter, C. Reese, J. Hormes, G. Heywang, and F. Jonas, Chem. Phys. 194 (1995) 207.

[11] A. Elschner, S. Kirchmeyer, W. Lövenich, U. Merker, K. Reuter, (Ed.) Taylor and Francis Group (2011), ISBN-13: 978-1-4200-6912-9.

[12] S. Bruckenstein, A.R. Hillman, J. Phys. Chem. 95 (1991) 10748.

[13] A. Bund, S. Neudeck, J. Phys. Chem. B 108 (2004) 17845.

[14] G. Tourillon, F. Garnier, J. Phys. Chem. 88 (1984) 5281.

[15] G.K. Chandler, D.J. Pletcher, Appl. Electrochem. 16 (1986) 62.

[16] K. Kost, D. Bartak, B. Kazee, Th. Kuwana, Anal. Chem. 60 (1988) 2379.

[17] J.C. Moutet, Y. Ouennoughi, S. Hamar-Thibault, Electrochim. Acta 40 (1995) 1827.

[18] Y.M. Maksimov, E.A. Kolyadko, Russ. J. Electrochem. 35 (1999) 1225.

116

[19] A. Yassar,J. Roncali, F. Garnier, J. Electroanal. Chem. 255 (1988) 53.

[20] J.Y. Lee, T.C. Tan, J. Electrochem. Soc. 137 (1990) 1402.

[21] V. Tsakova, A. Milchev, Electrochim. Acta 36 (1991) 1151.

[22] D.W. Hatchett, M. Josowicz, J. Janata, D.R. Baer, Chem. Mater. 11 (1999) 2989.

[23] B.J. Hwang, R. Santhanam, Y.L. Lin, Electronalysis 15 (2003) 1667.

[24] J.M. Kinyanjui, J. Hanks, M. Josowicz, J. Electrochem. Soc. 151(2004) 113.

[25] J.A. Smith, M. Josowicz, J. Janata Phys. Chem. Chem. Phys. 7 (2005) 3614.

[26] J.A. Smith, M. Josowicz, D.R. Baer, J. Janata Phys Chem (2005) 3619.

[27] Z. Wang, J. Yuan, M. Li, D. Han, A. Ivaska, J. Electroanal. Chem. 599 (2007) 121.

[28] A. Fedorczyk, J. Ratajczak, A. Czerwiński, M. Skompska, Electrochim. Acta 122 (2014) 267.

[29] V.-T. Gruia, A. Ispas, M. Wilke, I. Efimov, A. Bund, Electrochim. Acta 118 (2014) 88.

[30] D.K. Sarkar, X.J. Zhou, K.T. Leung, Solid. State. Commun. 125 (2003) 365.

[31] X.J. Zhou, A.J. Harmer, N.F. Heinig, K.T. Leung, Langmuir 20 (2004) 5109.

[32] T.F. Otero, S.O. Costa, M.J. Ariza, M. Marquez, J. Mater. Chem. 15 (2005) 1662.

[33] L.M. Abrantes, J.P. Correia, Electrochim. Acta 45 (2000) 4179.

[34] A. Zaoui, O. Stephan, A. Ourari, J.C. Moutet, Electrochim. Acta 46 (2000) 49.

[35] W. Wang, J. Shaowen, J. Lee, Applied Surface Science 283 (2013) 309.

References

[36] S. Fujii, H. Hamasaki, H Takeoka, T. Tsuruoka, K. Akamatsu, Y. Nakamura, Journal of Colloid and Interface Science 430 (2014) 47.

[37] F. Terzi, L. Pigani, R. Seeber, J. Electroanal. Chem., 619–620 (2008) 75.

[38] S. R. Hosseini, R. Hosseinzadeh, S. Ghasemi, N. Farzaneh, International Journal of Hydrogen Energy (2015).

[39] M. Haruta, Metal Nanoclusters in Catalysis and Materials Science (2008) 183.

[40] S.S. Kumar, J. Mathiyarasu, K.L. Phani, J. Electroanal. Chem. 578 (2005) 95.

[41] N.F. Atta, A. Galal, R.A. Ahmed, J. Electrochem. Soc. 158 (2011) 52.

[42] Teresa Łuczak, Electrochim. Acta 54 (2009) 5863.

[43] K. Wu, J. Fei, S. Hu, Analytical Biochemistry 318 (2003) 100.

[44] G. Inzelt,(2008) ISBN 978-3-540-75929-4.

[45] G. Heywang, F. Jonas, Adv. Mater. 4 (1992) 118.

[46] C. K. Chiang, C. B. Fincher, Jr., Y. W. Park, and A. J. Heeger, Physical Review Letters 39 (1977) 17.

[47] V. Rajendran, A. Gopalan,T.-Ch. Wen, Mat. Chem. Phys. 65 (2000) 320.

[48] Ch. Martin, L.S. van Dyke, in: R.W. Murray (Ed.), Molecular Design of Electrode Surfaces, Wiley, New York, 1992.

[49] G. Inzelt, M. Vorontynsev, J.W. Schultze, Electrochim. Acta 45 (2000) 2403.

[50] S. Richardson-Burns, J.L. Hendricks, B. Foster, L.K. Povlich, D.H. Kim, D.C.Martin, Biomaterials 28 (2007) 1552.

[51] L. Peponi, I. Navarro-Baena, J.M. Kenny, Smart Polymers and their Applications (2014) 204.

[52] N. Akkilic, W.M. de Vos, Switchable and Responsive Surfaces and Materials for Biomedical Applications (2015) 119.

118

[53] J. Bácskai, G. Inzelt, J. Electroanal. Chem. (1991) 310.

[54] G. Inzelt, J. Bácskai, J. Electroanal. Chem. (1991) 308.

[55] N. Oyama, T. Ohsaka, H. Yamamoto, M. Kaneko J. Phys. Chem. 90 (1986) 3850.

[56] Y. M. Tsou, H. Y. Lin, A. J. Bard J. Electrochem. Soc. 135 (1988)1669

[57] A. H. Schroeder, F. B. Kaufman, V. Patel, E. M. Engler, J. Electroanal. Chem. 113 (1980) 193.

[58] C. Degrand, J. Electroana.l Chem. 169 (1984) 259.

[59] P. M. Hoang, S. Holdcroft, B. L. Funt, J. Electrochem. Soc. 132 (1985) 2129.

[60] M. C. Pham, J. E. Dubois, J. Electroanal. Chem. 199 (1986) 153.

[61] C. Deslouis, M. M. Musiani, B. Tribollet, J. Phys. Chem. 98 (1994) 2936.

[62] A. Cook, A. Gabriel, N. Laycock J. Electrochem. Soc. 151 (2004) 529.

[63] D. Posadas, M. I. Florit, J. Phys. Chem. 108 (2004) 15470.

[64] M. C. Bernard, A. Hugot-Le Goff, Electrochim. Acta 52 (2006) 595.

[65] M. C. Bernard, A. Hugot-Le Goff, Electrochim. Acta 52 (2006) 728.

[66] A. R. Hillman, M. A. Mohamoud, Electrochim Acta 51 (2006) 6018.

[67] B. Palys, P. Celuch, Electrochim. Acta 51 (2006) 4115.

[68] P. S. Antonel, F. V. Molina, E. M. Andrade, J. Electroanal. Chem. 599 (2007) 52.

[69] M. A. Mohamoud, A. R. Hillman, J. Solid. State Electrochem. 11(2007) 1043.

[70] L. Komsiyska, V. Tsakova, G. Staikov Appl Phys 87 (2007) 405.

[71] P. A. Basnayaka, M. K. Ram, E. K. Stefanakos, A. Kumar, Electrochim. Acta 92 (2013) 376.

[72] G. Láng, M. Ujvári, G. Inzelt, Electrochim Acta 46 (2001) 4159.

[73] G. Láng, M. Ujvári, G. Inzelt, J. Electroanal. Chem. 572 (2004) 283.

References

[74] G. Láng, M. Ujvári, T. A. Rokob, G. Inzelt, Electrochim Acta 51 (2006) 1680.

[75] A. J. F. Romero, J. J. L. Cascales, T. F. Otero, J. Phys. Chem. B 109 (2005) 21078.

[76] I. L. Lehr, S. B. Saidman, Electrochim Acta 51 (2006) 3249.

[77] D. D. Ateh, H. A. Navsaria, P. Vadgama, J. Roy. Soc. Interface 3 (2006) 741.

[78] M. Heitzmann, C. Bucher, J. C. Moutet, E. Pereira, B. E. Saint-Aman E Electrochim. Acta 52 (2007) 3082.

[79] Hakanson E, Amiet A, Nahavandi S, Kaynak A (2007) Eur Polymer J 43:205.

[80] S. Koehler, M. Ueda, J. Efimov, A. Bund, Electrochim Acta 52 (2007) 3040.

[81] C. da Silva, A. R. Nogueira, J. Tonholo, A. S. Ribeiro, Solar Energy Materials and Solar Cells 95 (2011) 2255.

[82] H. Darwish, S. Okur, Sensors and Actuators B: Chemical 200 (2014) 325.

[83] L. Viau, J.Y. Hihn, S. Lakard, V. Moutarlier, V. Flaud, B. Lakard, Electrochim. Acta 137 (2014) 298.

[84] J. P. Correia, E. Vieil, L. M. Abrantes, J. Electroanal. Chem. 573 (2004) 299.

[85] Q. T. Vu, M. Pavlik, N Hebestreit, U. Rammelt, W. Plieth, J. Pfleger, React. Funct. Polym. 65 (2005) 69.

[86] M. Innocenti, F. Loglio, L. Pigani, R. Seeber, F. Terzi, R. Udisti, Electrochim. Acta 50 (2005) 1497.

[87] W. Alhalasah, R. Holze, J. Solid State Electrochem. 9 (2005) 836.

[88] C. Y. Wang, A. M. Ballantyne, S. B. Hall, G. Wallace J. Power Sources 156 (2006) 610.

120

[89] Y. Pang, X. Li, H. Ding, G. Shi, L. Jin, Electrochim Acta 52 (2007) 6172.

[90] S. I. Kuroda, K. Marumoto, T. Sakanaka, S. Abe, H. Kokubo, T. Yamamoto, Chem. Phys. Lett. 435 (2007) 273.

[91] A. S. Widge, M. Jeffries-El, X. Cui, C. F. Lagenaur, Y. Matsouka, Biosens Bioelectron 22 (2007) 1723.

[92] H.-J. Wang, L.-H. Chan, C.-P. Chen, S.-L. Lin, R.-H. Lee, R.-J. Jeng, Polymer 52 (2011) 326.

[93] B. Senthilkumar, P. Thenamirtham, R. Kalai Selvan, Applied Surface Science 257 (2011) 9063.

[94] P. Najafisayar, M.E. Bahrololoom, Electrochim. Acta 114 (2013) 462.

[95] X. Zhang, X. Ren, W. Cao, Y. Li, B. Du, Q. We, Analytica Chimica Acta, 845 (2014) 85.

[96] A. Bund, M. Schneider, J. Electrochem. Soc. 149 (2002) 331.

[97] V. Noël, H. Randriamahazaka, C. Chevrot, J. Electroanal. Chem. 558 (2003) 41.

[98] R. Hass, J. García-Canadas, G. Garcia-Belmonte, J Electroanal Chem 577 (2005) 99.

[99] R. Schweiss, J. F. Lübben, D. Johannsmann, W. Knoll, Electrochim Acta 50 (2005) 2849.

[100] K. Loganathan, P. G. Pickup, Electrochim. Acta 51 (2005) 41.

[101] W. Plieth, A. Bund, U. Rammelt, S. Neudeck, L. M. Duc, Electrochim Acta 51 (2006) 2366.

[101] F. Mouffouk, S. J. Higgins, Electrochem Commun 8 (2006) 15.

[102] A. Robert Hillman, Samantha J. Daisley, Stanley Bruckenstein, Electrochem. Comm. 9 (2007) 1316.

[103] A. Ispas, R. Peipmann, A. Bund, I. Efimov, Electrochim. Acta 54 (2009) 4668.

References

[104] A. Ispas, R. Peipmann, B. Adolphi, I. Efimov, A. Bund, Electrochim. Acta 56 (2011) 3500.

[105] A. Robert Hillman, Karl S. Ryder, Virginia C. Ferreira, Christopher J. Zaleski, Eric Vieil, Electrochim. Acta 110 (2013) 418.

[106] I. Efimov, A. Ispas, A. Bund, Electrochim. Acta 122 (2014) 16.

[107] V. Lyutov, I. Efimov, A. Bund, V. Tsakova, Electrochim. Acta 122 (2014) 21.

[108] A. Robert Hillman, Karl S. Ryder, Christopher J. Zaleski, E. Vieil, Electrochim. Acta 135 (2014) 42.

[109] M. Zhou, B. Geschke, J. Heinze, J. Phys. Chem. B (2002) 106, 10065

[110] J. Roncali, Chem. Rev., 92 (1992) 711.

[111] J. Heinze, B. A. Frontana-Uribe,S. Ludwigs, Chem. Rev. 110 (2010) 4724.

[112] A. Rasche, J. Heinze, Electrochim. Acta (2008) 53, 3812.

[113] M. Dietrich, J. Heinze, F. Jonas, J. ElectroanaI. Chem., 369 (1994) 87.

[114] J. Lukkari, M. Alanko, L. Heikkila, R. Laiho, J. Kankare, Chem. Mater. 5 (1993) 289.

[115] Q.B. Pei, G. Zuccarello, M. Ahlskog, O. Inganas, Polymer 35 (1994) 1347.

[116] S. A. Campbell, Y. Li, S. Breakspear, F. C. Walsh, J. R. Smith, Transactions of the Institute of Metal Finishing 85 (2007) 237.

[117] T. F. Otero, H. Grande, J. Rodriguez, Electrochim. Acta 41 (1996) 1863.

[118] T. F. Otero,I. Boyano, J. Phys. Chem. B 107 (2003) 6730.]

[119] S. Servagent, E. Vieil, J. Electroanal. Chem. 280 (1990) 227.

[120] J. Heinze, R. Bilger, Ber. Bunsen-Ges. Phys. Chem. 97 (1993) 502.

[121] L. Niu, C. Kvarnstrom, A. Ivaska, J. Electroanal. Chem. 569 (2004) 151.

[122] S. Koehler, A. Bund, I. Efimov, J. Electroanal. Chem. 589 (2006) 82.

[123] F. Chao, J. L. Baudoin, M. Costa, P. Lang, Makromol. Chem. Macromol. Symp.8 (1987) 173.

[124] Q.-X. Zhou,C. J. Kolaskie, L. L. Miller, J. Electroanal. Chem. 223 (1987), 283.

[125] S. Hotta, T. Hosaka, W. Shimotsuma, Synth. Met.,6 (1983) 319.

[126] P. Curie, J. Curie, C.R. Acad. Sci. 91 (1880) 294.

[127] Daniel A. Buttry, Chem. Rev. 92 (1992) 1355.

[128] G. Sauerbrey, Z. Phys. 155 (1959) 206.

[129] A. Bund, G. Schwitzgebel, Electrochim Acta 45 (2000) 3703.

[130] A. Bund, O. Schneider, V. Dehnke, Phys. Chem. Chem. Phys. 4 (2002) 3552.

[131] K. K. Kanazawa and J. G. Gordon, Analytica Chimica Acta 175 (1985) 99.

[132] K. S. Van Dyke, Proc. Annu. Freq. Control Symp. 1966, 10, 1.

[133] A. Bund, H. Chmiel, G. Schwitzgebel, Phys. Chem. Chem. Phys. 1, (1999) 3933.

[134] D. Johannsmann, K. Mathauer, G. Wegner, W. Knoll, Phys. Rev.46 (1992) 7808.

[135] C. S. Lu, O. Lewis, J. Appl. Phys. 43 (1972) 4385.

[136] S.J. Martin, V.E. Granstaff, G.C. Frye, Anal. Chem. 63 (1991) 2272.

[137] M. A. Vorontyntsev, E. Vieil, J. Heinze, Electrochim. Acta 41 (1996) 1913.

[138] I. Efimov, S. Winkels, J.W. Schultze, .J. Electroanal. Chem. 499 (2001) 169.

[139]. J. Li, X. Lin Sens Act B 124 (2007) 486.

[140] J. Mathiyarasu, S. Senthilkumar, K.L.N. Phani, V. Yegnaraman, Mater. Lett. 62 (2008) 571

References

[141] F. Terzi, C. Zanardi, L. Pigani, R. Seeber, J. Electroanal. Chem. 619–620 (2008) 75.

[142] N.F. Atta, M.F. El-Kady, A. Galal, Anal. Biochem. 400 (2010) 78.

[143] N. Tao, Z. Kaixin, X. Jingkun, L. Limin, B. Ling, J. Electroanal. Chem. 717–718 (2014) 1.

[144] J. Sophia, G. Muralidharan, J. Electroanal. Chem. 739 (2015) 115.

[145] M. Angelopoulos, IBM J. Res. Dev. 45 (2001) 57.

[146] W. Lian, J. Huang, X. Zhang, Q. Lin, X. Xing, S. Liu, Food Control 26 (2012) 620.

[147] N. Griffete, H. Frederich, A. Maitre, S. Ravaine, M.M. Chehimi, C. Mangeney, Langmuir 28 (2012) 1005.

[148] S. A. Nabi, A. M. Khan, Reactive and Functional Polymers 66 (2006) 495.

[149] Y. Yang, Y. Hao, J. Yuan, L. Niu, F. Xia, Carbon 84 (2015) 174.

[150] H. Hillaireau, T. Le Doan, H. Chacun, J. Janin, P. Couvreur, International Journal of Pharmaceutics 2 (2007) 148.

[151] Q. Cao, Y. Xu, F. Liu, F. Svec, J.M.J. Frechet, Anal. Chem. 82 (2010) 7416.

[152] M. Guerrouache, M.M. Chehimi, B. Carbonnier, Chem. Commun. 48 (2012) 7486.

[153] R. Bandaria, M.R. Buchmeiser, Catal. Sci. Technol. 2 (2012) 220.

[154] M. Omastova, M. Micusik, Chem. Pap. 66 (2012) 392.

[155] S. Thiagarajan, T.-H. Tsai, S.-M. Chen, Biosensors and Bioelectronics 24 (2009) 2712.

[156] A. Stoyanova, V. Tsakova, J Solid State Electrochem 14 (2010) 1947

[157] A. Stoyanova, V. Tsakova, J Solid State Electrochem 14 (2010) 1957.

[158] N.F. Atta, A. Galal, E. H. El-Ads, Electrochim. Acta 69 (2012) 102.

[159] S. Radhakrishnan, C.Sumathi, AhmadUmar, SangJaeKim, J.Wilson, V. Dharuman, Biosensors and Bioelectronics 47 (2013) 133.

[160] E. T. Kang, Y. P. Ting, K. G. Neoh, K. L. Tan, Polymer 34 (1993) 4494.

[161] Y. P. Ting, E. T. Kang, K. L.Tan, J. Chem. Technol. Biotechnol 59 (1994) 31.

[162] E. T. Kang, Y. P. Ting, K. G. Neoh, K. L. Tan Synth Met 69 (1995) 477.

[163] S. Ivanov, V. Tsakova Electrochim Acta 50 (2005) 5616.

[164] Ilieva M, Tsakova V, Erfurth W (2006) Electrochim Acta 52:816.

[165] M. Ocypa, M. Ptasinska, A. Michalska, K. Maksymiuk, Hall EAH J. Electroanal. Chem. 596 (2006) 157.

[166] H.L. Wang, W. Li, Q. X. Jia, E. Akhadov Chem Mater 19 (2007) 520.

[167] W. Wang, S. Ji, I. Lee, Applied Surface Science 283 (2013) 309.

[168] S. Biallozor, A. Kupniewska, V. Jasulajtene, Bull Electrochem 20 (2004) 231.

[169] S. Biallozor, A. Kupniewska, Bull Electrochem 20 (2004) 241.

[170] L. Niu, Q. Li, F. Wei, S. Wu, P. Liu, X. Cao, J. Electroanal. Chem. 578 (2005) 331.

[171] G. Wang, L. Li, J. H. Li, B. Q. Xu, Carbon 43 (2005) 2579.

[172] M. Trueba, S. P. Trasatti, S. Trasatti, Mater. Chem. Phys. 98 (2006) 165.

[173] C. W. Kuo, L. M. Huang, T. C. Wen, A. Gopalan, J. Power Sources 160 (2006) 65.

[174] J. M. Kinyanjui, N. R. Wijeratne, J. Hanks, D. W. Hatchett, Electrochim Acta 51 (2006) 2825.

[175] Coutanceau C, Croissant MJ, Napporn T, Lamy C (2000) Electrochim Acta 46:579

[176] Bouzek K, Mangold KM, Juettner K (2000) Electrochim Acta 46:661

[177] J. A. Smith, M. Josowicz, J. Janata Phys Chem Chem Phys 7 (2005) 3614

References

[178] A. Saheb, J.A. Smith, M. Josowicz, J. Janata, D.R. Baer, M.H. Engelhard, J. Electroanal. Chem. 621 (2008) 238.

[179] V. M. Jovanovic, S. Terzic, A. Dekanski, J Serb Chem Soc 70 (2005) 41.

[180] R. Dimeska, P. S. Murray, S. F. Ralph, G. G. Wallace Polymer 47 (2006) 4520.

[181] A. P. O'Mullane, S. E. Dale, T. M. Day, N. R. Wilson,P. R. Unwin PR, J. Solid State Electrochem. 10 (2006) 792.

[182] J. Wang, K. G. Neoh, E. T. Kang, J. Colloid Interface Sci. 239 (2001) 78.

[183] M. Ocypa, M. Ptasinska, A. Michalska, K. Maksymiuk, E.A.H. Hall, J. Electroanal. Chem. 596 (2006) 157.

[184] B. R. Panda,A. Chattopadhyay, J. Colloid Interface Sci., 316 (2007) 962.

[185] G. Hu,D.-P. Zhang, W. Wu, Z. Yang, Colloids Surf. 62 (2008) 199.

[186] C. Zanardi, F. Terzi, L. Pigani, A. Heras, A, Colina, Electrochim. Acta 53 (2008) 3916.

[187] A. Derlinkiewicz, M. Hasik, M. Choczynski (1998) Mater Res Bull 33:739.

[188] Z. H. Ma, K. L. Tan, E. T. Kang, Synth Met 114 (2000) 17.

[189] M. Lee, B. W. Kim, J. D. Nam, S. J. Seo, Y. Lee Mol. Cryst. Liq. Cryst. 407 (2003) 397.

[190] M. Hasik, E. Wenda, C. Paluskiewicz, A. Bernasik, J. Camra Synth Met 143 (2004) 341.

[191] V. W. L. Lim, E. T. Kang, K. G. Neo, Synth Met 123 (2001)107.

[192] A. Mourato, J.P. Correia, L.M. Abrantes, Electrochim Acta 53 (2007) 664.

[193] S. Ivanov, V. Tsakova, Electrochim Acta 49 (2004) 913.

[194] A.J. Bard, M. Stratmann, "Encyclopedia of Electrochemistry" (2007) ISBN: 978-3-527-30397-7

[195] Y. Liu, D. E. Krantz, C. Waites, R. H. Edwards, Trends in Cell Biology (1999) 356.

[196] Z. J. Li, C. H. Cho, European Journal of Pharmacology 667 (2011)22.

[197] V. Hook, L. Funkelstein, J. Wegrzyn, S. Bark, M. Kindy, G. Hook, Biochimica et Biophysica Acta (BBA) Proteins and Proteomics 1824 (2012) 89.

[198] T. L. Schwarz, Fundamental Neuroscience (Fourth Edition) (2013) 139.

[199] Y. Miyoshi, T. Oyama, R. Koga, K. Hamase, Journal of Neuroscience Methods 219 (2013) 5.

[200] C. Anne, B. Gasnier, Current Topics in Membranes 73 (2014) 149.

[201] A. Meneses, Identification of Neural Markers Accompanying Memory (2014) 5.

[202] G. H. Peters, M. Werge, M. N. Elf-Lind, J. J. Madsen, G. F. Velardez, P. Westh, Chemistry and Physics of Lipids 184 (2014) 7.

[203] A. A. Assareh, C. F. Sharpley, J. R. McFarlane, P. S. Sachdev, Neuroscience & Biobehavioral Reviews 49 (2015) 171.

[204] M. Hasanzadeh, N. Shadjou, E. Omidinia, Journal of Neuroscience Methods 219 (2013) 52.

[205] T. Łuczak, M. Bełtowska-Brzezinska, Electrochim. Acta 90 (2013) 634.

[206] R. Chellappan, T. Koichi, O.Takeo, Bioelectrochemistry 53 (2001) 183.

[207] N. F. Atta, M. F. El-Kady, Talanta 79 (2009) 647.

[208] I. A. Gesa, K. P.M. Currieb, F. Baudenbachera, Biosensors and Bioelectronics 34 (2012) 30.

[209] K. Yadav, B. Agrawal, M. Oyama, R. N. Goyal, Electrochim. Acta 125 (2014) 622.

[210] H. Hosseini, S. J. Rezaei, P. Rahmani, R. Sharifi, M. R. Nabid, A. Bagher, Sensors and Actuators B: Chemical 195 (2014) 85.

[211] S. A. Kumar, P.-H. Lo, S.-M. Chen, Biosensors and Bioelectronics 24 (2008) 518.

[212] H. W. Richter, W. H. Waddell, J. Am. Chem. SOC. 105 (1983) 5434.

References

[213] N. Sakmeche, J. J. Aaron, M. Fall, S. Aeiyach, M.Jouini, J. C. Lacroix, P. C. Lacaze, Chem. Commun. (1996) 2724.

[214] J. Kimling, M. Maier, B. Okenve, V. Kotaidis, H. Ballot, and A. Plech, J. Phys. Chem. B 110 (2006) 15700.

[215] I. J. Goldstein, D. E. Newburg, P. Echlin, D. C. Joy, C. Fiori, E. Lifshin, Scanning Electron Microscopy and X-Ray Microanalysis, second edition Plenum Press, New York and London (1984) .

[216] R.J. Hunter, Foundations of Colloid Science, 2nd edition, Oxford University Press, Oxford, New York (2001).

[217] Zetasizer Nano Series User Manual, Issue 2.1, Malvern Instruments Ltd., Worcestershire, United Kingdom (2004).

[218] R. L. Johnston, Atomic and Molecular Clusters, Taylor & Francis (2002).

[219] A. Knauer, A. Thete, S. Li, H. Romanus, A. Csáki, W. Fritzsche, J.M. Köhler, Chemical Engineering Journal 166 (2011) 1169.

[220] G.V. Andrievsky, V.K. Klochkov, A.B. Bordyuh, G.I. Dovbeshko, Chemical Physics Letters 364 (2002) 8.

[221] J. Heinze, A. Rasche, M. Pagels, B. Geschke, J. Phys. Chem. B 111 (2007) 989.

[222] G.P. Pandey, A.C. Rastogi, Electrochim. Acta 87 (2013) 168.

[223] C. Stromberg, V. Tsakova, J.W. Schultze, J. Electroanal Chem 547 (2003) 125

[224] F.H. Haegel, J. Schlupen, J.W. Schultze, S. Winkels, Ch. Stromberg, Electrochim. Acta 46 (2001) 3973.

[225] N. Sakmeche, J.J. Aaron, S. Aeiyach, P.C. Lacaze, Electrochim. Acta 45 (2000) 1921.

[226] V.Lisy, J.Tothova, A.Zatovsky, Condensed Matter Physics 9 (2006) 95.

[227] A.R. Hillman, M.A. Mohamoud, I. Efimov, Analytical Chem. 83 (2011) 5696.

[228] I. Jureviciute, S. Bruckenstein, A.R. Hillman, Electrochim. Acta 51 (2006) 2351.

[229] Péter S. Tóth, Emese Peintler-Kriván, Csaba Visy, Electrochem. Commun. 18 (2012) 16.

[230] Krzysztof Maksymiuk, Karl Doblhofer, Electrochim. Acta 39 (1994) 217.

[231] Krzysztof Maksymiuk, J. Electroanal. Chem. 373 (1994) 97.

[232] Péter S. Tóth, Csaba Janaky, Otto Berkesi, Tarmo Tamm, Csaba Visy, J. Phys. Chem. B 116 (2012) 5491.

[233] W. Plieth, A. Bund, S. Neudeck, L. Duc, Electrochim. Acta 51 (2006) 2366.

[234] A. R. Hillman, S. J. Daisley, S. Bruckenstein, Phys. Chem. Chem.Phys. (2007) 9, 2379.

[235] N. A. Pogulyaichenko, So Hui, V. V. Malev, V. Kondratiev, V. Russ. J. Electrochem. (2009) 45, 1267−1274.

[236] J. A. Harrison , H. R. Thirsk (1971) In: A. J. Bard (ed) Electroanalytical chemistry, vol 5. Marcel Dekker, New York, p 67

[237] E. Budevski, G. Staikov, W. J. Lorenz (1996) Electrochemical phase formation—an introduction to the initial stages of metal deposition. VCH, Weinheim

[238] M. Chen, G. Diao, Talanta 80 (2009) 815.

[239] J. Wang, W.-D. Zhang, J. Electroanal. Chem. 654 (2011) 79.

[240] M. Angberg, C. Nystriim. S. Castensson, lnternat. J. of Pharmaceutics 90 (1993) 19.

[241] P.R. Roy, T. Okajima, T. Ohsaka, Bioelectrochemistry 59 (2003) 1.

[242] P.R. Roy, T. Okajima, T. Ohsaka, J. Electroanal. Chem. 561 (2004) 75.

References

[243] B.J. Venton, K.P. Troyer, R.M. Wightman, Anal. Chem. 74 (2002) 539–546.

List of Figures

131

132

136

138

List of Tables

List of Abbreviations

AA	ascorbic acid
AFM	Atomic Force Microscopy
AuNPs	gold nanoparticles
BvD	Butterworth van Dyke model
CE	counter electrode
CP	conductive polymer
CV	cyclic voltammetry
DA	dopamine
DC	direct current
DCS	differential centrifugal sedimentation
DPV	differential pulse voltammetry
EDOT	3,4-Ethylendioxythiophen
EDX	Energy Dispersive X-Ray
EQCM	Electrochemical Quartz Crystal Microbalance
ESCR	Electrochemically Stimulated Conformational Relaxation Model
FHWM	full width at half maximum
GC	glassy carbon electrode
GD-OES	glow discharge optical emission spectrometry
PBS	phosphate buffer solution
PP	pulse plating
PEDOT	Poly-3,4-Ethylendioxythiophen
RE	reference electrode
SCE	Saturated Calomel Electrode
SDS	Na dodecylsulfate

SEM	Scanning Electron Microscopy
TEM	transmission electron microscopy
WE	working electrode
5-HT	serotonin

List of symbols used in the text

A	active area of the working electrode
$a_{Me^{z+}}$	activity of Me^{z+}_{solv} ions in electrolyte
c	concentration
C_0	capacitance
D	diffusion coefficient or particle diameter
E	electrical potential, or electrolyte
E_0	standard electrode potential
E_{dep}	deposition potential
E_a	anodic potential
E_c	cathodic potential
f_0	resonance frequency of an unloaded quartz
f	resonance frequency
F	Faraday constant (96485 C mol^{-1})
Δf	shift of the resonance frequency
Δf^*	complex resonance shift ($\Delta f^* = \Delta f + i\Delta w$)
G	shear modulus ($G = G' + jG''$)
G'	storage moduli
G''	loss moduli
ΔH	Enthalpy
I	imaginary part ($i^2 = -1$)
I	electric current
I	current density
I_0	intensity of the incident light

142

L	inductance
Δm	mass density
M_a	molar mass of anions
M_K	molar mass of cations
Me	metal
Me_{ads}	adsorbed Me atoms
n	the number of electrons or cycle number
Q_{poly}	polymerization charge
$\tau,$	the conformational relaxation time or total polymerizationtime
ϱ	density
ρ_l	density of the liquid
ϱ_q	density of the quartz crystal (2684 Kg m^{-3})
R	resistance or universal gas constant (8.315 J K^{-1} mol^{-1})
R_f	final radius of rotation
R_i	initial radius of rotation
$[R]_1^{+\cdot}$	number of cation radicals
t_q	thickness of the quartz crystal
T	temperature
v	scan rate
z_c	is the charge consumed to reduce, close, and compact one mole of polymeric segments
Z^*_m	mechanical impedance ($Z^*_m = Z'_m + i\, Z''_m$)
Z_q	mechanical impedance of the quartz ($Z_q = (\mu_q * \varrho_q)^{1/2}$)
μ_q	shear modulus of the quartz crystal (2.957*10^{10} N m^{-2})

$\mu_{a,K}^{0(s)}$	standard chemical potential
η_C	cathodic overpotential
η	anodic overpotential
η_l	viscosity of the liquid
ω	rotational velocity
Δw	full width at half maximum, FWHM
$\emptyset^s$	potential in solution
$\emptyset^P$	potential in the polymer film
γ	molar equivalents of doping anion
ε	dielectric permittivity
λ	wavelength (of the X-Ray, for example)

List of Original Publications

This thesis is based on the following publications and presentations, respectively.

V.-T. Gruia, S. Ivanov, R. Peipmann, A. Ispas, C. Gheorghies, A. Bund
"Preparation and electrochemical performance of PEDOT – gold nanocomposite layers for the selective detection of dopamine"
EnFI 2011 Workshop Linz, Austria, 19-20.07.2011, poster presentation

V.-T. Gruia, R. Peipmann, A. Ispas, C. Gheorghies, A. Bund
"Comparative methods for preparation and electrochemical performance of PEDOT – gold nanocomposite layers for the detection of serotonin "
Pulse Plating Conference Austria, Viena, 09.03.2012, poster presentation

V.-T. Gruia, A. Ispas,V. Tsakova , A. Bund
"Comparative methods for preparation and electrochemical performance of PEDOT – gold nanocomposite layers for the selective detection of dopamine and serotonin"
WEEM Conference Hungary, Szeged, 3-8.06.2012, poster presentation

V.-T. Gruia, A. Ispas, A. Bund
"Preparation and electrochemical performance of PEDOT – gold nanocomposite layers for the selective detection of dopamine and serotonin in the presence of ascorbic acid"
Nanofair 2012, Dresden, 12.07. 2012, poster presentation

V.-T. Gruia, I. Efimov, A. Ispas, A. Bund

„Electrochemical formation and characterization of Poly (3,4-ethylenedioxythiophene) layers in aqueous electrolytes by direct and pulse plating methods, using EQCM technique"

Nanocoatings 2013, Milano. 8-9.07.2013, oral presentation

V.-T. Gruia, I. Efimov, A. Ispas, A. Bund

„Electrochemical formation and characterization of PEDT layers in aqueous electrolytes by direct and pulse plating methods"

WEEM Conference Germany, Bad Herenalb, 31.05-5.06.2015, poster presentation

V.-T. Gruia, A. Ispas, M. Wilke, I. Efimov, A. Bund

"Application of acoustic impedance method to monitoring of sensors:Metal deposition on viscoelastic polymer substrate"

Electrochimica Acta 118 (2014) 88– 91

I. Efimov, V.-T. Gruia, F. Rumiche, A. Bund, A. Ispas

"An electrochemical quartz crystal microbalance study on adsorption of single walled carbon nanotubes onto poly[3,4-ethylenedioxythiophene] layers"

J Solid State Electrochem 19 (2015) 2581-2589

V. Lyutov; V.-T. Gruia, I. Efimov, A. Bund, V. Tsakova

"An acoustic impedance study of PEDOT layers obtained in aqueous solution"

Electrochimica Acta (2016) 285-293